Coherent control of optical pulse propagation through multi-level atomic media

A thesis submitted in partial fulfilment of the requirements for the award of

Doctor of Philosophy

by

Rajitha K V

Department of Physics
Indian Institute of Technology Guwahati
Guwahati 781039, India.

May 2016

Dedicated to my family

Declaration

I hereby declare that the contents of this thesis are original and have not been submitted for consideration for any other degree or qualification in this, or any other university. This dissertation is my own work and contains nothing which is the outcome of work done by others, except for the collaboration as specified in the text and Acknowledgements.

Rajitha K V
May 2016

Certificate

This is to certify that the work contained in the thesis entitled "**Coherent control of optical pulse propagation through multi-level atomic media"** submitted by Rajitha K V in the partial fulfillment of the requirement for the award of the degree of Doctor of Philosophy in Physics, Department of Physics, Indian Institute of Technology Guwahati, is a record of the candidate's own work carried out by her under my supervision and guidance. The matter embodied in this report has not been submitted in part or full to any other university or institute for the award of any degree.

Dr. Tarak Nath Dey
Associate Professor
Department of Physics
Indian Institute of Technology Guwahati
Guwahati - 781039
Assam, India.

May 2016

Acknowledgements

First and foremost, I sincerely thank my supervisor Dr. Tarak Nath Dey for his guidance, constant help and support throughout the period of my research.
I would also like to thank my doctoral committee, chairman Dr. B. R. Boruah and members Dr. S. B Santra and Dr. A. N. Panda, for their comments and suggestions.
Particular thanks go to my co-authors, Dr. Martin Kiffner, Dr. Pankaj K. Jha, Dr. Sumanta Das and Dr. Jörg Evers for their valuable help and contributions.
I acknowledge the computational and other facilities provided by the department and institute for smooth conduct of the research.
I acknowledge the financial assistance from MHRD for successful completion of my research work.
I extend my thanks to the group members Sandeep and Nawaz, my family and all other people directly or indirectly helped in completing this thesis.

Abstract

In this thesis, we are dealing with the propagation of optical pulses through coherently prepared atomic media. Coherent control techniques make use of the quantum interference effects of probability amplitudes to control and manipulate optical properties of quantum systems. Different optical phenomena are found to be effectively controlled with this coherent preparation by engineering the dispersion and absorption properties of the medium. The development of new schemes for pulse shaping and control is important in many fields of optics and atomic physics, some of which includes preparation of atoms and molecules in desired quantum states, optical communication systems with tailored pulses, ultrafast spectroscopy and so on. One prominent example of coherent quantum control is electromagnetically induced transparency(EIT), a quantum interference effect that allows the propagation of light pulses through an otherwise opaque medium. EIT leads to many interesting new phenomena, including lasing without inversion, slow light, stopped light, and efficient non-linear wave mixing to name a few. This work shows the controllability of different phenomena arise by modifying the EIT media with more fields and level structures.

The first system investigated is a four-level N-type atomic medium, with two transitions coupled by the probe field simultaneously. The propagation dynamics of a Gaussian probe pulse through the medium is investigated. It is observed that at two-photon resonance of probe and control fields, weaker probe pulses may propagate through the medium with low absorption and pulse shape distortion. In contrast, we find that increasing the probe pulse intensity leads to a splitting of the initially Gaussian pulse into a sequence of sub-pulses in the time domain.

It is known that microwave coupled optical systems offers new possibilities of optical control. In our second work, by making use of microwave field coupling hyperfine levels in a three level Λ system, we could generate a frequency comb with frequencies of Raman sub harmonics. The sub-harmonics generated is found to be stable within the length of the medium.

The closed Λ system is again investigated in our third work, with a microwave pulse coupling the hyperfine levels. We observed frequency conversion from microwave to optical frequency with the proper choice of couplings in this system. The efficiency of

generation and stability against propagation is controlled by tuning different parameters of the system.

Combining nonlinear fiber systems with atomic systems opens up new possibilities for efficient pulse control. In the fourth work in this thesis, a system describing doped optical nonlinear fibers with three level atoms is studied. We have observed generation of gray and bright coupled soliton solutions in such systems.

Contents

List of figures

Chapter 1

Introduction

Optical properties of quantum systems are known to be manipulated by using different techniques based on quantum interference effects. Coherent laser light is being used to control the dispersive and absorptive properties of the medium. One of the remarkable consequences of one's ability to manage dispersive and absorptive properties of an optical medium has been the manipulation of the dynamics of optical pulses through it. Optical pulse propagation through coherently prepared media is one important area of research for many years. The key elements in the control of optical properties of a resonant medium are atomic coherences and quantum interference effects.

Quantum mechanical systems are characterized by probability amplitudes, the products of which give rise to either a probability of an atom being in a particular quantum state or an atomic coherence between the levels. These coherences are generally produced by coherent resonant laser fields. The ability to couple light to resonant systems made possible harnessing the quantum mechanical properties of light. Atomic systems were naturally used for studies of coherent processes since they have discrete energy level structure. The atom light coupled systems allow controlled manipulations of the optical properties of atomic or atom-like media via strong coupling of near-resonant optical signal fields and collection of atoms [1]. The prevalence of optical coherence in various fields of optics can be seen from the amount of many diverse works done on this. Controlled quantum systems can be exploited for exploring fundamental aspects of quantum physics, quantum information processing, light storage [2], atomic clocks [3], precision measurements [2, 4, 5], magnetometers [6–8] and metrology [9].

The foundations for many strong-field coherent effects in optics were laid in the classic papers of McCall and Hahn on self-induced transparency(SIT)[10, 11], a phenomenon where a single pulse creates transparency for itself. Two-level atomic media have been used in these resonant pulse propagation and spectroscopic studies for a long time. In a two-level system, coherent evolution is characterized by oscillatory population transfer (Rabi flopping). Irradiating atomic medium by more than one electromagnetic

field simultaneously enabled multi-photon transitions and other nonlinear phenomena are observed to develop. In coherent population trapping(CPT), application of two continuous wave(cw) optical fields to a three level atomic system results in preparation of atoms in a coherent superposition of states which is immune to absorption of radiation [12]. CPT was first experimentally observed by Alzetta *et. al* in sodium vapor in three level atomic configuration [13]. In 1990, Harris and co-workers experimentally observed the remarkable property of Electromagnetically Induced Transparency (EIT) in an atomic system in three level configuration [14]. EIT is observed in three level systems where the absorption of a probe laser field expected near an atomic transition can be suppressed almost completely, making use of coherence induced between two atomic levels, due to the presence of a second 'coupling' field that couples to a third state. Within the narrow transparency window, dispersion is steep and normal, which leads to ultra slow group velocities [15–17]. Since then atomic system with more than one levels became a constant case of study. EIT is closely related to CPT , the difference between the two being that EIT modifies both optical property of the medium and the optical fields themselves while CPT involves only modifications to the material states.

The possibility of building a short-wavelength laser operating without the need to achieve population inversion in the atomic medium has been recognized as a consequence of EIT [18]. This property termed as 'Lasing without inversion' (LWI), has been demonstrated in Na and Rb in the visible range [19]. LWI and EIT effects are observed in semiconductor quantum wells using laser-induced processes [20] or bandgap engineering [21] to create the necessary coherences.

EIT has become a versatile tool for realization of controllable atom-light coupling for the past decades. Some of the interesting EIT phenomena are slowing and stopping of light [15–17, 22–26], the coherent storage and retrieval of light [15, 22, 23, 27], and stationary light [28–37]. EIT can also be used to enhance the nonlinear susceptibility [38–42]. These phenomena exhibited in atomic and atom-like media allows the effective manipulation of optical pulse propagation through it.

Conventional EIT system is a three level atomic system in ladder, V or Λ configurations. Among these, the Λ system is the most extensively studied theoretical model in comparison to its other two counterparts because of the long living metastable ground level. Modifications of EIT system with more optical fields coupling same or additional levels is found to exhibit many interesting behavior. One important way to modify the Λ system is by coupling the ground state levels by a low frequency rf or microwave field. Switching from subluminal to superluminal is shown to be possible in this system [43]. It is possible to enhance the Kerr non-linearity of the medium by adding an extra ground state and coupling field to the Λ system [44]. The emergence of a 'double dark' state, a splitting of the dark state resonance associated with EIT is also observed in this

system [45, 46]. Another EIT modified system studied often is N-level configuration, formed by the addition of an excited state to the Λ-system [45, 47]. The N-system also exhibits double dark state. It was the original candidate for achieving high Kerr non-linearities [48]. The system has also been used to study electromagnetically induced absorption (EIA) both theoretically [49] and experimentally [50]. In addition to the EIT Kerr nonlinearity, there have been many advances in using EIT to provide more efficient low-light-level nonlinear optical phenomena. The field of EIT enhanced nonlinear optics began in the mid 1990's, only a few years after the first experiments on EIT. In 1995 Hemmer*et al.* demonstrated that EIT could be used to realize efficient phase conjugate effects [51]. In 1996, efficient frequency conversion via EIT has been demonstrated by several groups [52, 53].

Pulse propagation through such modified media making use of EIT-related effects is an interesting subject for investigation. The propagation of electromagnetic fields through a medium is governed by the Maxwell field equations. Combining these with the Bloch formalism, the complete spatio-temporal evolution of the pulse can be investigated. Depending on the level structure and couplings involved, the pulse dynamics is shown to exhibit new effects. In this chapter, we investigate the theory of light-matter interaction in atomic system. We follow semiclassical treatment in which the atomic system under consideration is treated quantum mechanically with discrete energy levels while the electromagnetic field is treated classically using Maxwell equations. This approach is physically more intuitive than the full quantum mechanical approach and can explain most of the frequently observed phenomena. It is only in the extreme conditions like light levels are of a few quanta that this approach is not adequate. Some of the phenomena which the semiclassical approach fails to explain are spontaneous emission, free induction decay and photon echoes [54]. For our purpose of investigating narrow bandwidth optical pulse propagation through atomic media consists of alkali atoms, below given semiclassical theory suffices.

1.1 Theoretical background of atom-field interaction

Before beginning the detailed discussion on light-matter interaction in quantum optics, it is important to first understand the fundamentals of semiclassical theory. The dynamics of atoms are governed by appropriate density operator obeying the Liouville equation. The basic Maxwell's equations of classical electrodynamics are used to describe the propagation of electromagnetic fields. We start with the derivation of propagation eqation of an electromagnetic field through a dielectric medium.

1.1.1 Maxwell Equations

The propagation of electromagnetic(em) field through an optical medium is governed by Maxwell's fundamental equations. We adopt Gaussian units throughout this thesis considering the symmetry properties and physical usefulness. In the classical theory of electromagnetism, the electric and magnetic field vectors are related through the four fundamental equations

$$\nabla .\ \mathbf{D} = 4\pi\rho, \qquad \text{(Gauss's law)} \tag{1.1a}$$

$$\nabla .\ \mathbf{B} = 0, \qquad \text{(no name)} \tag{1.1b}$$

$$\nabla \times \mathbf{E} = -\frac{1}{c}\frac{\partial \mathbf{B}}{\partial t}, \qquad \text{(Faraday's law)} \tag{1.1c}$$

$$\nabla \times \mathbf{H} = \frac{4\pi}{c}\mathbf{J} + \frac{1}{c}\frac{\partial \mathbf{D}}{\partial t}. \qquad \text{(Maxwell-Ampere law)} \tag{1.1d}$$

In these equations the basic electric and magnetic field vectors are given by $\mathbf{E}$ and $\mathbf{H}$ and c represents the velocity of light in vacuum. $\mathbf{D}$ and $\mathbf{B}$ are the electric displacement and the magnetic induction vectors in material medium related through the equations,

$$\mathbf{D} = \mathbf{E} + 4\pi\mathbf{P}, \tag{1.2}$$

$$\mathbf{B} = \mathbf{H} + 4\pi\mathbf{M}, \tag{1.3}$$

where $\mathbf{P}$ and $\mathbf{M}$ are the electric and magnetic polarizations respectively. In free space, both $\mathbf{P}$ and $\mathbf{M}$ vanish. The systems considered in this thesis is nonmagnetic ($\mathbf{M} = 0$), non-conducting ($\mathbf{J} = 0$) and there are no free charges ($\rho = 0$). Taking the curl of Eq. (1.1c) and using the constitutive relation for $\mathbf{B}$, we obtain

$$\nabla \times \nabla \times \mathbf{E} + \frac{1}{c^2}\frac{\partial^2}{\partial t^2}(\mathbf{E} + 4\pi\mathbf{P}) = 0. \tag{1.4}$$

We use the trigonometric identity $\nabla \times \nabla \times \mathbf{A} = \nabla(\nabla \cdot \mathbf{A}) - \nabla^2\mathbf{A}$, use Eq. 1.2 and the fact that for a charge free isotropic medium, $\nabla \cdot \mathbf{D}$ (and hence $\nabla \cdot \mathbf{E}$) $= 0$. Thus the equation Eq. 1.4 is reduced into the simplified form,

$$\nabla^2\mathbf{E} - \frac{1}{c^2}\frac{\partial^2 \mathbf{E}}{\partial t^2} = \frac{4\pi}{c^2}\frac{\partial^2 \mathbf{P}}{\partial t^2}. \tag{1.5}$$

This equation is the Maxwell wave equation for propagation of electromagnetic field through a material medium. The term on right hand side of the equation is the source term and represents the material response. For an unpolarized medium, the above equation Eq. 1.5 reduces to

$$\nabla^2\mathbf{E} - \frac{1}{c^2}\frac{\partial^2 \mathbf{E}}{\partial t^2} = 0. \tag{1.6}$$

This is the wave equation in vacuum. The transverse variations of the field can be ignored in the optical wavelength limit. The structure of the equation Eq. 1.6 allows to write the general solution of this equation in the simple form,

$$\mathbf{E} = \mathbf{E_1}(z - ct) + \mathbf{E}_2(z + ct), \tag{1.7}$$

where $\mathbf{E_1}$ and $\mathbf{E_2}$ are arbitrary functions representing fields propagating with velocity c in the positive and negative z-direction respectively. We are dealing with pulse propagation through dielectric media where polarization is non-zero. In the presence of a polarized medium, the wave equation Eq. 1.5 is nonlinear. Since the exact analytical solution of a nonlinear equation is difficult to obtain, we apply numerical methods for a complete solution. But if we employ some approximations valid in the regime of our application, an analytical solution is also obtainable.

Consider a quasi-monochromatic wave propagating in the z-direction. The medium effects cause the light to get polarized. Its electric field and induced polarization can be described by

$$\mathbf{E}(x, y, z, t) = \hat{\mathbf{e}}\mathcal{E}(x, y, z, t)e^{i(kz-\omega t)} + c.c., \tag{1.8}$$

$$\mathbf{P}(x, y, z, t) = \hat{\mathbf{e}}\mathcal{P}(x, y, z, t)e^{i(kz-\omega t)} + c.c., \tag{1.9}$$

where $\mathcal{E}(x, y, z, t)$ and $\mathcal{P}(x, y, z, t)$ are the envelope functions of the field. The unit vector $\hat{\mathbf{e}}$ denotes the direction of polarization, ω is the central angular frequency of the field and $k = \omega/c$ is the wave number. The complex conjugate ($c.c.$) term has been added to the complex electric field expression to make it real.

The required derivatives of Eq. 1.4 are obtained as:

$$\nabla^2\mathbf{E} = \hat{\mathbf{e}}(\nabla_\perp^2\mathcal{E} + \frac{\partial^2\mathcal{E}}{\partial z^2} + 2ik\frac{\partial\mathcal{E}}{\partial z} - k^2\mathcal{E})e^{i(kz-\omega t)} + c.c., \tag{1.10}$$

$$\frac{\partial^2\mathbf{E}}{\partial t^2} = \hat{\mathbf{e}}(\frac{\partial^2\mathcal{E}}{\partial t^2} - 2i\omega\frac{\partial\mathcal{E}}{\partial t} - \omega^2\mathcal{E})e^{i(kz-\omega t)} + c.c., \tag{1.11}$$

$$\frac{\partial^2\mathbf{P}}{\partial t^2} = \hat{\mathbf{e}}(\frac{\partial^2\mathcal{P}}{\partial t^2} - 2i\omega\frac{\partial\mathcal{P}}{\partial t} - \omega^2\mathcal{P})e^{i(kz-\omega t)} + c.c., \tag{1.12}$$

where Laplacian operator $\nabla_\perp^2 = \partial^2/\partial x^2 + \partial^2/\partial y^2$ represents the variation in the transverse direction of the field. At this point we make an important approximation. We assume that the variations in time and space of envelope functions $\mathcal{E}$ and $\mathcal{P}$ are very small within the optical period and optical wavelength. This is a quasi monochromatic field assumption and can be represented mathematically by following inequalities:

$$\left|\frac{\partial^2\mathcal{E}}{\partial z^2}\right| \ll \left|k\frac{\partial\mathcal{E}}{\partial z}\right| \ll |k^2\mathcal{E}|, \quad \left|\frac{\partial^2\mathcal{E}}{\partial t^2}\right| \ll \left|\omega\frac{\partial\mathcal{E}}{\partial t}\right| \ll |\omega^2\mathcal{E}|, \tag{1.13}$$

$$\left|\frac{\partial^2\mathcal{P}}{\partial z^2}\right| \ll \left|k\frac{\partial\mathcal{P}}{\partial z}\right| \ll |k^2\mathcal{E}|, \quad \left|\frac{\partial^2\mathcal{P}}{\partial t^2}\right| \ll \left|\omega\frac{\partial\mathcal{P}}{\partial t}\right| \ll |\omega^2\mathcal{E}|. \tag{1.14}$$

The above approximation is known as the **slowly varying envelope approximation (SVEA)** which leads to major mathematical simplifications. The SVEA approximation plays a central role in laser physics and pulse propagation problems.
Substituting above derivatives into Eq. 1.5 and use the above inequalities in ignoring the higher order partial derivatives with respect to z and t,

$$\frac{1}{2ik}\nabla_\perp^2\mathcal{E} + \frac{\partial\mathcal{E}}{\partial z} + \frac{1}{c}\frac{\partial\mathcal{E}}{\partial t} = 2\pi ik\mathcal{P}. \tag{1.15}$$

This equation is the wave quation governing the dynamics of slowly varying electric field envelope $\mathcal{E}$ through the material medium.
We are working in the regimes where the transverse variation of the field is little in comparison with the variation in the propagation direction, z. So the first term in Eq. 1.15 can be ignored.

$$\frac{\partial\mathcal{E}}{\partial z} + \frac{1}{c}\frac{\partial\mathcal{E}}{\partial t} = 2\pi ik\mathcal{P}. \tag{1.16}$$

For ease of numerical integration, we transform this equation into new variables

$$\tau = t - z/c, \;\; \zeta = z. \tag{1.17}$$

so that ,

$$\partial/\partial z + c^{-1}\partial/\partial t = \partial\zeta, \; \partial/\partial t = \partial/\partial\tau, \tag{1.18}$$

and the wave equation Eq. 1.16 further simplified into an equation in one independent variable ζ:

$$\frac{\partial\mathcal{E}}{\partial\zeta} = 2\pi ik\mathcal{P}. \tag{1.19}$$

The propagation of an em wave through the atomic medium is governed by this equation. This equation determines how light propagates through a material medium with polarization given by $\mathcal{P}$. The real and imaginary parts of the complex polarization drives the dispersion and absorption of the medium respectively.

1.1.2 Polarization and susceptibility of the medium

Equation 1.16 tells us how a plane electromagnetic wave responds to a given polarization of the medium. But the polarization in turn is also affected by the em field. For atomic gases without permanent polarization, it is the electromagnetic field itself that induces the polarization. Thus the applied electromagnetic field drives the polarization of the medium and vice versa. For a complete description, we need a relation between the

induced polarization and the field. The response of a dielectric medium for intense electromagnetic fields, as in the case of lasers, is nonlinear in the field amplitude. On a fundamental level, the anharmonic motion of bound electrons under the influence of an applied field is attributed to as the origin of this nonlinear response. So, in the most general case, polarization is a nonlinear function of the electric field expressed by

$$\mathbf{P} = \chi^{(1)}\mathbf{E} + \chi^{(2)}\mathbf{EE} + \chi^{(3)}\mathbf{EEE} + \cdots , \tag{1.20}$$

where $\chi^{(j)}$ is called jth order susceptibility. In general $\chi^{(j)}$ is a tensor of rank $j+1$. The dominant contribution to $\mathbf{P}$ is the linear susceptibility $\chi^{(1)}$. Its effects are expressed through the refractive index n and the attenuation coefficient α of the medium. The second-order susceptibility $\chi^{(2)}$ is nonzero only for media that lack an inversion symmetry. It is responsible for nonlinear effects such as second-harmonic generation and sum-frequency generation. The lowest order nonlinear term for atomic medium is thus $\chi^{(3)}$ which causes effects such as third-harmonic generation and four-wave mixing. We can write Eq. 1.20 such that the total susceptibility is defined as the coefficient of proportionality relating $\mathbf{E}$ and $\mathbf{P}$.

$$\mathbf{P} = \left[\chi^{(1)} + \chi^{(2)}\mathbf{E} + \chi^{(3)}\mathbf{EE} + \cdots\right]\mathbf{E} = \chi\mathbf{E}. \tag{1.21}$$

The induced polarization Eq. 1.20 can be separated into linear and nonlinear parts as

$$\mathbf{P}(\mathbf{r},t) = \mathbf{P}_L(\mathbf{r},t) + \mathbf{P}_{NL}(\mathbf{r},t). \tag{1.22}$$

All the nonlinear terms are included in $\mathbf{P}_{NL}(\mathbf{r},t)$. Generally, the only significant contribution to the nonlinear polarization is limited upto third order, because all higher order terms are small enough to be neglible. Because of the complex tensor nature of polarization expressions, we can make some simplifying assumptions without hindering the physical applicability. The nonlinear polarization $\mathbf{P}_{NL}$ in Eq. 1.22 is treated as a small perturbation to the total induced polarization. This is justified because we are probing optical pulses which are weak in intensity to cause any significant nonlinear effect. The envelope function of linear polarization is related to the electric field through the relation:

$$\mathcal{P}_L(\mathbf{r},t) = \sum_\beta \int_{-\infty}^{+\infty} \int_{-\infty}^{t} dt'dr' \chi_{\alpha\beta}(r-r', t-t')\mathcal{E}_\beta(r',t'), \tag{1.23}$$

where the linear susceptibility coefficient $\chi_{\alpha\beta}$ is a tensor of rank two for an anisotropic medium, in which the response of the medium is different for different components of the electric field. In the present thesis, the medium is isotropic and the complex

susceptibility, $\chi_{\alpha\beta} \equiv \chi$ is a scalar quantity. Let us also assume that the medium response is local which is justified in the electric-dipole approximation that will be introduced in section 1.2. Thus Eq. 1.23 can be written as

$$\mathcal{P}_L(\mathbf{r},t) = \int_{-\infty}^{t} dt' \chi^{(1)} \mathcal{E}(r,t'). \tag{1.24}$$

It is useful to write the wave equation Eq. 1.6 in the frequency domain by identifying that the $\partial^2/\partial t^2$ becomes $-\omega^2$ in Fourier domain.

$$(\nabla^2 + \frac{\omega^2}{c^2})\ \tilde{\mathbf{E}}(\mathbf{r},\omega) = -\frac{4\pi\omega^2}{c^2}\tilde{\mathbf{P}}(\mathbf{r},\omega), \tag{1.25}$$

where $\tilde{\mathbf{E}}(\mathbf{r},\omega)$ is the Fourier transform of $\mathbf{E}(\mathbf{r},t)$ defined by

$$\tilde{\mathbf{E}}(\mathbf{r},\omega) = \int_{-\infty}^{+\infty} \mathbf{E}(\mathbf{r},t) e^{i\omega t} dt. \tag{1.26}$$

In frequency domain, the linear part of the polarization $\mathcal{P}$ simply reduces into $\chi^{(1)}(\omega)\tilde{\mathcal{E}}(\omega,t)$. The linear susceptibility $\chi^{(1)}(\omega)$ is in general a complex quantity. In the optical wavelength domain, $\chi^{(1)} \ll 1$. Therefore an approximate linear relation can be obtained connecting the refractive index $n(\omega)$ and the absorption coefficient $\alpha(\omega)$ of the medium with the real and imaginary parts of $\chi(\omega)$ as given by

$$n(\omega) = 1 + 2\pi Re[\chi^{(1)}(\omega)], \tag{1.27}$$

$$\alpha(\omega) = \frac{4\pi\omega}{c} Im[\chi^{(1)}(\omega)], \tag{1.28}$$

where Re and Im stand for the real and imaginary parts, respectively. Eq. 1.19 for a linear polarization can be expressed in frequency space as

$$\frac{\partial \mathcal{E}}{\partial \zeta} = 2\pi i k \chi(\omega)\mathcal{E}(\omega). \tag{1.29}$$

For a constant χ, the above equation is valid in the time domain also. For a medium of length L, the output field after propagation can be obtained by solving this equation. In general, the electric filed $\mathcal{E}$ is a function of time and space. We can find a steady state limit in the linear regime so that $\mathcal{E}$ is independent of z. Then Eq. 1.29 in time can readily be integrated to get for the output filed

$$\vec{E}_{out}(z=L,t) = \hat{e}\mathcal{E} e^{2\pi i k L \chi} e^{-i(\omega t - kz)} + c.c.. \tag{1.30}$$

In general, when the optical frequency is near a medium resonance, the evaluation of $\mathcal{P}$ requires a quantum-mechanical approach. In the next section, we will discuss the Bloch formalism to determine the microscopic description of the polarization. This leads to the description of the interaction between the matter and field to be expressed in terms of coupled nonlinear partial differential equations which have to be solved "self-consistently". A complete description of atom-light coupling is given by Maxwell-Bloch equations, which account for both time evolution of atomic states and propagation of light through it.

1.2 Atom-field interaction Hamiltonian

As mentioned before, in semiclassical theory of light matter interaction, the atoms constituting the medium are treated quantum mechanically, with their discrete energy levels and interacting electromagnetic field obey Maxwell equations of motion. The atom dynamics is described by density matrix formalism using Liouville's equations of motion. In this section we start with the derivation of atom field interaction Hamiltonian. The dipole approximation is introduced to reduce this Hamiltonian into a simple yet valid form. The density matrix formalism is subsequently given. The atomic gas medium under consideration consists of alkali metal atoms with a single outer electron. The outer electron is bound by Coulomb interaction potential $V(\mathbf{r})$, $\mathbf{r}$ being the position vector of the electron with respect to the nucleus. The classical expression for Hamiltonian of such a bound electron of mass m and charge $-e$ is expressed as

$$H_0 = \frac{\mathbf{p}^2}{2m} + V(\mathbf{r}), \tag{1.31}$$

where $\mathbf{p}$ is the canonical momentum of the electron. This electron is acted on by an external em field. From the fundamental theory of electromagnetism, the electric field $\mathbf{E}$ and magnetic induction $\mathbf{B}$ associated with an em field can be expressed in terms of the scalar and vector potentials $\Phi(\mathbf{r}, t)$ and $\mathbf{A}(\mathbf{r},\mathrm{t})$ as:

$$\mathbf{E}(\mathbf{r}, t) = -\nabla\Phi(\mathbf{r}, t) - \frac{1}{c}\frac{\partial}{\partial t}\mathbf{A}(\mathbf{r}, t), \tag{1.32}$$

$$\mathbf{B}(\mathbf{r}, t) = \nabla \times \mathbf{A}(\mathbf{r}, t). \tag{1.33}$$

The modified form of the above Hamiltonian for the atom-field system is obtained from comparison of Lorentz force equation: $\mathbf{F} = -e[\mathbf{E} + (\mathbf{V} \times \mathbf{B})/c]$ and classical Lagrange's equation. We use the above forms of electric and magnetic fields in the

expression for **F** and arrive at the Hamiltonian of atom-field system:

$$H' = \frac{1}{2m}\left[\mathbf{p} + \frac{e}{c}\mathbf{A}(\mathbf{r},t)\right]^2 - e\Phi(\mathbf{r},t). \tag{1.34}$$

Thus the total Hamiltonian of atom-field system takes the following form

$$H = \frac{1}{2m}\left[\mathbf{p} + \frac{e}{c}\mathbf{A}(\mathbf{r},t)\right]^2 - e\Phi(\mathbf{r},t) + V(\mathbf{r}). \tag{1.35}$$

Quantization of equation Eq. 1.35 is done by replacing the classical variables with the corresponding quantum operators. Thus, momentum $\mathbf{p} \rightarrow \hat{\mathbf{p}} = -i\hbar\nabla$, and the total energy $\mathbf{E} \rightarrow \hat{\mathbf{E}} = -i\hbar\partial/\partial t$, where $\hbar = h/2\pi$ is the reduced Planck's constant. The same Hamiltonian can be derived for a quantum system from a gauge invariant point of view. We discuss it below. The dynamics of a quantum system is described by the non-relativistic Schrödinger equation:

$$i\hbar\frac{\partial}{\partial t}\Psi(\mathbf{r},t) = H\Psi, \tag{1.36}$$

where $\Psi(\mathbf{r},t)$ is the wave function of the quantum system so that quantity $|\Psi(\mathbf{r},t)|^2$ gives the probability density of finding an electron at position **r** and time t. The electronic motion under Coulomb potential is described by,

$$i\hbar\frac{\partial}{\partial t}\Psi(\mathbf{r},t) = \left[\frac{-\hbar^2}{2m_e}\nabla^2 + V(\mathbf{r})\right]\Psi(\mathbf{r},t). \tag{1.37}$$

The general solution of Eq. 1.36 can be written as:

$$\Psi(\mathbf{r},t) = \psi(\mathbf{r},t)e^{i\chi(\mathbf{r},t)}, \tag{1.38}$$

where χ is an arbitrary scalar function. Note that χ appears as a phase factor and does not affect the physical state of the system. However, if the phase is a function of both space and time variables, then the above solution does not satisfy the Schrödinger equation Eq. 1.36. Since the probability density still remains invariant under this transformation, we can modify the Schrödinger equation in order to satisfy phase invariance. The modified Schrödinger equation is given by

$$i\hbar\frac{\partial}{\partial t}\Psi(\mathbf{r},t) = \left\{\frac{1}{2m}\left[-i\hbar\nabla + \frac{e}{c}\mathbf{A}(\mathbf{r},t)\right]^2 - e\Phi(\mathbf{r},t) + V(\mathbf{r})\right\}\Psi(\mathbf{r},t), \tag{1.39}$$

where the functions **A**(**r**,t) and $\Phi(\mathbf{r},t)$ on right hand side of Eq. 1.39 represent the usual vector and scalar potentials of the external electromagnetic field, respectively.

The expanded form of total Hamiltonian $\hat{H}$ from this equation is written as

$$\hat{H} = -\frac{\hbar^2}{2m}\nabla^2 - \frac{ie\hbar}{2mc}\left[\mathbf{A}(\mathbf{r},t)\cdot\nabla + \nabla\cdot\mathbf{A}(\mathbf{r},t)\right] + \frac{e^2}{2mc^2}\mathbf{A}(\mathbf{r},t)\cdot\mathbf{A}(\mathbf{r},t) - e\Phi(\mathbf{r},t) + V(\mathbf{r}). \tag{1.40}$$

It is to be noted that the fields **E** and **B** and the wave equation Eq. 1.6 remain invariant under the following gauge transformations

$$\mathbf{A}(\mathbf{r},t) \rightarrow \mathbf{A}'(\mathbf{r},t) = \mathbf{A}(\mathbf{r},t) - \frac{\hbar c}{e}\nabla\chi(\mathbf{r},t), \tag{1.41}$$

$$\Phi(\mathbf{r},t) \rightarrow \Phi'(\mathbf{r},t) = \Phi(\mathbf{r},t) + \frac{\hbar}{e}\frac{\partial\chi(\mathbf{r},t)}{\partial t}. \tag{1.42}$$

This allows us to select Coulomb gauge or radiation gauge given by $\Phi(\mathbf{r},t) = 0$ and $\nabla\cdot\mathbf{A}(\mathbf{r},t) = 0$. The total Hamiltonian in radiation gauge becomes,

$$\hat{H} = -\frac{\hbar^2}{2m}\nabla^2 - \frac{ie\hbar}{2mc}\mathbf{A}(\mathbf{r},t)\cdot\nabla + \frac{e^2}{2mc^2}\mathbf{A}(\mathbf{r},t)\cdot\mathbf{A}(\mathbf{r},t) + V(\mathbf{r}). \tag{1.43}$$

Now we introduce an important and useful approximation known as "dipole approximation' which leads to substantial simplification of the interaction Hamiltonian.

Electric dipole Approximation

The vector potential describing the incident plane electromagnetic wave is expressed by a vector $\mathbf{A}(\mathbf{r_0}+\mathbf{r},t)$ defined as

$$\mathbf{A}(\mathbf{r_0}+\mathbf{r},t) = \mathbf{A}(t)exp[i\mathbf{k}\cdot(\mathbf{r_0}+\mathbf{r})], \tag{1.44}$$

where $\mathbf{r}_0$ is location of nucleus of the atom. Now we make an assumption that the wavelength of the interacting em field is much larger than the typical size of the atom, *i.e.*, $kr \ll 1$, where $|k| = 2\pi/\lambda$. This is known as the "electric dipole approximation" which essentially means that the spatial variation of electromagnetic field is nearly constant over the dimension of the atom. Atomic size is of the order of Bohr radius $a_0 \approx 0.5$ Å and optical wavelength $\approx 10^{-7}m$. Therefore it is safe to assume the dipole approximation in our problems.
The vector potential can be written as

$$\mathbf{A}(\mathbf{r_0}+\mathbf{r},t) = \mathbf{A}(t)exp[i\mathbf{k}\cdot(\mathbf{r_0}+\mathbf{r})] \tag{1.45}$$

$$= \mathbf{A}(t)exp(i\mathbf{k}\cdot\mathbf{r_0})[1 + i\mathbf{k}\cdot\mathbf{r} + \cdots] \tag{1.46}$$

$$\approx \mathbf{A}(t)exp(i\mathbf{k}\cdot\mathbf{r_0}). \tag{1.47}$$

The total Hamiltonian for the atom-field interaction in the dipole approximation is given by

$$\hat{H} = -\frac{\hbar^2}{2m}\nabla^2 + V(\mathbf{r}) - \frac{ie\hbar}{2mc}\mathbf{A}(\mathbf{r_0}, t)\cdot\nabla + \frac{e^2}{2mc^2}\mathbf{A}^2(\mathbf{r}_0, t). \tag{1.48}$$

We now perform a gauge transformation using $\chi(\mathbf{r}, t) = (-e/\hbar c)\mathbf{A}(r_0, t)$. This transforms the wave function $\Psi(\mathbf{r}, t)$ into the new form

$$\Psi(\mathbf{r}, t) = exp\left[\frac{-ie}{\hbar c}\mathbf{A}(\mathbf{r_0}, t)\right]\psi(\mathbf{r}, t). \tag{1.49}$$

The electric field $\mathbf{E}$ at $\mathbf{r_0}$ in terms of the Coulomb potential is $\mathbf{E}(\mathbf{r}_0, t) = -\frac{1}{c}\frac{\partial}{\partial t}\mathbf{A}(\mathbf{r}_0, t)$. Putting this along with Eqs. (1.49) and (1.48) into Eq. 1.39 and simplifying,

$$i\hbar\frac{\partial}{\partial t}\psi(\mathbf{r}, t) = \left\{-\frac{\hbar^2}{2m}\nabla^2 + V(\mathbf{r}) + e\mathbf{r}\cdot\mathbf{E}(\mathbf{r}_0, t)\right\}\psi(\mathbf{r}, t) \tag{1.50}$$

$$= (H_0 + H_I)\psi(\mathbf{r}, t), \tag{1.51}$$

where H_0 and H_I denotes the unperturbed and interaction parts of the Hamiltonian respectively. The simplified interaction Hamiltonian can be expressed in terms of the dipole operator $\mathbf{d} = -e\mathbf{r}$ as

$$H_I = e\mathbf{r}\cdot\mathbf{E} = -\mathbf{d}\cdot\mathbf{E}. \tag{1.52}$$

This is the form of interaction Hamiltonian being used in our study of atom-light interaction problems. One of the simplest problems involving atom-light interaction is a two-level atomic model system. In the next section, we present the basic theory and results of a two-level atom interacting with a near resonant laser field.

1.3 Density matrix formalism

There are many mathematical tools available to treat problems in nonlinear and quantum optics. We choose the density matrix formalism in treating our atomic system because the density matrix has features that make it a natural choice. For example, it permits one to ignore irrelevant parts of a problem and to focus mathematically on the dynamics of interest. Also, it can be reduced to a rate equation treatment, if desired. Density matrix is an excellent tool for problems involving light either to probe, control or alter systems. It incorporates all important phases of fields and polarizations responsible for some of the surprising phenomena encountered in optical science. It can describe dephasing, coherent control, and relaxation processes in a manner consistent with the occupation of various states of the system. Also, it

eliminates the need for detailed wavefunctions in predicting the important dynamics in new systems. This section gives the basics of density matrix formalism and gives the polarization expression in terms of density operator. This form of the polarization will be used in our microscopic treatment of atomic medium.

In quantum theory, all possible information about a physical system is contained in its state vector ψ. We define the density operator ρ as

$$\rho = \Sigma_i P_i |\psi_i\rangle\langle\psi_i|, \tag{1.53}$$

where P_i is the probability of the system to be in state ψ_i such that $\Sigma_i P_i = 1$. In the particular case when all probabilities of states P_i of the system is zero except for one, say ψ_0, the system is said to be in a pure state. Pure state density operator is defined by,

$$\rho = |\psi_0\rangle\langle\psi_0|. \tag{1.54}$$

The trace of any quantum mechanical operator $\mathbf{O}$ is defined by the expression:

$$Tr\left[\mathbf{O}\right] = \sum_i \langle i|\mathbf{O}|i\rangle \tag{1.55}$$

Some of the properties of density matrix operator are:

$$\text{(i) } Tr(\rho) = 1, \quad \text{normalization}$$

$$\text{(ii) For a pure state, } Tr(\rho^2) = 1.$$

We know that any physically relevant quantity of a quantum system can be extracted from the wave function ψ by calculating the expectation value of the corresponding operator $\mathbf{O}$,

$$\langle \mathbf{O} \rangle_{qm} = \langle\psi|\mathbf{O}|\psi\rangle. \tag{1.56}$$

For an ensemble of identical systems, we need to take an ensemble average over similarly prepared systems,$\langle\langle O\rangle_{qm}\rangle_{ensemble}$, in addition to the quantum mechanical average. This is done using density operator. Using the completeness relation $\Sigma_i |i\rangle\langle i| = 1$, it is straight forward to show that the expectation value of any operator O can be expressed as

$$\langle O \rangle = Tr(O\rho). \tag{1.57}$$

It follows from the definition of density operator that the above average is ensemble average:

$$\langle\langle O\rangle_{QM}\rangle_{ensemble} = Tr(O\rho). \tag{1.58}$$

Also, it can be easity shown that $Tr(O\rho) = Tr(\rho O)$.

1.3.1 Liouville's equation of motion for Density matrix

Taking time derivative of density operator (Eq. 1.53),

$$\dot{\rho} = \sum_i P_i(|\dot{\psi_i}\rangle\langle\psi_i| + |\psi_i\rangle\langle\dot{\psi_i}|), \tag{1.59}$$

where dot denots time derivative. Using Schrödinger equation of motion, $i\hbar|\dot{\psi}\rangle = H\psi$, the equation of motion for the density matrix can be expressed as

$$\dot{\rho} = -\frac{i}{\hbar}[H, \rho]. \tag{1.60}$$

This equation is known as Liouville or Von Neumann equation of motion for the density matrix. This equation contains both quantum as well as statistical information of the system and so is more general than Schrödinger equation. Various decay mechanisms in the system such as spontaneous emission and collisional effects can be incorporated by adding phenomenological decay terms to this equation such that Eq. 1.60 is modified into

$$\dot{\rho} = -\frac{i}{\hbar}[H, \rho] - \frac{1}{2}\{\Gamma, \rho\}, \tag{1.61}$$

where $\{\Gamma, \rho\} = \Gamma\rho + \rho\Gamma$, and the relaxation matrix Γ is given by

$$\langle n|\Gamma|m\rangle = \gamma_n\delta_{nm}, \tag{1.62}$$

where γ_n are various decay constants.
Eq. 1.61 can be expanded for a single element ρ_{ij} as

$$\dot{\rho}_{ij} = -\frac{i}{\hbar}\sum_k(H_{ik}\rho_{kj} - \rho_{ik}H_{kj}) - \frac{1}{2}\sum_k(\Gamma_{ik}\rho_{kj} + \rho_{ik}\Gamma_{kj}). \tag{1.63}$$

This formula is the key formula used in our treatment of pulse propagation in many level atomic media for calculating $\rho_{ij}(t)$ to reveal population and polarization dynamics.

Induced polarization

Coupling between the light and the atomic medium through which it propagates proceeds via polarization of the medium or atoms. The simple microscopic theory of polarization is given below. During propagation, atom interacts with an external electromagnetic field via its bound charges. The charge distribution of the atom is

distorted in this process, creating a multipole moment. In the electric-dipole approximation introduced in the previous section, this moment is dominated by the electric dipole d, neglecting all other terms of the multipole. This is because the wavelength of light is much larger than the average distance of the electron from the nucleus. The dipole is a quantity used in both classical and quantum mechanics. This provides a rather convenient link between the behaviour of the classical electric and magnetic fields, and the operator-based formalism underpinning the evolution of the atomic ensemble. Treated classically, an electric dipole is a measure of charge separation in a system of particles. A dielectric medium composed of $\mathcal{N}$ particles per unit volume has a macroscopic polarization density $\mathcal{P} = \mathcal{N}\hat{\mathbf{d}}$, where $\hat{\mathbf{d}}$ is the mean dipole moment. In quantum mechanics, the dipole operator $\hat{\mathbf{d}}$ is related to the quantum states that the particles reside in. Since Eq. 1.57 is true for any operator, we can express the induced polarization operator of the medium in this form. In the microscopical quantum level, the polarization of a medium consisting of an ensemble of atoms with number density $\mathcal{N}$ and dipole operator $\hat{\mathbf{d}}$ is defined as

$$\mathbf{P} = \mathcal{N}\langle\hat{\mathbf{d}}\rangle = \mathcal{N}Tr\{\rho\hat{\mathbf{d}}\}. \tag{1.64}$$

Once we know the density of the medium and relevant dipole moment operator, the induced polarization can be calculated from the density matrix elements using this equation. As can be seen from Eq. 1.63, the density operator contains the macroscopic field information through the interaction Hamiltonian that we derived earlier in the dipole approximation. So this gives an essential link between the microscopic and macroscopic properties of the light-matter interacting system.

1.4 Two level systems

One of the simplest problems in atom-light interaction is a two level atom coupled with a single mode of electromagnetic field. An atomic system is approximated as two level system if a driving filed of single frequency is in resonance or nearly resonance with only two levels of the atom while all other levels are highly detuned. Many essential features of atom-light coupled system can be extracted from this simple model under certain realistic approximations.

1.4.1 Rabi oscillations

Consider the incident single mode radiation of frequency ω interacting with two levels of an atomic system, upper level $|1\rangle$ and lower level $|2\rangle$. These levels are the eigen states of the unperturbed Hamiltonian H_0 of the atom with eigen values $\hbar\omega_1$ and $\hbar\omega_2$

respectively. The state of the system can be expressed as a linear combination of these

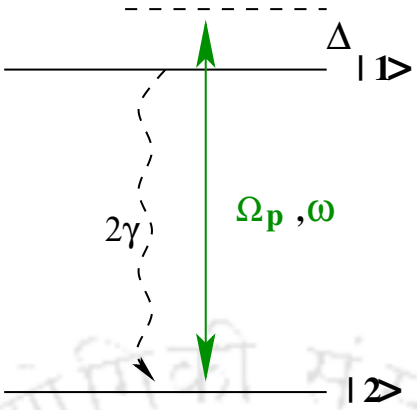

Fig. 1.1 The energy level diagram of a two-level atom. A monochromatic laser field is in nearly resonant with the transition between ground level $|2\rangle$ and excited level $|1\rangle$. ω gives the frequency of the field, Δ is detuning from resonance, Ω_p is the Rabi frequency and 2γ is the spontaneous emission rate from upper level $|1\rangle$ to $|2\rangle$.

two states:

$$\psi = c_1|1\rangle + c_2|2\rangle, \tag{1.65}$$

where c_1 and c_2 are the probability amplitudes of states $|1\rangle$ and $|2\rangle$. The corresponding density operator can be constructed from its definition:

$$\begin{aligned}\rho = |\psi\rangle\langle\psi| &= (c_1|1\rangle + c_2|2\rangle)(c_1^*\langle 1| + c_2^*\langle 2|) \\ &= |c_1|^2|1\rangle\langle 1| + |c_2|^2|2\rangle\langle 2| + c_1c_2^*|1\rangle\langle 2| + c_1^*c_2|2\rangle\langle 1|.\end{aligned} \tag{1.66}$$

From this equation, we can see that the the elements of density matrix operator are the bilinear combinations of probability amplitudes:

$$\rho_{11} \equiv |c_1|^2 \qquad \rho_{12} \equiv c_1c_2^* \qquad \rho_{21} \equiv c_2c_1^* = \rho_{12}^* \qquad \rho_{22} \equiv |c_2|^2$$

The unperturbed Hamiltonian H_0 is given by

$$\begin{aligned}H_0 &= (|1\rangle\langle 1| + |2\rangle\langle 2|)H_0(|1\rangle\langle 1| + |2\rangle\langle 2|) \\ &= \hbar\omega_1|1\rangle\langle 1| + \hbar\omega_2|2\rangle\langle 2|.\end{aligned} \tag{1.67}$$

The total Hamiltonian for the atom light coupled system is obtained by including the interaction term to this.

$$H = H_0 + H_I, \tag{1.68}$$

where H_I is the interaction Hamiltonian representing the interaction of the atom with the radiation field. In the dipole approximation, we have

$$H_I = -\, e\hat{r} \cdot \mathbf{E}(\mathbf{r}, t) \tag{1.69}$$

$$
\begin{aligned}
&= -e(|1\rangle\langle 1| + |2\rangle\langle 2|)\hat{r}(|1\rangle\langle 1| + |2\rangle\langle 2|) \cdot \mathbf{E} \\
&= -(\mathbf{d}_{12}|1\rangle\langle 2| + \mathbf{d}_{21}|2\rangle\langle 1|) \cdot \mathbf{E}.
\end{aligned}
$$

In Eq. 1.69, the electric dipole matrix element is defined by $\mathbf{d}_{12} = \mathbf{d}_{21}^* = e\langle 1|\hat{\mathbf{r}}|2\rangle$, $\hat{\mathbf{r}}$ is the position of the atom and $\mathbf{E}(\mathbf{r}, t)$ is the electric field at the atomic position. For a linearly polarized field along the z direction, $\hat{\mathbf{r}}$ replaces z. The total Hamiltonian Eq. 1.68 thus takes the form,

$$
H = \hbar\omega_{12}|1\rangle\langle 1| - (\mathbf{d}_{12} \cdot \mathbf{E}(\mathbf{r}, t)|1\rangle\langle 2| + \mathbf{d}_{21} \cdot \mathbf{E}(\mathbf{r}, t)|2\rangle\langle 1|), \tag{1.70}
$$

where we defined $\omega_{12} = \omega_1 - \omega_2$ and the ground level $|2\rangle$ is taken as zero energy level. The electric field of the incident field can be expressed as

$$
\mathbf{E}(\mathbf{r}, t) = \hat{\mathbf{e}}\mathcal{E}(\mathbf{r}, t)e^{i(\mathbf{k}.\mathbf{r}-\omega t)} + c.c., \tag{1.71}
$$

where $\mathcal{E}(\mathbf{r}, t)$ is the slowly varying envelope, $\hat{\mathbf{e}}$ the polarization unit vector, $\mathbf{k}$ wave vector and ω frequency of the field. Substituting the above form of the field in 1.70, the complete expression for the Hamiltonian is expressed as

$$
\begin{aligned}
H = \hbar\omega_{12}|1\rangle\langle 1| &- (\mathbf{d}_{12} \cdot \hat{\mathbf{e}}\mathcal{E}(\mathbf{r}, t)e^{i(\mathbf{k}.\mathbf{r}-\omega t)} + \mathbf{d}_{12} \cdot \hat{\mathbf{e}}\mathcal{E}^*(\mathbf{r}, t)e^{-i(\mathbf{k}.\mathbf{r}-\omega t)})|1\rangle\langle 2| \\
&- (\mathbf{d}_{21} \cdot \hat{\mathbf{e}}\mathcal{E}(\mathbf{r}, t)e^{i(\mathbf{k}.\mathbf{r}-\omega t)} + \mathbf{d}_{21} \cdot \hat{\mathbf{e}}\mathcal{E}^*(\mathbf{r}, t)e^{-i(\mathbf{k}.\mathbf{r}-\omega t)})|2\rangle\langle 1|.
\end{aligned} \tag{1.72}
$$

We define quantities called Rabi frequencies as

$$
\Omega_p = \frac{\mathbf{d}_{12} \cdot \hat{\mathbf{e}}\mathcal{E}(\mathbf{r}, t)}{\hbar}e^{i\mathbf{k}.\mathbf{r}} \ , \ \tilde{\Omega}_p = \frac{\mathbf{d}_{12} \cdot \hat{\mathbf{e}}\mathcal{E}^*(\mathbf{r}, t)}{\hbar}e^{-i\mathbf{k}.\mathbf{r}}. \tag{1.73}
$$

The Hamiltonian is reduced into the simplified form,

$$
H = \hbar\omega_{12}|1\rangle\langle 1| - \hbar(\Omega_p e^{-i\omega t} + \tilde{\Omega}_p e^{i\omega t})|1\rangle\langle 2| - \hbar(\Omega_p^* e^{i\omega t} + \tilde{\Omega}_p^* e^{-i\omega t})|2\rangle\langle 1|. \tag{1.74}
$$

Rotating wave approximation

Now we make a unitary transformation of the state vector :

$$
\begin{aligned}
|\psi(\mathbf{r}, t)\rangle &= \hat{U}|\phi(\mathbf{r}, t)\rangle \\
&= e^{-i\omega t|1\rangle\langle 1|}|\phi(\mathbf{r}, t)\rangle,
\end{aligned} \tag{1.75}
$$

so that the Schrödinger equation takes the new form in the transformed frame

$$
i\hbar\frac{\partial}{\partial t}|\phi(\mathbf{r}, t)\rangle = H_{eff}|\phi(\mathbf{r}, t)\rangle, \tag{1.76}
$$

where the effective Hamiltonian $H_{eff} = \hat{U}^\dagger H \hat{U} - i\hbar \hat{U}^\dagger \frac{\partial \hat{U}}{\partial t}$ can be written in the following form,

$$H_{eff} = \hbar\Delta|1\rangle\langle 1| - \hbar(\Omega_p + \tilde{\Omega}_p e^{2i\omega t})|1\rangle\langle 2| - \hbar(\Omega_p^* + \tilde{\Omega}_p{}^* e^{-2i\omega t})|2\rangle\langle 1|. \tag{1.77}$$

In this equation we can ignore the highly oscillating terms involving frequency $2\omega t$ in favour of the other terms because these averages out to zero within the time scales involved since $\tilde{\Omega}_p \ll 2\omega$. This approximation is known as "rotating wave approximation"(RWA) in optical physics. We use this approximation throughout this thesis in defining the effective Hamiltonian involved. So the effective Hamiltonian is free form explicit time dependence and is reduced into the simple form:

$$H_{eff} = \hbar\Delta|1\rangle\langle 1| - \hbar\Omega_p|1\rangle\langle 2| - \hbar\Omega_p^*|2\rangle\langle 1|. \tag{1.78}$$

Using this Hamiltonian, the Lioville's equation of motion Eq. 1.60 for the density matrix elements takes the form,

$$\dot{\rho_{11}} = i\Omega_p\rho_{21} - i\Omega_p^*\rho_{12}, \tag{1.79a}$$

$$\dot{\rho_{12}} = \dot{\rho_{21}}^* = i\Delta\rho_{12} + i\Omega_p(\rho_{22} - \rho_{11}). \tag{1.79b}$$

These equations are known as Optical Bloch equations because of its structural resemblance to the Bloch equations of magnetic spin 1/2 system [54]. The solution of these equations have the following physical meaning : The diagonal elements ρ_{ii} gives the probability of the atom being in state $|i\rangle$ while the off-diagonal elements ρ_{ij} gives the coherence between the levels $|i\rangle$ and $|j\rangle$. These coherences are related to the polarization of the atomic system. The above equations can be solved by assuming the initial condition that atoms are initially in the ground state $|2\rangle$. The following solutions are obtained:

$$\rho_{11} = \frac{4|\Omega_p|^2}{\Omega^2}\sin^2\left(\frac{\Omega t}{2}\right), \tag{1.80}$$

$$\rho_{12} = \frac{2|\Omega_p|}{\Omega^2}\sin\left(\frac{\Omega t}{2}\right)\left\{-\Delta\sin\left(\frac{\Omega t}{2}\right) + i\Omega\cos\left(\frac{\Omega t}{2}\right)\right\}, \tag{1.81}$$

where $\Omega = \sqrt{\Delta^2 + 4|\Omega_p|^2}$ is called the generalized Rabi frequency of the system. In figure Fig.1.2, the population of upper level ρ_{11} is plotted against normalized time for different values of Δ normalized with the input amplitude of the field. It is observed from the figure that in the special case of $\Delta = 0$, the population oscillates between its maximum and minimum values 0 and 1 symmetrically. These oscillations of the population is known as Rabi oscillations. The frequency of oscillation $\Omega = 2\Omega_p$ is

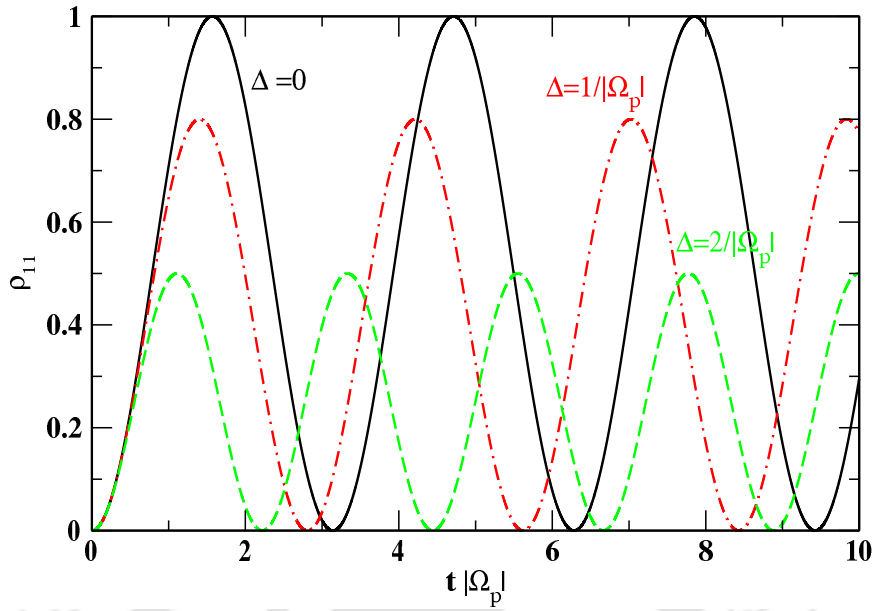

Fig. 1.2 The Rabi oscillations in two-level atomic system. The excited state population ρ_{11} as a function of normalized time for three values of field detuning.

called Rabi frequency of the system. For non-zero value of detuning, that is , the off-resonant transitions, we can see that the maximum population in the upper level is less than zero and the frequency of the oscillations increases. Ω here is the generalized Rabi frequency.

1.4.2 Optical Bloch Equations with Decay

The optical Bloch equations described above, Eqs. (1.79) are not applicable to cases where relaxation mechanisms are present. Some of the relaxation mechanisms present in an atomic gas medium are spontaneous emission from upper level to lower level, elastic collisions between atoms, inelastic collisions leading to decoherence. One advantage of describing the atomic system in terms of a density operator ρ is that the physical interpretation of its elements allows us to phenomenologically add various relaxation terms directly to its elements. In presence of these decay processes, we need to solve the full density matrix equations Eq. 1.61. The optical Bloch equations are modified in this case into

$$\dot{\rho_{11}} = -2\gamma\rho_{11} + i\Omega_p\rho_{21} - i\Omega_p^*\rho_{12}, \tag{1.82a}$$

$$\dot{\rho_{22}} = 2\gamma\rho_{11} - i\Omega_p\rho_{12} - i\Omega_p^*\rho_{12}, \tag{1.82b}$$

$$\dot{\rho_{12}} = -[\Gamma - i\Delta]\rho_{12} + i\Omega_p(\rho_{22} - \rho_{11}), \tag{1.82c}$$

$$\dot{\rho_{21}} = -[\Gamma + i\Delta]\rho_{21} - i\Omega_p(\rho_{22} - \rho_{11}). \tag{1.82d}$$

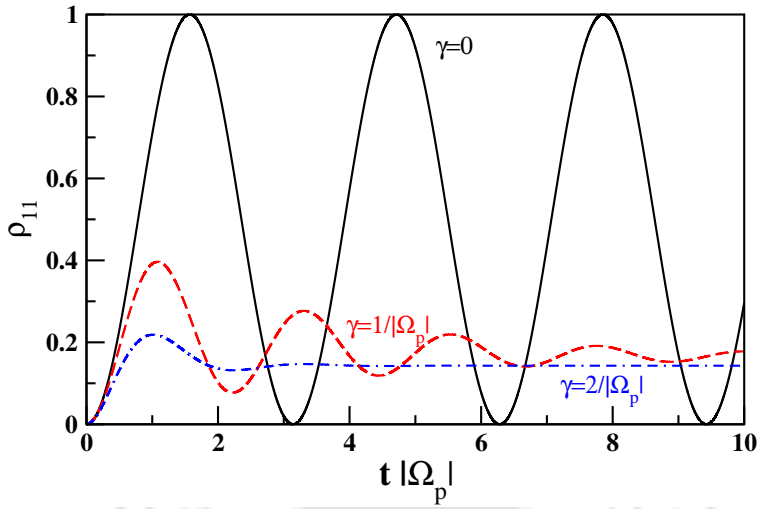

Fig. 1.3 The excited state population ρ_{11} of a two level system with decay, plotted as a function of normalized time for three values spontaneous decay rate.

where 2γ is the spontaneous radiation decay rate from the excited state $|1\rangle$ to the ground state $|2\rangle$. $\Gamma = \gamma + \gamma_{ph}$ is the dephasing rate of the coherence ρ_{12} and it is sum of radiative and collisional rates. Figure 1.3 shows the plots of population including spontaneous emission, with different values of emission rate γ. It shows that the Rabi oscillations damped out rapidly and after a certain time, the system reaches a steady state. So equations Eq. 1.82 can be solved by setting all time derivatives to zero. The solutions obtained are

$$\rho_{11} = \frac{|\Omega_p|^2}{(\gamma^2 + \Delta^2) + 2|\Omega_p|^2}, \tag{1.83}$$

$$\rho_{12} = \frac{i\Omega_p(\gamma + i\Delta)}{(\gamma^2 + \Delta^2) + 2|\Omega_p|^2}. \tag{1.84}$$

The induced polarization is obtained by using Eq. 1.64.

$$\mathbf{P} = \mathcal{N}\langle\hat{\mathbf{d}}\rangle = \mathcal{N}Tr\{\rho\hat{\mathbf{d}}\} = \mathcal{N}(d_{21}\rho_{12} + d_{12}\rho_{21}). \tag{1.85}$$

As the susceptibility is the constant of proportionality relating $\mathcal{E}$ and $\mathcal{P}$, using definition of Ω_p and the relation $\mathcal{P} = \chi\mathcal{E}$, we have for the susceptibility of the medium,

$$\chi = \frac{\mathcal{N}|d_{12}|^2}{\hbar} \frac{i(\gamma + i\Delta)}{(\gamma^2 + \Delta^2) + 2|\Omega_p|^2}. \tag{1.86}$$

Note that this expression includes both linear and nonlinear parts of the susceptibility. It is a complex function of Rabi frequency and detuning. For a weak intensity of the light field, only linear part can be retained without losing any physical information of the system. As we have seen before, the transmission of the medium is given by

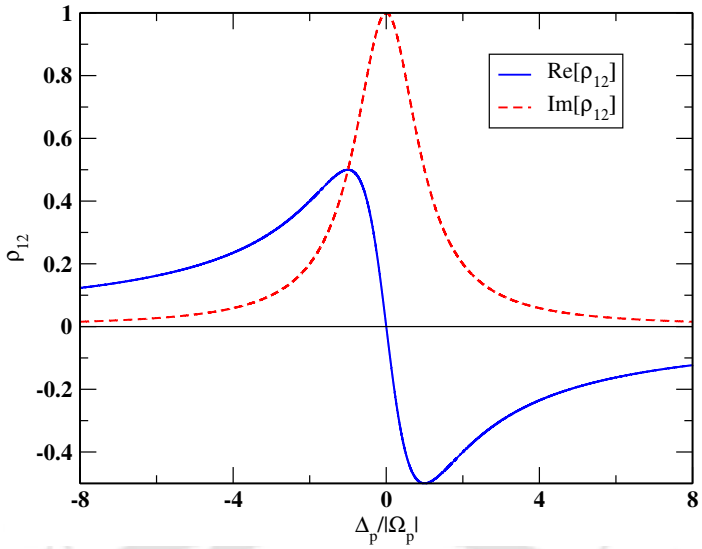

Fig. 1.4 Real and imaginary parts of the normalized susceptibility plotted as a function of normalized detuning, for a two level system. $\Omega_p = 0.01\gamma$

.

it's imaginary part and the real part gives refractive index. In Fig.1.4, the real and imaginary parts of the susceptibility are plotted against the normalized detuning (scaled frequency) of the system for a weak intensity pulse. It is clear from the large peak of the imaginary part in the figure that the light field experience very large absorption near resonance. This limits utilization of the high dispersion as observed from the plot of real part of susceptibility, because most of the light gets absorbed by the medium.

However, atomic ensembles like phaseonium [55] exhibits less absorption and high refractive index although its practical realization is limited mainly because of the high pressure requirements which leads to various broadening. To get rid of this, saturation absorption technique (SAT) is used in which an extra strong field applied takes medium into a saturation stage and protects the weak probe field [56].

Self Induced Transparency

The coherence effects associated with a pulsed electric field are more diverse than the simple Rabi flopping associated with a cw field. The simplest observable effect in a pulsed system is the oscillation of the excited state population with pulse area, described with the area theorem [10]. The area theorem shows that a pulse with area less than π will be absorbed by the resonant medium, area of the pulse with initial area lying between π and 2π eventually increses to 2π and a pulse of area 2π shows an absorption free propagation. This pattern repeats and pulses having multiples of 2π area eventually breaks up into series of 2π area pulses.

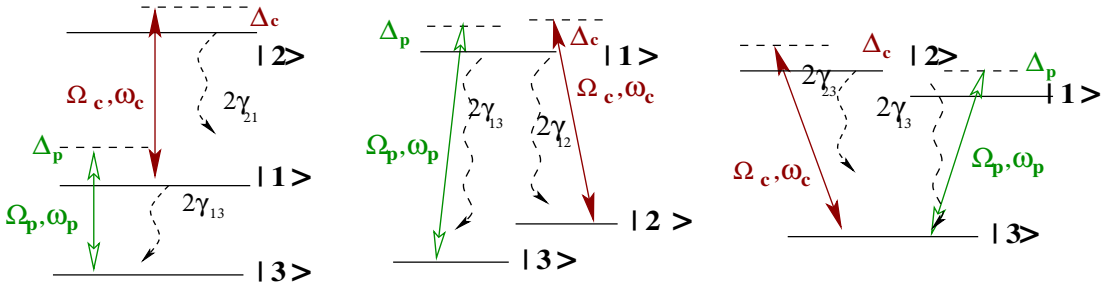

Fig. 1.5 Three configurations of a three level system with two optical fields of Rabi frequencies Ω_p and Ω_c

The ability of a 2π area pulse to travel through the medium without getting absorbed is referred to as self-induced transparency (SIT) [57, 58], where a single pulse creates transparency for itself. SIT was the first demonstration of atomic coherence at optical frequencies.

McCall and Hahn showed that only pulse envelope of *sech* shape is consistent with the area theorem as solution to the combined Maxwell-Schrödinger equations. Pulse envelopes of different shapes were shown to undergo reshaping through the coherent interaction with the medium so that the steady state pulse shape is always of *sech*. Processes that cause incoherence such as spontaneous emission and collisional broadening degrade the SIT phenomenon.

The susceptibility behavior of two-level atomic medium can be drastically modified by introducing another field called control field into the system, essentially making it a three-level configuration. This not only suppresses the high absorption, but also gives steep dispersion properties of the medium which can be utilized in many diverse areas of atom and optical physics. This will be discussed in detail in the next section.

1.5 Three level atomic system

Many aspects of atomic physics such as Rabi oscillations, radiation force used in laser cooling and atomic clocks can be described on the basis of interaction between light and matter in a two-level system. Natural generalization of two-level system is three-level system, where two laser field couples two atomic transitions. It was realised from early nineties that three-level systems can display novel features not possible in the two-level system.

In this section we analyze the three level system dynamics and the phenomenon of EIT in detail. An atomic system is called a three level system when each of the atom can be modelled as a system consisting of three energy levels. First we will introduce

the three level Λ system and following the procedure of the preceding section, get the susceptibility of the system.

Formalism

Three level systems can be modelled in three different configurations based on the energy levels chosen to represent the system. These are called ladder, V and Λ configurations, so named because of the Greek letter the energy level diagram pictorially resembles to. The three configurations are shown in figure Fig.1.5. Among the three different

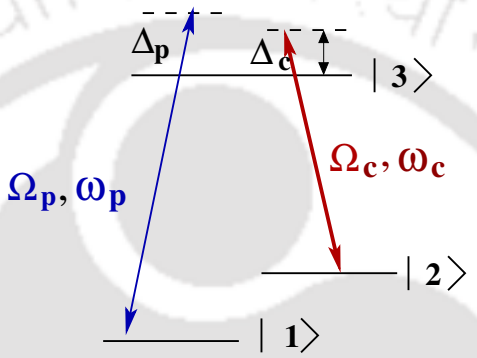

Fig. 1.6 Energy level diagram of a three level Λ system

.

level structures, we analyze the Λ system in detail in this section. The studies in this thesis is mainly based on the Λ system. The long living intermediate ground level of Λ configuration allows longer coherence between the levels, making it a preferred choice over the other two configurations.

The system under consideration is shown in figure Fig.1.6 which constitutes an upper level $|3\rangle$ and two ground levels $|1\rangle$ and $|2\rangle$ which are hyperfine levels of same ground state. A strong control field of frequency ω_c couples the levels $|2\rangle$ and $|3\rangle$. The field under study, weak probe field, connects to the levels $|1\rangle$ and $|3\rangle$. The transitions $|1\rangle \leftrightarrow |2\rangle$ and $|2\rangle \leftrightarrow |3\rangle$ are dipole allowed whereas the transition $|2\rangle \leftrightarrow |3\rangle$ is dipole forbidden. Δ_c and Δ_p represents corresponding detuning of the two fields from resonance to the transition defined by,

$$\Delta_p = \omega_p - \omega_{13}, \quad \Delta_c = \omega_c - \omega_{12}. \tag{1.87}$$

The structure of the two input fields coupling the levels are

$$\mathbf{E}_c(\mathbf{r},t) = \hat{\mathbf{e}}_c \mathcal{E}_c(t) e^{ik_c \cdot \mathbf{r} - \omega_c t} + c.c., \tag{1.88}$$

$$\mathbf{E}_p(\mathbf{r},t) = \hat{\mathbf{e}}_p \mathcal{E}_p(t) e^{ik_p \cdot \mathbf{r} - \omega_p t} + c.c., \tag{1.89}$$

where $\mathcal{E}_p(t)$ and $\mathcal{E}_c(t)$ are slowly varying amplitudes, $\hat{\mathbf{e}}_p$ and $\hat{\mathbf{e}}_c$ are the polarization unit vectors, k_p and k_c are the state vectors of the probe and control field respectively. The interaction between a three level Λ atomic system and the light filed can be expressed in terms of the Hamiltonian

$$H = H_0 + H_I, \tag{1.90}$$

where H_0 represent the unperturbed Hamiltonian of the atomic system and H_I the interaction term of the atom-light coupled system. Interaction between the atom and field is limited to the dipole interaction term as described earlier. The unperturbed part of the Hamiltonian, considering level $|1\rangle$ as zero energy level, can be expressed as

$$H_0 = \hbar\omega_{12}|2\rangle\langle 2| + \hbar\omega_{13}|3\rangle\langle 3|. \tag{1.91}$$

The dipole interaction term between the atom and the optical field is expressed as:

$$H_I = -\left[\mathbf{d}_{13}\cdot\mathbf{E}_p(\mathbf{r},t) + \mathbf{d}_{12}\cdot\mathbf{E}_c(\mathbf{r},t)\right]. \tag{1.92}$$

Now we define the Rabi frequencies of the system

$$\Omega_p = \frac{\mathbf{d}_{13}\cdot\hat{\mathbf{e}_p}\mathcal{E}_p(t)}{\hbar}e^{ik_p\cdot\mathbf{r}}, \quad \Omega_p^* = \frac{\mathbf{d}_{13}\cdot\hat{\mathbf{e}_p}\mathcal{E}_p^*(t)}{\hbar}e^{-ik_p\cdot\mathbf{r}}, \tag{1.93}$$

$$\Omega_c = \frac{\mathbf{d}_{12}\cdot\hat{\mathbf{e}_c}\mathcal{E}_c(t)}{\hbar}e^{ik_c\cdot\mathbf{r}}, \quad \Omega_c^* = \frac{\mathbf{d}_{12}\cdot\hat{\mathbf{e}_c}\mathcal{E}_c^*(t)}{\hbar}e^{-ik_c\cdot\mathbf{r}}. \tag{1.94}$$

The state vector of an atomic system is represented by $|\psi(\mathbf{r},t)\rangle$. Now we introduce the rotating frame by applying a unitary transformation to the state vector $\psi(\mathbf{r},t)$:

$$|\psi(\mathbf{r},t)\rangle = U|\phi(\mathbf{r},t)\rangle = e^{-i(\omega_p|1\rangle\langle 1| + (\omega_p-\omega_c)|2\rangle\langle 2|)t}|\phi(\mathbf{r},t)\rangle, \tag{1.95}$$

so that the Schrödinger equation can be expressed in the new frame with the effective Hamiltonian H_{eff}:

$$i\hbar\frac{\partial}{\partial t}|\phi(r,t)\rangle = H_{eff}|\phi(r,t)\rangle. \tag{1.96}$$

Following the similar procedure applied for two level systems, using the above mentioned unitary transformation, the effective Hamiltonian for this system under rotating wave approximation can be expressed as

$$H_{eff} = \hbar\Delta_p|3\rangle\langle 3| + \hbar(\Delta_p - \Delta_c)|2\rangle\langle 2| - \hbar(\Omega_p|3\rangle\langle 1| + \Omega_c|3\rangle\langle 2|) + h.c.. \tag{1.97}$$

In this equation for effective Hamiltonian, we have ignored the counter rotating terms in favour of the co-rotating terms.
The system dynamics is governed by the Liouville's equation of motion for the density matrix,

$$\partial_t \rho = -\frac{i}{\hbar}\left[\mathscr{H}_{eff}, \rho\right] + \mathcal{L}_\gamma[\rho], \tag{1.98}$$

where the relaxation matrix is given by

$$\begin{aligned}\mathcal{L}_\gamma[\rho] = &-\frac{\gamma_2}{2}\left(|3\rangle\langle 3|\rho - 2|2\rangle\langle 2|\rho_{33} + \rho|3\rangle\langle 3|\right)\\ &-\frac{\gamma_1}{2}\left(|3\rangle\langle 3|\rho - 2|1\rangle\langle 1|\rho_{33} + \rho|3\rangle\langle 3|\right)\ .\end{aligned} \tag{1.99}$$

In Eq. 1.99, decay constants $\gamma_{1(2)}$ represents spontaneous emission from upper state to state $|1(2)\rangle$. With the Hamiltonian Eq. 1.97, the density matrix equations of motion of populations and atomic coherences are written as:

$$\dot{\rho}_{33} = -(\gamma_1+\gamma_1)\rho_{33} + i\Omega_c\rho_{23} - i\Omega_c^*\rho_{32} + i\Omega_p\rho_{13} - i\Omega_p^*\rho_{31}, \tag{1.100a}$$
$$\dot{\rho}_{32} = -\Gamma_{32}\rho_{32} - i\Omega_c(\rho_{33}-\rho_{22}) + i\Omega_p\rho_{12}, \tag{1.100b}$$
$$\dot{\rho}_{31} = -\Gamma_{31}\rho_{31} - i\Omega_p(\rho_{33}-\rho_{11}) + i\Omega_c\rho_{21}, \tag{1.100c}$$
$$\dot{\rho}_{22} = \gamma_2\rho_{33} - i\Omega_c\rho_{23} + i\Omega_c^*\rho_{32}, \tag{1.100d}$$
$$\dot{\rho}_{21} = -\Gamma_{21}\rho_{21} - i\Omega_p\rho_{23} + i\Omega_c^*\rho_{31}, \tag{1.100e}$$
$$\dot{\rho}_{11} = \gamma_1\rho_{33} - i\Omega_p\rho_{13} + i\Omega_p^*\rho_{31}. \tag{1.100f}$$

In Eq. 1.100, we define the quantities,

$$\Gamma_{31} = (\gamma_1+\gamma_2) + i\Delta_p, \quad \Gamma_{32} = (\gamma_1+\gamma_2) + i\Delta_c, \quad \Gamma_{21} = \Gamma - i(\Delta_p - \Delta_c). \tag{1.101}$$

Decoherence of the ground level coherence ρ_{12} is given by Γ. The total population conservation $\rho_{11}+\rho_{22}+\rho_{33}=0$ is assumed in this system. Also, $\rho_{ij} = \rho_{ji}^*$ from the definition of density matrix. For simplicity in calculations, we asssume $\gamma_1 = \gamma_2 = \gamma$.

Steady state analysis of density matrix

The induced polarization of the medium of number density $\mathcal{N}$ for the probe field acts as the source term in Maxwell's propagation equation. The total polarization is calculated as usual,

$$\mathbf{P} = \mathcal{N}\langle\hat{\mathbf{d}}\rangle = \mathcal{N}Tr\{\rho\hat{\mathbf{d}}\} = \mathcal{N}(d_{31}\rho_{13} + d_{13}\rho_{31} + d_{32}\rho_{23} + d_{23}\rho_{32}). \tag{1.102}$$

We are interested in the optical susceptibility $\chi(\omega_p)$ at the probe frequency as given by,

$$P = \chi(\omega_p)E(\omega_p). \tag{1.103}$$

To calculate the absorption and dispersion co-efiiceients of the probe field with frequency ω_p in the $|3\rangle - |1\rangle$ transition, we derive a steady-state solution for ρ_{31}. Since the probe field intensity is small compared to that of control field, we can employ pertubative solution to the equation Eq. 1.100. The polarization is expanded as a power series in Ω_p. In the steady state limit we can take $\rho_{11} \approx 1$ since all population settles into ground state. The linear part of the susceptibility $\chi^{(1)}(\omega_p)$ obtained is given by the expression:

$$\chi^{(1)}(\omega_p) = \frac{\mathcal{N}|d_{13}|^2}{\hbar} \frac{i\left[\Gamma - i(\Delta_p - \Delta_c)\right]}{(2\gamma - i\Delta_p)\left[\Gamma - i(\Delta_p - \Delta_c)\right] + |\Omega_c|^2}. \tag{1.104}$$

This equation reduces to the two-level susceptibility when $\Omega_c = 0$. In Fig.1.7, the

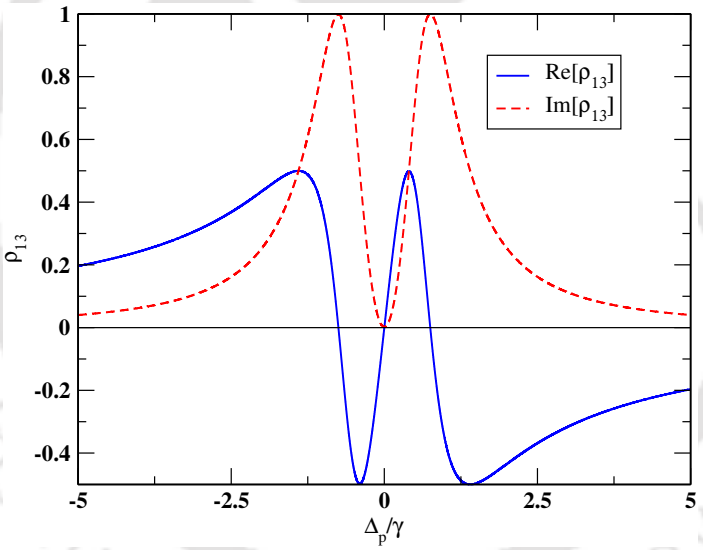

Fig. 1.7 Real and imaginary parts of the normalized susceptibility plotted as a function of normalized detuning, of a Λ system. $\Omega_p = 0.01\gamma$, $\Omega_c = 0.75\gamma$.

real and imaginary parts of the linear susceptibility in the presence of strong control field is plotted as a function of normalized detuning Δ_p/γ. The imaginary part of the susceptibility plot in Fig.1.7 shows the vanishing of expected absorption of the probe field at the line center. This means that in the presence of a strong control field, the coherently driven medium becomes transparent to the weak probe field. This phenomenon is referred to as "*Electromagnetically induced transparency*", a term first used by S. E. Harris [14]. The plot of real part of susceptibility shows a steep normal dispersion, in contrast to the anomalous dispersion in two-level case, in the region of transparency. This leads to ultra slow velocities, this point will be explained below.

The steepness of dispersion curve can further be controlled by lowering the control field strength and increasing the probe field strength. For example, at $\Omega_c = \gamma \approx \Omega_p$, a much narrower transparency window than the case of strong control field can be obtained. The EIT is also accompanied by larger nonlinearities.
The vanishing of absorption at the line center can be understood by using the quantum interference theory. It is well known that the transition amplitudes of atomic states coupled via several possible alternative transition processes, interfere either constructively or destructively to give the total transition probability [59]. In our case, the atom from ground state $|1\rangle$ can excite to the upper state $|3\rangle$, that is, can be absorbed in two ways. In addition to the direct path $|1\rangle \rightarrow |3\rangle$, the strong control field creates a new path for the atom to reach the upper state, via $|1\rangle \rightarrow |3\rangle \rightarrow |2\rangle \rightarrow |3\rangle$. When the two-photon detuning is zero, a destructive interference between these two probability amplitudes occurs. This permits the propagation of a weak probe pulse through an otherwise opaque atomic medium. Thus, it is the interference between alternative excitation pathways between atomic states that lead to the effect of electromagnetically induced transparency.

1.5.1 Dressed state analysis of three level system

Another way of explaining electromagnetically induced transparency applies the notion of dressed states. Dressed states are the eigen states of the coupled atom-field system. The effective Hamiltonian Eq. 1.97 in the rotating frame can be written in matrix form taking the bare states $|1\rangle$, $|2\rangle$ and $|3\rangle$ as basis:

$$H_{eff} = -\hbar \begin{pmatrix} 0 & 0 & \Omega_p^* \\ 0 & -(\Delta_p - \Delta_c) & \Omega_c^* \\ \Omega_p & \Omega_c & -\Delta_p \end{pmatrix}$$

Eigen states and eigen values of this matrix is found in the usual way. For the case of two photon resonance, $\Delta = \Delta_p - \Delta_c = 0$, the eigen vectors are expressed as:

$$|a^0\rangle = \cos\theta|1\rangle - \sin\theta|2\rangle, \tag{1.105}$$

$$|a^+\rangle = \sin\theta\sin\phi|1\rangle + \cos\theta\sin\phi|2\rangle + \cos\phi|3\rangle, \tag{1.106}$$

$$|a^-\rangle = \sin\theta\cos\phi|1\rangle + \cos\theta\cos\phi|2\rangle - \sin\phi|3\rangle. \tag{1.107}$$

In these equations, the quantities θ and ϕ are defined by the relations,

$$\tan\theta = \frac{\Omega_p}{\Omega_c}, \quad \tan 2\phi = \frac{2\sqrt{|\Omega_p|^2 + |\Omega_c|^2}}{\Delta_p}. \tag{1.108}$$

These eigen states are a coherent superposition of the bare states and are referred to as dressed states. Corresponding eigen values are obtained to be,

$$\lambda_0 = 0, \tag{1.109}$$

$$\lambda_+ = \frac{\hbar}{2}\left[\Delta_p + \sqrt{\Delta_p^2 + 4(|\Omega_p|^2 + |\Omega_c|^2)}\right], \tag{1.110}$$

$$\lambda_- = \frac{\hbar}{2}\left[\Delta_p - \sqrt{\Delta_p^2 + 4(|\Omega_p|^2 + |\Omega_c|^2)}\right]. \tag{1.111}$$

Note that the eigen value of the superposition state $|a^0\rangle$ is zero. This state is a linear combination of the two ground states $|2\rangle$ and $|1\rangle$ and does not involve the excited state $|3\rangle$. The zero energy corresponding to this level means there is no coupling to the laser field with this level. This level is known as *dark state*. If the systems is prepared in this state, the population cannot be excited to the upper level and the population remains trapped between the two ground states. This phenomenon is known as " *Coherent Population Trapping*". It is first observed by Alzetta *et.al.* [13] as decrease in fluorescence emission of sodium in three level Λ configuration. The phenomenon appeared as a dark line inside bright fluorescent cell, hence the name dark resonance is associated with it. In the usual CPT scheme, both coupling field strengths are of comparable magnitude, $\Omega_p \approx \Omega_c$. So interference effects arise from both the fields. Now we consider the special case when the probe field is much weaker than the control field, i.e, $\Omega_p \ll \Omega_c$. In this case, only interference effects due to processes driven by Ω_c will be important. This is the situation in EIT schemes. The dressed states of this case is given as

$$|a^0\rangle = |1\rangle, \tag{1.112}$$

$$|a^+\rangle = \frac{1}{\sqrt{2}}(|3\rangle + |2\rangle), \tag{1.113}$$

$$|a^-\rangle = \frac{1}{\sqrt{2}}(|3\rangle - |2\rangle). \tag{1.114}$$

It is clear that state $|a^0\rangle$, which is ground state $|1\rangle$, is identical to the dark state here. The weak probe field does not couple to the excited state $|3\rangle$ from this level, whereas strong control field creates superposition of state $|2\rangle$ and $|3\rangle$. Two absorption peaks are formed at $\Delta_p = \pm\Omega_c$ due to transition to dressed states. The EIT effect in terms of dressed states can be explained as follows. The total probability of excitation of population to the upper level is a linear combination of the probabilities to the dressed states $|a^\pm\rangle$. These probabilities destructively interfere to give total probability of excitation from ground state to excited state zero. This is illustrated in Fig.1.8.

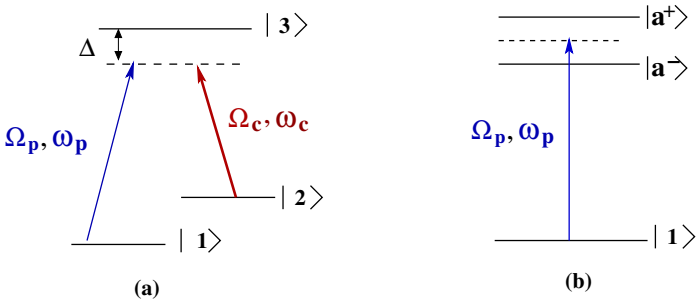

Fig. 1.8 (a) EIT scheme in bare states. (b) The dressed states. Destructive interference between the probe absorption amplitudes due to these two dressed states leads to EIT.

EIT in Doppler averaged media

The optical frequency as seen by a moving atom is different from the frequency of the laser beam because of the Doppler effect. In thermal vapor, the atoms are usually in constant motion and have a Maxwellian velocity distribution. This results in an inhomogeneous line-broadening, which is termed as Doppler broadening. For an atom moving along the z direction with velocity v, the Doppler shift in frequency is given by

$$\omega' \simeq \omega \left(1 + \frac{v}{c}\right). \tag{1.115}$$

Thus the shift in detuning becomes,

$$\Delta_{doppler} = kv, \tag{1.116}$$

where $k = \omega/c$, the propagation constant. Doppler broadening plays a crucial role to control the width of the absorption or gain window of the thermal media. The spectral features of the window become narrower in a Doppler broadened medium as compared with the homogeneous medium [60, 61].

1.5.2 Pulse propagation in EIT media

The discussions so far considers EIT with monochromatic fields. Since our studies are coherent control of pulse propagation, a brief discussion of pulse propagation though EIT media is given here. The action of the EIT medium on the light pulses is quite substantial, and a number of interesting new propagation phenomena are observed. These effects are very important for a variety of applications.

Slow light

Form the Taylor series expansion of susceptibility $\chi(\omega)$ of the medium and substituting the resulting polarization expression into the Maxwell propagation equation, retaining

terms upto first order, we can identify the group velocity of a pulse as :

$$v_g \equiv Re\left[\frac{d\omega}{dk}\right] = Re\left[\frac{c}{1+2\pi\chi(\omega_0)+2\pi\omega_0\frac{d\chi}{d\omega}|_{\omega_0}}\right], \tag{1.117}$$

provided $Im\left[\chi(\omega_0)\right]$ is vanishingly small or zero. The refractive index of the medium given by $n(\omega) = \sqrt{1+4\pi Re[\chi^{(1)}(\omega)]}$ can be approximated by $n(\omega) \approx 1+2\pi Re[\chi^{(1)}(\omega)]$, since $\chi(\omega) \ll 1$. So the group velocity expression can be conveniently written as

$$v_g \equiv Re\left[\frac{d\omega}{dk}\right] = Re\left[\frac{c}{n+\omega_0\frac{dn}{d\omega}}\right] = Re\left[\frac{c}{n_g}\right]. \tag{1.118}$$

The quantity $n_g = n + \omega_0\frac{dn}{d\omega}$ is the group index. For normal dispersive medium, $dn/d\omega > 0$. It leads to light propagating through the medium with subluminal velocity, that is, group velocity slower in the medium than in vacuum. For the case of anomalous dispersion, $dn/d\omega > 0$, which implies that $n + dn/d\omega < 1$. This results in light pulse propagation at a superluminal velocity, group velocity faster than in vacuum. When $v_g = \infty$, the condition $n + dn/d\omega = 0$ is satisfied. In this rare situation, the response of the medium to the applied field is local. This indicates that by manipulating the refractive index of the medium, the velocity of propagation of a light pulse can be controlled [62]. In the EIT medium, the high positive value of $dn/d\omega$, from steep normal dispersion at the resonance, allows for ultra-slow group velocities within the transparency region. This lossless slowdown of a light pulse in a medium is associated with a number of important effects. For example, the pulse becomes spatially compressed in the propagation direction, which can lead to photons or electromagnetic energy be temporarily stored in the combined system of atoms and coupling field [40].

Stimulated Raman transitions

In a Raman transition, two atomic levels are coupled by absorption of a photon from one laser beam (pump beam) and by stimulated emission of another photon into the other beam (Stokes beam). The Λ configuration shown in Fig.1.6 can be used to explain this, with $\Delta_p = \Delta_c = \Delta$, Raman detuning. The pump beam couples levels $|1\rangle$ and $|3\rangle$, while the Stokes beam couples levels $|2\rangle$ and $|3\rangle$. As a result the levels $|1\rangle$ and $|2\rangle$ become coherently coupled by the Raman beams. The condition $\Delta \gg \Gamma$, Γ being the linewidth is to be satisfied by the system to avoid spontaneous emission from the excited state and prevent resonant excitation to it. Both Raman beams are characterized by the Rabi frequency Ω_i. If the optical frequencies of the Raman beams

are ω_p and ω_s, respectively, the Raman detuning δ is defined as $\delta = \omega_p - \omega_c - \omega_{12}$, the detuning from the two-photon resonance. It is shown experimentally by Harada *et. al* that stimulated Raman scattering can disrupt EIT, where the incident probe beam is depleted and new fields are generated via Raman processes [63].

Chapter 2

Pulse-splitting in light propagation through N-type atomic media

2.1 Introduction

It is known that EIT can be used to enhance the nonlinear susceptibility [38–42]. However, conventional EIT schemes are limited in their enhancement of nonlinear effects due to the presence of considerable absorption [64]. Multilevel EIT-related atomic systems are a possible route to circumvent these limitations. In this spirit, Schmidt and Imamŏglu proposed a four-level N-configuration system in which the standard EIT level scheme is augmented by an additional off-resonantly-driven transition for the enhancement of the Kerr-nonlinearity [48]. This Kerr-nonlinearity was experimentally observed in [65] and has many interesting applications. For example, the N-type level system has been shown to exhibit cross-Kerr interactions [66] as well as the phenomena of optical bistability [67] and optical switching [68] in cavity systems and hollow-core optical fibres [69]. On the quantum level, the N-level system gives rise to nonlinear optical interactions that can be conservative [70] or dissipative [71]. These two-particle interactions were employed for the realization of strongly correlated polariton systems [72–74].

From a practical point of view, it is important to measure the effect of the Kerr-nonlinearity on the probe field. An obvious and common way of probing an optical system is by studying its response to an optical pulse. In particular, the polariton systems in [72–74] involve a sequence where an input pulse is stored, processed and then released for readout. An evident question is thus how the Kerr-nonlinearity in the N-level system modifies the propagation of a weak, classical probe pulse. However, up to now this problem has not received much attention [75].

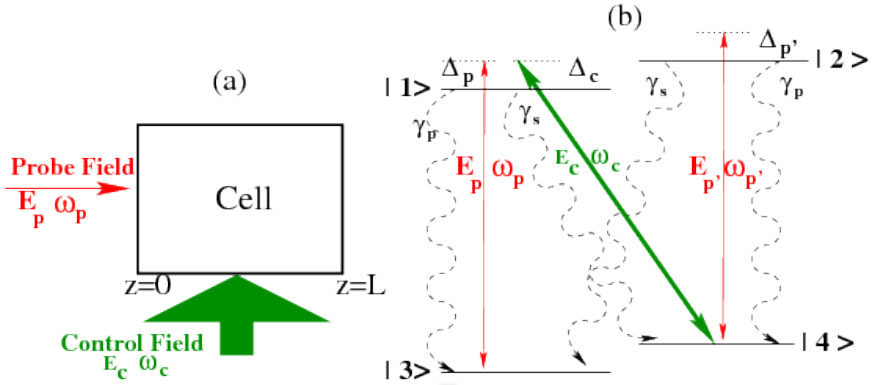

Fig. 2.1 (a) A block diagram of the system of interest. We assume that the control field intensity is constant along the propagation direction. (b) Schematic representation of four-level atoms in N-type configuration. We consider two $J = 1/2$ Zeeman manifolds with excited states $|1\rangle = |m_e = -1/2\rangle$ and $|2\rangle = |m_e = 1/2\rangle$ and ground states $|3\rangle = |m_g = -1/2\rangle$ and $|4\rangle = |m_g = 1/2\rangle$. The σ^--polarized control field $\boldsymbol{E}_c$ couples to the transition $|1\rangle \leftrightarrow |4\rangle$, and the π-polarized probe field $\boldsymbol{E}_p$ interacts with the $|1\rangle \rightarrow |3\rangle$ and $|2\rangle \rightarrow |4\rangle$ transitions.

Motivated by this, in this work, we investigate the pulse propagation through a coherent medium in N-type configuration, see Fig. 2.1. We solve the Maxwell-Bloch equations governing the propagation dynamics numerically and consider resonant driving of the Raman transition within the Λ sub-system. As a first result, we find that a weak probe may propagate through the medium with low absorption and pulse shape distortion, provided that the Kerr detuning of the probe field is sufficiently large. However, at stronger probe pulse intensities, the numerical simulations predict a splitting of the initially Gaussian pulse into sub-pulses, which subsequently propagate through the medium without further splittings. To interpret these results, we derive a simple analytical model for nonlinear pulse propagation through the N-type medium. From this model, we conclude that the pulse splitting is a direct manifestation of the self-phase modulation associated with the Kerr nonlinearity in the presence of group velocity dispersion. The group velocity dispersion can be adjusted via the detuning of the probe and control fields with respect to the excited state of the Λ sub-system. Measuring the temporal pulse shape of the probe pulse at the output thus indicates the strength of the Kerr nonlinearity experienced inside the medium. A similar pulse splitting phenomenon should be observable in other systems with EIT-enhanced nonlinearities giving rise to self-phase modulation effects. For example, EIT in Rydberg systems [76] can give rise to giant photon non-linearities mediated by the interaction between the Rydberg atoms [77–79].

2.2 Theoretical model

We consider a homogeneous atomic medium interacting with two laser fields as shown in Fig. 2.1(a). The weak probe and the strong control fields propagate in perpendicular directions. The atomic four-level system in N-type configuration is depicted in Fig. 2.1(b). In the following, we assume that this level scheme is realized with two $J = 1/2$ Zeeman manifolds via polarization selection. The weak probe field with central frequency ω_p couples to the π-transitions $[|1\rangle \leftrightarrow |3\rangle$ and $|2\rangle \leftrightarrow |4\rangle]$ and is defined as

$$\boldsymbol{E}_p(t) = \boldsymbol{e}_\pi \mathcal{E}_p e^{i(k_p x - \omega_p t)} + \text{c.c.}, \tag{2.1}$$

where $\boldsymbol{e}_\pi$ is the polarization unit vector, $k_p = \omega_p/c$ and c is the speed of light. The strong σ^--polarized control field with frequency ω_c couples to the $|1\rangle \leftrightarrow |4\rangle$ transition and can be written as

$$\boldsymbol{E}_c(t) = \boldsymbol{e}_{\sigma^-} \mathcal{E}_c e^{i(k_c z - \omega_c t)} + \text{c.c.}, \tag{2.2}$$

where $k_c = \omega_c/c$. In electric-dipole and rotating-wave approximation, the semiclassical Hamiltonian of the system is

$$\begin{aligned} H_{\text{int}} &= -\hbar(\Delta_p - \Delta_c)|4\rangle\langle 4| - \hbar\Delta_p|1\rangle\langle 1| \\ &- \hbar(\Delta_p + \Delta_{P'} - \Delta_c)|2\rangle\langle 2| \\ &- [(|2\rangle\langle 4| - |1\rangle\langle 3|)\Omega_p + |1\rangle\langle 4|\Omega_c + \text{H.c.}] \,. \end{aligned} \tag{2.3}$$

The Rabi frequencies of the probe and control fields in Eq. (2.3) are defined as

$$\Omega_p = \frac{\boldsymbol{d}_{24} \cdot \boldsymbol{e}_\pi}{\hbar} \mathcal{E}_p \,, \tag{2.4a}$$

$$\Omega_c = \frac{\boldsymbol{d}_{14} \cdot \boldsymbol{e}_{\sigma^-}}{\hbar} \mathcal{E}_c \,, \tag{2.4b}$$

where $\boldsymbol{d}_{ij}$ is the electric dipole moment for the transition between levels $|i\rangle$ and $|j\rangle$. Note that $\boldsymbol{d}_{24} = -\boldsymbol{d}_{13}$ according to the Clebsch-Gordan coefficients of the considered $J = 1/2 \leftrightarrow J = 1/2$ level scheme. The detunings of probe and control fields are given by

$$\Delta_p = \omega_p - \omega_{13} \,, \tag{2.5a}$$

$$\Delta_{P'} = \omega_p - \omega_{24} \,, \tag{2.5b}$$

$$\Delta_c = \omega_c - \omega_{14} \,. \tag{2.5c}$$

We model the quantum dynamics of the atoms using the master equation approach. The matrix elements of the atomic density operator ρ obey the following equations,

$$\begin{aligned}
\dot{\rho}_{11} &= -(\gamma_p+\gamma_s)\rho_{11} - i\Omega_p\rho_{31} + i\Omega_p^*\rho_{13} \\
&\quad + i\Omega_c\rho_{41} - i\Omega_c^*\rho_{14}\ , && \text{(2.6a)}\\
\dot{\rho}_{12} &= -[\gamma_p+\gamma_s - i(\Delta_c-\Delta_{P'})]\rho_{12} + i\Omega_c\rho_{42} \\
&\quad - i\Omega_p\rho_{32} - i\Omega_p^*\rho_{14}, && \text{(2.6b)}\\
\dot{\rho}_{13} &= -[(\gamma_p+\gamma_s)/2 - i\Delta_p]\rho_{13} + i\Omega_c\rho_{43} \\
&\quad - i\Omega_p(\rho_{33}-\rho_{11}), && \text{(2.6c)}\\
\dot{\rho}_{14} &= -[(\gamma_p+\gamma_s)/2 - i\Delta_c]\rho_{14} - i\Omega_p(\rho_{34}+\rho_{12}) \\
&\quad + i\Omega_c(\rho_{44}-\rho_{11}), && \text{(2.6d)}\\
\dot{\rho}_{22} &= -(\gamma_p+\gamma_s)\rho_{22} + i\Omega_p\rho_{42} - i\Omega_p^*\rho_{24}\ , && \text{(2.6e)}\\
\dot{\rho}_{23} &= -\left[(\gamma_p+\gamma_s)/2 + i(\Delta_c-(\Delta_p+\Delta_{P'}))\right]\rho_{23} \\
&\quad + i\Omega_p\rho_{43} + i\Omega_p\rho_{21}\ , && \text{(2.6f)}\\
\dot{\rho}_{24} &= -\left[(\gamma_p+\gamma_s)/2 - i\Delta_{P'}\right]\rho_{24} + i\Omega_p(\rho_{44}-\rho_{22}) \\
&\quad - i\Omega_c\rho_{21}\ , && \text{(2.6g)}\\
\dot{\rho}_{33} &= \gamma_p\rho_{11} + \gamma_s\rho_{22} - i\Omega_p^*\rho_{13} + i\Omega_p\rho_{31}\ , && \text{(2.6h)}\\
\dot{\rho}_{34} &= \left[\Gamma + i(\Delta_p-\Delta_c)\right]\rho_{34} - i\Omega_p^*\rho_{14} \\
&\quad - i\Omega_p\rho_{32} - i\Omega_c\rho_{31}, && \text{(2.6i)}
\end{aligned}$$

where γ_p [γ_s] is the decay rate of the π [σ] transition. These decay constants are related through the Clebsch-Gordan coefficients of the level scheme and obey $\gamma_s = 2\gamma_p = 2\gamma/3$, where γ is the total decay rate of each excited state. The decay rate of the ground state coherence is denoted by Γ. The medium polarization induced by the probe field can be expressed in terms of the off-diagonal density matrix elements ρ_{13} and ρ_{24} as

$$\boldsymbol{P} = \mathcal{N}(\boldsymbol{d}_{31}\rho_{13} + \boldsymbol{d}_{42}\rho_{24})\,, \tag{2.7}$$

where $\mathcal{N}$ is the number density of the medium. The spatio-temporal evolution of the probe pulse through the medium is governed by Maxwell's equations. In the slowly varying envelope approximation, we find

$$\left(\frac{\partial}{\partial x} + \frac{1}{c}\frac{\partial}{\partial t}\right)\Omega_p = i\eta\,(\rho_{24}-\rho_{13})\ , \tag{2.8}$$

where

$$\eta = \gamma \frac{\mathcal{N}\lambda^2}{8\pi} \tag{2.9}$$

is the coupling constant and λ is the wavelength of the transition $|1\rangle \leftrightarrow |3\rangle$. In order to facilitate the numerical integration of the coupled Maxwell-Bloch equations in Eqs. (2.6) and (2.8), we introduce a co-moving coordinate system

$$\tau = t - \frac{x}{c}, \qquad \zeta = x. \tag{2.10}$$

This change of coordinates reduces the partial differential equation in Eq. (2.8) to an ordinary differential equation with respect to the independent variable ζ,

$$\frac{\partial \Omega_p}{\partial \zeta} = i\eta \left(\rho_{24} - \rho_{13}\right). \tag{2.11}$$

Typical parameter values are $\mathcal{N} = 5\times10^{11}\text{atoms/cm}^3$, $\lambda = 780$ nm, and $\gamma = 2\pi\times10^6$ Hz. Throughout this work, we assume that the depletion of the strong control field throughout its propagation can be neglected such that its intensity is independent of position. We further choose values of Δ_p and Δ_c compatible with the resonant Raman condition $\Delta_p = \Delta_c$, and hence we define

$$\Delta = \Delta_p = \Delta_c\,. \tag{2.12}$$

2.3 Numerical Analysis

We start our discussion with a numerical analysis of the probe field propagation through the atomic four-level medium. To this end, we assume that the shape of the input pulse at the medium boundary at $\zeta = 0$ is given by

$$\Omega_p(\zeta = 0, \tau) = \Omega_p^0 e^{-\frac{(\tau-\tau_0)^2}{2\sigma_p^2}}, \tag{2.13}$$

where Ω_p^0 and σ_p are the amplitude and temporal width of the Gaussian pulse, respectively. Furthermore, all atoms are assumed to be in the ground state $|3\rangle$ initially.
Our choice of parameters is guided by the following considerations. For suitable parameters, the N-type level scheme gives rise to self-phase modulation (SPM) due to the optical Kerr effect [48, 71]. As a consequence, the probe field experiences an intensity-dependent refractive index and thus acquires a time-dependent phase shift in accordance with its temporal intensity profile. This time-varying phase can be interpreted as a transient frequency shift. Furthermore, if the intensity of the probe

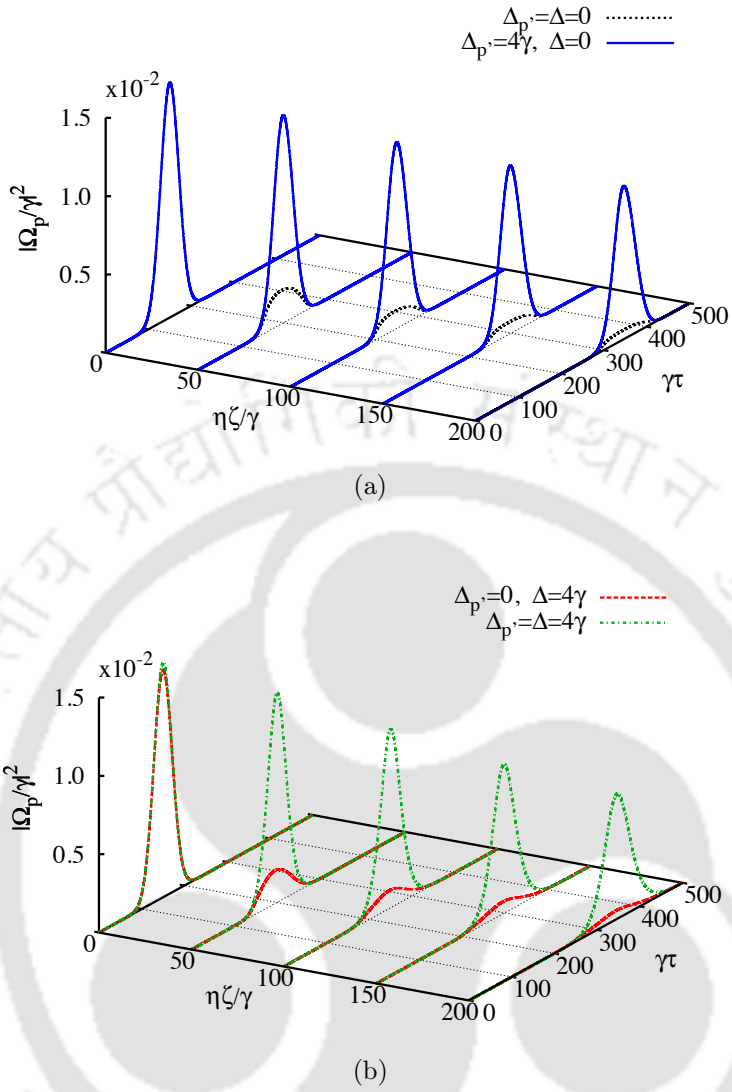

Fig. 2.2 Intensity $|\Omega_p/\gamma|^2$ of a weak probe pulse as a function of position and time for different detuning conditions. The parameters in (a) and (b) are $\Omega_c = \gamma$, $\Omega_p = \sqrt{0.015}\gamma$, $\sigma_p = 30/\gamma$, and $\Gamma = 0$.

pulse is sufficiently large, the SPM gives rise to characteristic modification of its Fourier spectrum. For example, an initially Gaussian Fourier spectrum typically break up into several peaks in the Fourier domain [80].

2.3.1 Weak probe pulses

In a first step we focus on weak probe pulses such that the effect of SPM is negligible. To this end, we evaluate the Fourier spectra inside the medium and verify that typical manifestations of SPM are absent. In this parameter regime the remaining system parameters governing the probe pulse propagation are given by Δ and Δ_c. In the following we discuss four different detuning conditions in order to systematically

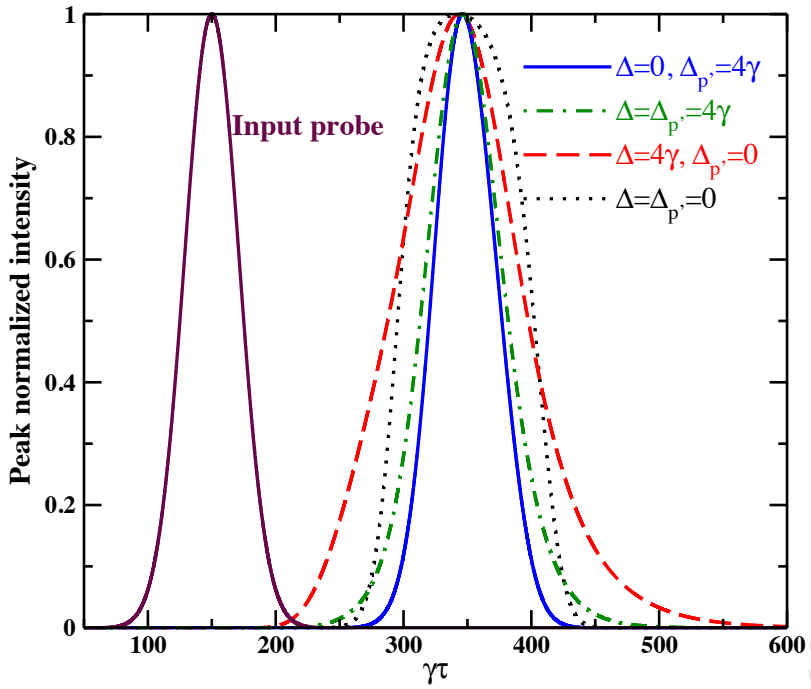

Fig. 2.3 Probe pulse intensities at the medium exit at $\eta\zeta/\gamma = 200$. Parameters are as in Fig. 2.2. To facilitate the analysis of the pulse widths, all pulses are shown normalized to their respective peak values.

investigate the influence of the Raman detuning Δ and Kerr detuning $\Delta_{P'}$. For this, we evaluate all four combinations of Δ and $\Delta_{P'}$ being either 0 or 4γ:

$$
\begin{aligned}
&(i) && \Delta = 0 && \text{and} \quad \Delta_{P'} = 4\gamma\,, \\
&(ii) && \Delta = 4\gamma && \text{and} \quad \Delta_{P'} = 4\gamma\,, \\
&(iii) && \Delta = 0 && \text{and} \quad \Delta_{P'} = 0\,, \\
&(iv) && \Delta = 4\gamma && \text{and} \quad \Delta_{P'} = 0\,.
\end{aligned}
$$

The resulting pulse propagation dynamics is shown in Fig. 2.2. It can be seen that $\Delta_{P'}$ crucially affects the absorption. The two cases with $\Delta_{P'} = 0$ lead to a transmission of less than 10% of the probe pulse intensity through the medium. In contrast, the cases $\Delta_{P'} = 4\gamma$ give rise to approximately 75% probe intensity transmission. This behavior can be traced back to the absorption on the $|4\rangle \leftrightarrow |2\rangle$ transition. Figure 2.3 shows the effect of Δ, which affects the shape and width of the transmitted pulse, whereas its effect on the transmitted intensity is small.

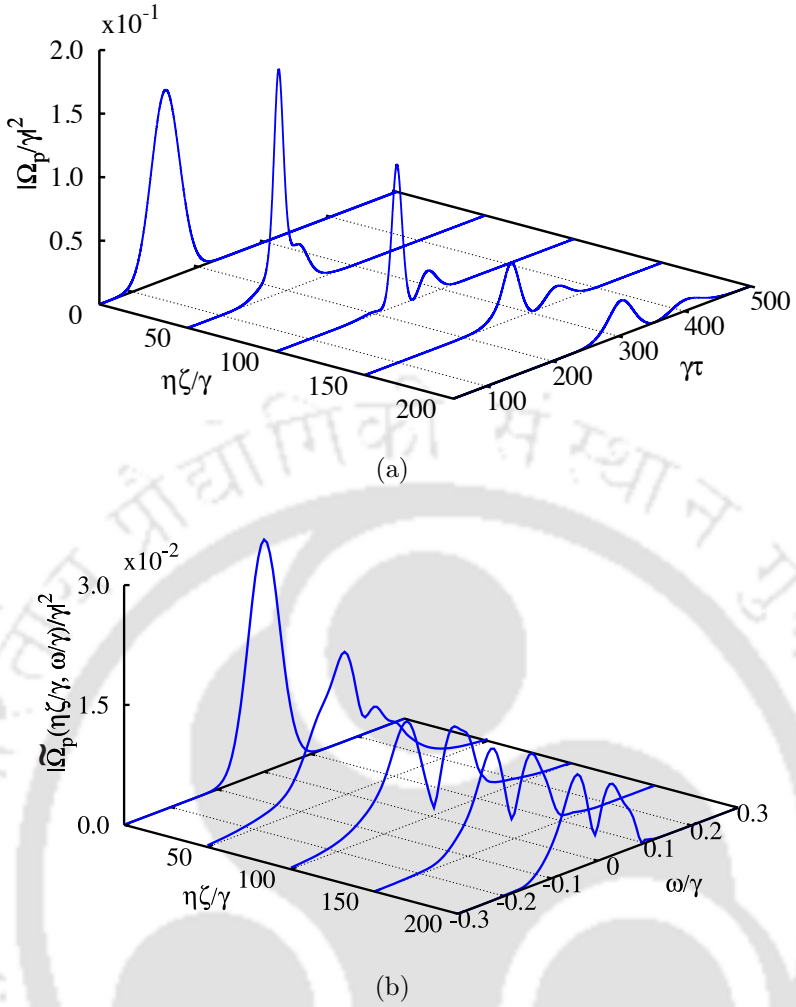

Fig. 2.4 (a) Intensity $|\Omega_p/\gamma|^2$ of a stronger probe pulse as function of the propagation distance. Parameters are $\Delta = \Delta_{P'} = 4\gamma$ and $\Omega_p = \sqrt{0.15}\gamma$; all other parameters are chosen as in Fig. 2.2. (b) shows the corresponding probe pulse power spectra obtained by Fourier transformation as function of the propagation distance.

2.3.2 Strong probe pulses

Next, we consider probe pulses with higher intensities such that the effect of SPM is expected to become of relevance. Figure 2.4 shows the probe pulse propagation dynamics as function of the propagation distance for case (ii), i.e., $\Delta_{P'} = \Delta = 4\gamma$. The other parameters are chosen as in Figs. 2.2 and 2.3, except for the intensity higher by a factor of 10. Panel (a) shows the temporal probe pulse shape throughout the propagation. We find that the pulse gradually breaks up, until two fully separated pulses are obtained at $\eta\zeta/\gamma = 100$. The shapes of these sub-pulses remain Gaussian, and they are found to subsequently propagate through the medium without further break-up. However, the individual subpulses broaden as they propagate through the medium, as it was also found in the corresponding weak probe pulse case of Fig. 2.2.

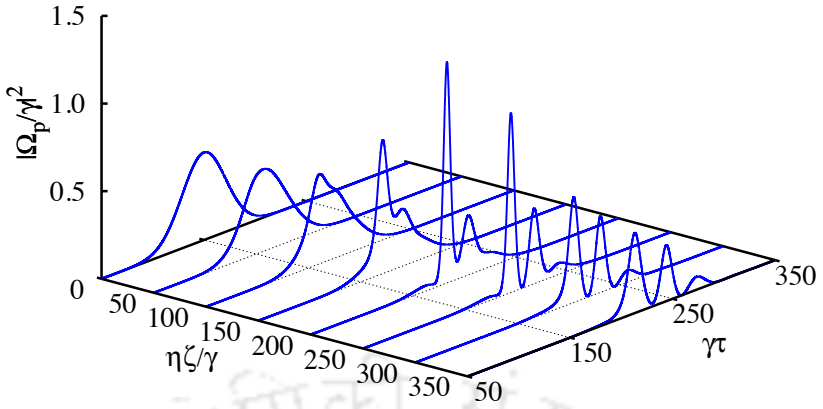

Fig. 2.5 Propagation dynamics of a probe pulse with $\Omega_p = \sqrt{0.5}\gamma$ and $\Delta = \Delta_{P'} = 4\gamma$. All other parameters are chosen as in Fig. 2.2.

To further analyze this pulse break-up, Fig. 2.4(b) shows the power spectra of the probe pulse throughout its propagation, obtained by Fourier transformation of the temporal pulse shape. The power spectrum evolves from the Gaussian input spectrum into a double-peaked structure which is a characteristic signature of the SPM effect.
A further numerical study reveals that the number of generated subpulses depends on the initial probe field intensity. Figure 2.5 demonstrates that a three-peak pulse can be generated from a single Gaussian probe pulse if the initial probe field intensity is suitably increased. As expected, the precise shape of the output pulse depends sensitively on the probe pulse intensity and the value of the detuning Δ. For example, the three-peak shape in Fig. 2.5 turns into a two-peak structure if the three-photon detuning is increased to $\Delta = 8\gamma$. Finally, we verified that the shaping and splitting of the probe pulse does not rely on the initial Gaussian pulse shape and can also be observed with non-Gaussian initial pulse shapes, such as secant-hyperbolic pulses.

2.4 Theoretical Analysis

Next, we provide a theoretical interpretation of the numerical results presented in Sec. 2.3. To this end, we adapt the standard description of pulse propagation in optical fibers [80] to our system.
We find that this model reproduces our numerical results accurately for weak probe pulses where the SPM phenomenon is small. For parameters where the SPM effect becomes dominant our model allows us to gain qualitative insights and provides an intuitive explanation for the pulse splitting phenomenon described in Sec. 2.3.
Details on our simple model for the propagation of optical pulses in nonlinear media inspired by the standard fiber optics approach [80] are provided in Appendix 2.5. There,

we perform a perturbative analysis with respect to the probe field strength to derive the linear susceptibility $\chi(\omega)$ of the probe field, and find that the spatio-temporal evolution of the probe pulse can be described by

$$\left(\frac{\partial}{\partial x}+\frac{1}{c}\frac{\partial}{\partial t}\right)\Omega_p = i\eta\left(\sum_{n=0}^{3}\beta_n\frac{i^n}{n!}\frac{\partial^n\Omega_p}{\partial t^n}\right)+i\eta R_p\left|\Omega_p\right|^2\Omega_p\,. \tag{2.14}$$

The parameters β_n and R_p are determined by the microscopic model introduced in Sec. 2.2. In particular,

$$\beta_n = \left.\frac{\partial^n\chi}{\partial\omega^n}\right|_{\Delta_p=\Delta_c}^{\omega=0} \tag{2.15}$$

is the n-th derivative of the medium susceptibility $\chi(\omega)$ evaluated at the center frequency $\omega = 0$ of the probe pulse [see Eq. (2.28)]. Note that due to the approximations used throughout the derivation, our model described by Eq. (2.14) is valid under the following conditions. (α) The probe pulse must be sufficiently long in time such that the atomic medium follows the probe pulse dynamics adiabatically. (β) The probe field spectrum must be sufficiently narrow such that the Taylor expansion of the linear susceptibility is justified [see Appendix 2.5 for details]. (γ) The probe field intensity must be weak enough such that all non-linear effects are well described by the third-order term proportional to R_p.

We start by analyzing the relevant model parameters, see Fig. 2.6. Panel (a) shows the linear susceptibility $\chi(\omega)$ as a function of frequency ω scanned across the probe pulse center frequency $\omega = 0$ [see Eq. (2.24)]. The parameter β_0 is the linear susceptibility χ of the probe field evaluated at $\omega = 0$, and vanishes for resonant Raman fields [see Eq. (2.12)] if the ground-state decoherence rate Γ is neglected. β_1 is related to the group velocity of the pulse via $v_g = [1/c + \eta\mathrm{Re}(\beta_1)]^{-1}$, where Re denotes the real part. The parameters β_2 and β_3 account for group velocity dispersion. The real and imaginary parts of β_2 [β_3] are shown in Fig. 2.6(b) [(c)] as a function of the detuning Δ. Both real and imaginary parts of β_2 and β_3 determine the width and amplitude of the probe pulse at the output. For $\Delta = 0$ only the imaginary part of β_2 is different from zero. This term accounts for absorption due to the finite width of the EIT window in frequency space. For larger values of Δ the real part of β_2 increases and describes the change of the group velocity for frequencies away from the central frequency of the pulse. In general, β_3 represents a higher-order correction to the group velocity dispersion. The nonlinearity due to the Kerr transition is proportional to R_p defined in Eq. (2.23), and the dependence of R_p on $\Delta_{P'}$ is shown in Fig. 2.6(d). The imaginary part of R_p is only large for $\Delta_{P'} \approx 0$, and hence absorption on the Kerr transition is

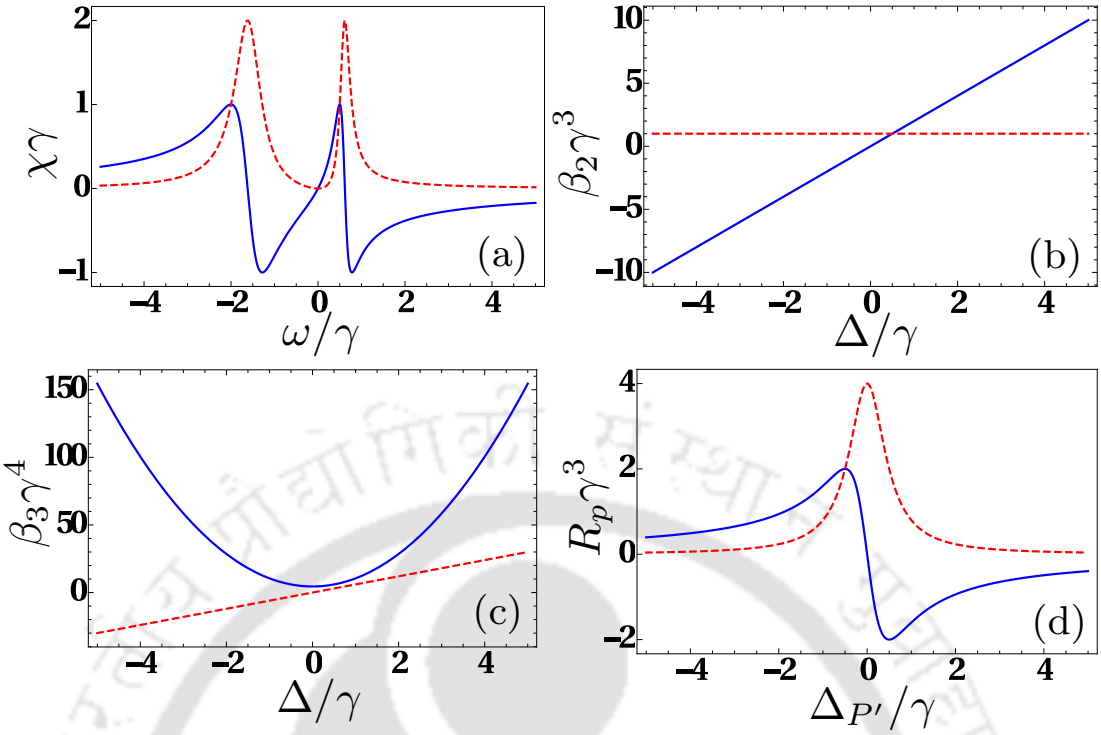

Fig. 2.6 (a) Real and imaginary parts of the linear susceptibility χ in Eq. (2.27) as a function of the Fourier component ω of the probe pulse envelope. We have $\beta_0 = \chi(0) = 0$, and β_n is the nth derivative of χ at $\omega = 0$, see Appendix 2.5. The real and imaginary parts of β_2 [β_3] are shown in (b) [(c)]. (d) Real and imaginary parts of R_p as a function of the Kerr detuning $\Delta_{p'}$ for $\Delta = 4\gamma$. In (a)-(d), blue solid (red dashed) lines show real (imaginary) parts and $\Omega_c = \gamma$.

small for $\Delta_{P'}/\gamma \gg 1$. Note that the quantitative impact of the term proportional to R_p in Eq. (2.14) depends on the probe pulse intensity.

Equation Eq. (2.14) can be numerically solved using the split-step Fourier method [80]. We find excellent agreement with the numerical results obtained in Sec. 2.3 for parameters where the model conditions (α)-(γ) are met.

In particular, this is the case for all parameters where the SPM effect is small, and in this regime the explanation of all phenomena in terms of the parameters β_i and R_p is straightforward. We begin with a weak probe pulse and a large detuning $\Delta_{P'}$ on the Kerr transition [cases (i) and (ii) in Sec. 2.3]. Since the imaginary part of R_p and hence the absorption on the Kerr transition is small for these parameters, the probe pulse can propagate through the medium without significant losses. The additional broadening of the probe pulse in case (ii) as compared to (i) can be explained by the non-zero group velocity dispersion for the parameters in (ii). Next we consider a resonant Kerr field $\Delta_{P'} = 0$ [cases (iii) and (iv) in Sec. 2.3]. The strong damping of the probe pulse found in Sec. 2.3 can be explained by the large imaginary part of R_p. The Kerr transition hence destroys the EIT phenomenon and leads to absorption of

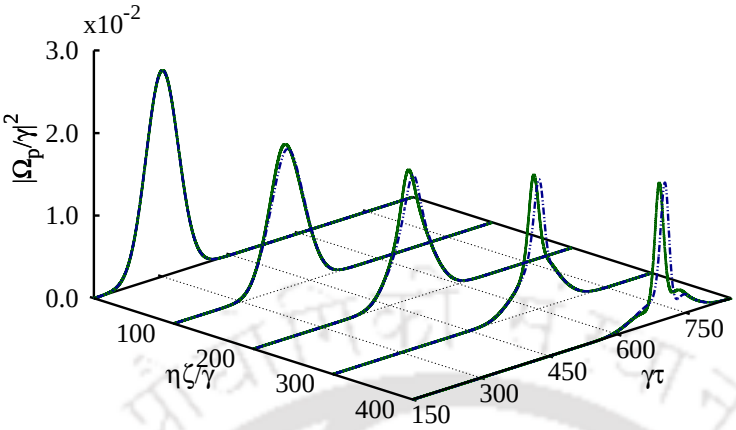

(a)

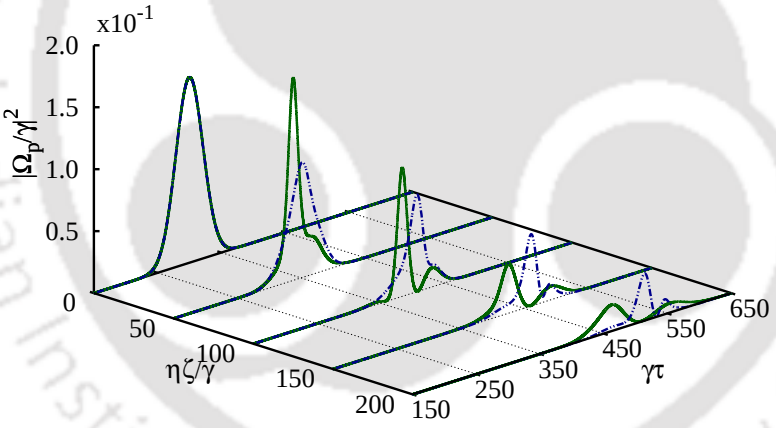

(b)

Fig. 2.7 Comparison between the full numerical solution to Eqs. (2.6) and (2.8) [green solid line] and the simple model in Eq. (2.14) [blue dot-dashed line]. The parameters in (a) are $\Omega_p = 0.025\gamma$, $\sigma_p = 50/\gamma$, $\Delta = \gamma$ and $\Delta_{P'} = 3\gamma$.. Results in (b) correspond to $\Omega_p = \sqrt{0.15}\gamma$, $\sigma_p = 30/\gamma$, and $\Delta = \Delta_{P'} = 4\gamma$.

the probe pulse. The non-vanishing group velocity dispersion in case (iv) leads to an additional broadening of the pulse as compared to (iii).

For a moderate probe pulse intensity, in our numerical analysis we found that the pulse splits into two pulses as it propagates through the medium [see Fig. 2.4(b)]. In this regime where the SPM effect is significant, our model in general is not sufficient for a

quantitative description of the pulse propagation, since part or all of the conditions (α, β, γ) are violated. However, in order to gain a qualitative insight into the pulse splitting phenomenon, we identify a parameter regime where the pulse splitting occurs and our model is still valid. This is shown in Fig. 2.7(a), where the pulse starts splitting at the end of the medium, and there is a reasonable agreement between the full numerical calculations and our theoretical model. From the model, the pulse splitting effect can be understood as follows. The SPM associated with R_p results in a splitting of the probe pulse in frequency space. In the presence of group velocity dispersion described by β_2 and β_3, these pulses propagate at different speeds. This explains the emergence of two different pulses in the temporal domain. Note that the pulse splitting reduces the intensity of the individual pulses, and suppresses nonlinear effects. Hence, the two pulses in Fig. 2.4(a) do not split again. Higher intensities such as in Fig. 2.5 lead to three pulses in the temporal domain. Interestingly, this result does not agree with the naive expectation that the pulse first breaks up in two pulses that subsequently split up in two pulses each, giving rise to a total of four pulses. This outcome is a manifestation of the non-linearity of the SPM phenomenon.
Finally, in Fig. 2.7(b) we compare the theoretical model to the full numerical simulation for parameters as in Fig. 2.4(a). The pulse splitting effect is more pronounced than for the parameters in Fig. 2.7(a). But clearly, for these parameters, the model is not capable of reproducing the full result. The reason for the discrepancy between the simple model in Eq. (2.14) and the numerical approach is that the conditions (α)-(γ) for the validity of the model are not met for the considered parameters. In particular,the probe pulse width in frequency space is not narrow enough to justify the adiabatic approximation rigorously. Second, the linear susceptibility χ varies too strongly over the width of the pulse in frequency space for $\Delta = 4\gamma$ such that the expansion of χ up to third order is insufficient. Third, the probe pulse intensity is not small enough such that higher order terms beyond the third-order nonlinearity will contribute. An improved model could be obtained by continuing the perturbative analysis to higher orders, which, however, would not qualitatively affect our interpretation of the pulse splitting phenomenon. The development of a more accurate model describing pulse propagation in the non-perturbative regime is subject to further investigation.

2.5 Chapter conclusion

In this chapter, we have studied the propagation dynamics of a Gaussian pulse through an atomic medium in four-level N-type configuration under different input conditions of control and probe field intensities and detunings. As our first result, we have found that at two-photon resonance condition with large Kerr detuning, distortionless

propagation of the probe pulse with low absorption is possible. In contrast, when the intensity of the probe pulse becomes higher, a splitting of the single Gaussian input pulse into a sequence of pulses may occur. To interpret the origin of this pulse splitting, we have derived a simple theoretical model for nonlinear pulse propagation in our model system. The parameters of this model can be calculated from the system's steady state density matrix. We conclude that in particular an interplay between Kerr nonlinearity and group velocity dispersion leads to the pulse splitting. The nonlinearity leads to a decomposition of the probe pulse in frequency space. Subsequently, the such formed subpulses propagate with different velocity due to group velocity dispersion, such that a splitting in the time domain arises. The temporal shape of the probe pulse at the output does thus indicate the strength of the self-phase modulation induced by the Kerr-nonlinearity. Our numerical analysis has shown that the number of peaks can be controlled by adjusting the laser parameters. For example, the group velocity can be controlled by the detuning of the probe and control fields with the excited state of the Λ sub-system. In addition, the Kerr-detuning and the laser intensities control the magnitude of the self-phase modulation.

Appendix - model parameters

Here we outline the derivation of the model in Eq. (2.14) from Eqs. (2.6) and (2.8). We assume that the probe field is sufficiently weak ($|\Omega_p| \ll \gamma, |\Omega_c|$) and pursue the perturbative approach outlined in [81, 82]. The atomic density operator is expanded as

$$\rho = \sum_{k=0}^{\infty} \rho^{(k)}, \tag{2.16}$$

where $\rho^{(k)}$ denotes the contribution to ρ in kth order in the probe field Hamiltonian

$$H_p = -(|2\rangle\langle 4| - |1\rangle\langle 3|)\Omega_p + \text{H.c.}\,. \tag{2.17}$$

In order to obtain the solutions $\rho^{(k)}$ we re-write the master equation (2.6) as

$$\mathcal{L}\rho = \mathcal{L}_0\rho - \frac{i}{\hbar}[H_p, \rho]\,, \tag{2.18}$$

where the linear super-operator $\mathcal{L}_0$ is independent of the probe field. Inserting the expansion (2.16) into Eq. (2.18) leads to the following set of coupled differential

equations

$$\dot{\rho^{(0)}} = \mathcal{L}_0 \rho^{(0)} \,, \tag{2.19}$$

$$\dot{\rho^{(k)}} = \mathcal{L}_0 \rho^{(k)} - \frac{i}{\hbar}[H_p, \rho^{(k-1)}], \quad k > 0. \tag{2.20}$$

Equation (2.19) describes the interaction of the atom with the control field to all orders and in the absence of the probe field. Higher-order contributions to ρ can be obtained if Eq. (2.20) is solved iteratively. Equations (2.19) and (2.20) must be solved under the constraints $\mathrm{Tr}(\rho^{(0)}) = 1$ and $\mathrm{Tr}(\rho^{(k)}) = 0$ $(k > 0)$.

First we consider the nonlinear term where we employ the adiabatic approximation, i.e., we assume that the temporal length of the probe pulse is much longer than the lifetime of the excited states. In this case we can find the nonlinear response of the medium to the probe field by solving for the steady state of Eqs. (2.19) and (2.20) up to third order in H_p and obtain

$$\rho^{(0)} = |3\rangle\langle 3| \,. \tag{2.21}$$

Under the resonance condition $\Delta = \Delta_p = \Delta_c$ the only non-zero terms contributing in Eq. (2.8) are $\rho_{24}^{(3)}$ and $\rho_{13}^{(3)}$. We find

$$\rho_{24}^{(3)} - \rho_{13}^{(3)} = R_p |\Omega_p|^2 \Omega_p \,, \tag{2.22}$$

where

$$R_p = -\frac{2}{(\Delta_{P'} + i\gamma/2)|\Omega_c|^2} \,. \tag{2.23}$$

Next we calculate the dominant correction arising from the spread of the probe pulse in frequency space. To this end we consider the Fourier expansion of the slowly varying probe pulse envelope,

$$\Omega_p(t) = \int_{-\infty}^{\infty} \tilde{\Omega}_p(\omega) e^{-i\omega t} \mathrm{d}\omega \,. \tag{2.24}$$

We solve Eqs. (2.19) and (2.20) up to first order and obtain

$$\rho_{13}^{(1)}(t) = -\int_{-\infty}^{\infty} \chi(\omega) \tilde{\Omega}_p(\omega) e^{-i\omega t} \mathrm{d}\omega \,, \tag{2.25}$$

where

$$\chi(\omega) = -\frac{\omega + \Delta_p - \Delta_c}{(\omega + \Delta_p + i\gamma/2)(\omega + \Delta_p - \Delta_c) - |\Omega_c|^2}\,. \tag{2.26}$$

There are no other terms up to first order contributing to the coherences ρ_{13} or ρ_{24}, and χ is shown in Fig. 2.6. If χ is slowly varying over the typical width of the probe pulse, we can expand χ in a Taylor series around $\omega = 0$. For $\Delta_p = \Delta_c = \Delta$ and up to third order we obtain

$$\chi(\omega) \approx \sum_{n=0}^{3} \frac{\omega^n}{n!}\beta_n\,, \tag{2.27}$$

where

$$\beta_n = \left.\frac{\partial^n \chi}{\partial \omega^n}\right|_{\Delta_p=\Delta_c}^{\omega=0}\,. \tag{2.28}$$

The coefficients β_k are shown in Fig. 2.6 and given by

$$\beta_0 = 0\,, \tag{2.29}$$

$$\beta_1 = \frac{1}{|\Omega_c|^2}\,, \tag{2.30}$$

$$\beta_2 = \frac{2(\Delta + i\gamma/2)}{|\Omega_c|^4}\,, \tag{2.31}$$

$$\beta_3 = \frac{6[|\Omega_c|^2 + (\Delta + i\gamma/2)^2]}{|\Omega_c|^6}\,. \tag{2.32}$$

Inserting the expansion (2.27) into Eq. (2.25) gives

$$\rho_{13}^{(1)}(t) \approx -\sum_{n=0}^{3} \beta_n \frac{i^n}{n!}\frac{\partial^n \Omega_p}{\partial t^n}. \tag{2.33}$$

In summary, the right-hand side of Eq. (4.7) can be written as

$$i\eta(\rho_{24} - \rho_{13}) \approx i\eta\left[\rho_{24}^{(3)} - \rho_{13}^{(3)} - \rho_{13}^{(1)}\right]\,. \tag{2.34}$$

Substituting the results from Eqs. (2.22) and (2.33) into Eq. (2.34) allows us to obtain Eq. (2.14).

Chapter 3

Microwave controlled efficient Raman sub-harmonic generation

3.1 Introduction

Optical systems in three level atomic configuration generalized by introducing more levels and couplings between different levels with optical and low-frequency microwave fields is shown to exhibit many new properties [83, 84] . Some of the interesting observations in these systems include four-wave mixing of optical and microwave fields[85, 86], study of double dark resonances[45, 87]. A low frequency field coupling two lower levels (LL) along with two optical fields form closed three level Λ system [88–93]. In closed Λ systems, the LL field perturbes the EIT and induces new coherences which lead to better control over optical properties of the media such as dispersion, absorption and nonlinearity [88–96]. Studies in closed Λ system make use of perturbed low frequency coherence induced by the additional field resulting in better storage and retrieval of light, phase manipulation of EIT, generation of new frequencies [89, 91, 94, 96]. In nonlinear wave mixing process , the interaction of two or more frequencies results in the generation of new frequencies. It is known that nonlinear wave mixing [97] between intense Stokes and anti-Stokes optical fields of Raman processes interacting in multilevel atomic system can produce a comb of Raman sub-harmonics [98]. The generation of such broad comb of Raman side bands has been an active area of research [99–103] owing to the fact that these sidebands can be synthesized as short pulse trains [104, 105]. The efficient short pulses generation has important applications in material processing, laser surgery, optical frequency metrology, and communications. Competition between stimulated Raman scattering (SRS) and electromagnetically induced transparency (EIT) has been studied experimentally by Harada *et al*[63]. They showed that an inhomogeneously broadened dense atomic

medium can destroy intensities of the incident fields whereas new fields via Raman processes can be successfully generated. Linear [63] and non-linear [106] theory have been adopted to understand SRS and EIT processes. The optical density is found to be the controlling parameter of this processes [63, 106]. In this work, we propose a novel scheme for efficient Raman sub-harmonic generation by exciting hyperfine coherences of the lower level metastable states in an atomic system with atoms in a closed three level Λ-configuration. Note that, such hyperfine coherence between ground levels of a Λ system has been investigated earlier in connection to manipulation of EIT effects for sub and superluminal light propagation, and modulation of line shape for CPT masers[107–109].

The key feature underlying Raman sub-harmonics generation is microwave induced hyperfine coherence between the two lower level metastable states. We show explicitly how the amplitude and phase of the microwave field generate controllable spectral amplitudes of Raman sub-harmonics. The main feature of our work is the creation of lower and higher order sub frequency Raman sidebands by manipulating the hyperfine coherence with variable amplitude and phase of the microwave. Our scheme is viable in currently available atomic vapor cells thereby opening the way for efficient sub-harmonic generation in standard experimental setups.

3.2 Theoretical model

The system under consideration is an atomic vapor modelled in closed Λ configuration as depicted in Fig. 3.1. The dipole allowed transitions $|a\rangle \leftrightarrow |i\rangle (i = b, c)$ are coupled by the weak optical fields and the dipole forbidden transition $|b\rangle \leftrightarrow |c\rangle$ is further coupled by a strong microwave field. The dynamics of the atomic system thus becomes notably different from a typical EIT scheme [see Fig. 1(a)], and other nonlinear processes starts to become significant. Here we show that a band of Raman sub-harmonics can be generated efficiently in this atomic system with the amplitudes, phases and detuning parameters of the three fields properly selected.

The input field $E(z,t)$ is selected such that it couples to both transitions $|a\rangle \leftrightarrow |c\rangle$ and $|a\rangle \leftrightarrow |b\rangle$ simultaneously. The form of input field is written as,

$$E(z,t) = \mathcal{E}(z,t)e^{-i\nu_c t} + \text{c.c}, \tag{3.1}$$

where $\mathcal{E}(z,t)$ denotes the net field . It gives the generated field at the output of the medium. At the input face of the medium $\mathcal{E}(z,t)$ contains both control and probe field components:

$$\mathcal{E}(z,t) = \mathcal{E}_c + \mathcal{E}_p e^{-i(\nu_p - \nu_c)t}. \tag{3.2}$$

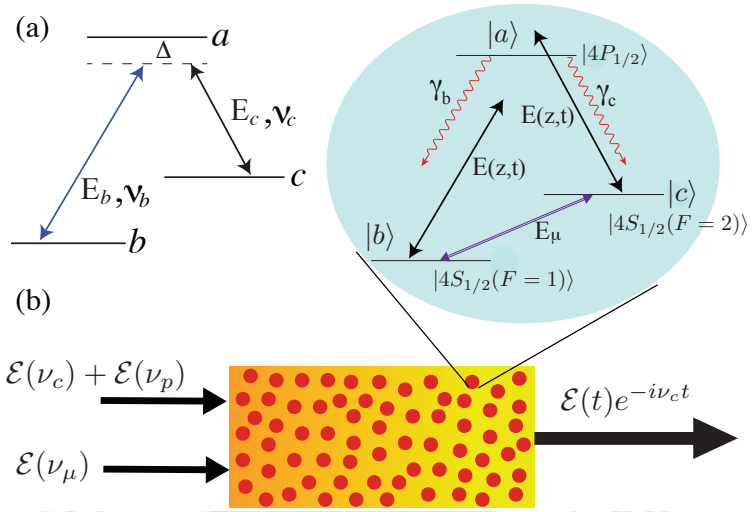

Fig. 3.1 (a) Schematic diagram of a three-level atomic system with energy spacing ω_{bc} between two ground states $|c\rangle$ and $|b\rangle$ in a typical EIT setup. The control field with frequency ν_c and probe field with frequency ν_p act on the atomic transitions $|a\rangle \leftrightarrow |c\rangle$ and $|a\rangle \leftrightarrow |b\rangle$, respectively. (b) Same three-level Λ system as (a) but in presence of the microwave field. The space-time-dependent field $E(z,t)$ can now couple to both the optical transitions generating Raman Stokes and anti-Stokes frequencies along with the pump and probe frequencies.

The cell is placed in a microwave cavity and microwave field couples the dipole forbidden lower levels This creats coherence among the lower states which as we will see later are responsible for generation of the Raman sub-harmonic fields in the system.

We consider the form of microwave field as,

$$E_\mu(z,t) = \mathcal{E}_\mu(z)e^{-i(\nu_\mu t+\theta_\mu)}, \tag{3.3}$$

where $\mathcal{E}_\mu(z) = \mathcal{E}_\mu e^{ik_\mu z}$ is the amplitude of the microwave field inside the cavity, ν_μ is the microwave frequency, and θ_μ is the phase of the microwave field.

The Hamiltonian for our three level system in the dipole approximation can be written as,

$$\begin{aligned}\mathscr{H} &= \sum_k \hbar\omega_k|k\rangle\langle k| - [\wp_{ab}E(z,t)|a\rangle\langle b| \\ &+ \wp_{ac}E(z,t)|a\rangle\langle c| + \wp_{cb}E_\mu(z,t)|c\rangle\langle b| + \text{h.c}]\end{aligned} \tag{3.4}$$

where $k = a, b, c$ and $\wp_{\alpha\beta} = \langle\alpha|\hat{\wp}|\beta\rangle$ is the dipole moment of the corresponding transition ($|\alpha\rangle \leftrightarrow |\beta\rangle$).

3.2.1 Density matrix equations of atomic system

We take a master equation approach to investigate the space-time dependent dynamics of the atomic system in presence of relaxation processes. The corresponding Louville equation of motion is given by,

$$\partial_t \rho = -\frac{i}{\hbar}\left[\mathscr{H}, \rho\right] + \mathcal{L}_\gamma[\rho] \tag{3.5}$$

where ρ is the density operator of the system, and $\mathcal{L}_\gamma[\rho]$ is the Lindbald operator representing the relaxation processes.

$$\begin{aligned}\mathcal{L}_\gamma[\rho] = &-\frac{\gamma_b}{2}\left(|a\rangle\langle a|\rho - 2|b\rangle\langle b|\rho_{aa} + \rho|a\rangle\langle a|\right) \\ &-\frac{\gamma_c}{2}\left(|a\rangle\langle a|\rho - 2|c\rangle\langle c|\rho_{aa} + \rho|a\rangle\langle a|\right) .\end{aligned} \tag{3.6}$$

The relaxation rates of the coherences in our model system are given by $\Gamma_{ab} = (\gamma_b + \gamma_c)/2 + i\Delta', \Gamma_{ac} = (\gamma_b + \gamma_c)/2 + i\Delta$ and $\Gamma_{bc} = \gamma_p + i\omega_{bc}$ respectively with $\Delta' = \omega_{bc} - \Delta$ and $\Delta = \nu_c - \omega_{ac}$. Here $\gamma_k (k = b, c)$ being the spontaneous emission rate of the excited state $|a\rangle$ to the states $|b\rangle$ and $|c\rangle$ respectively. The non-radiative decay rate of the lower levels is taken to be γ_p. The population and coherences can be evaluated by expanding equation (3.5) in the basis $\{|a\rangle, |b\rangle, |c\rangle\}$[106]. In doing so we work in a frame rotating with frequency ν_c to eliminate the highly oscillating terms. The full density matrix equations of motion for populations and coherences under rotating wave approximation is written as

$$\sigma_{aa} = -(\gamma_b + \gamma_c)\sigma_{aa} + i\Omega\sigma_{ba} - i\Omega^*\sigma_{ab} + i\Omega\sigma_{ca} - i\Omega^*\sigma_{ac}, \tag{3.7a}$$

$$\sigma_{ab} = -\Gamma_{ab}\sigma_{ab} - i\Omega\sigma_{aa} - \sigma_{bb} + i\Omega\sigma_{cb} - i\Omega_\mu e^{-i\Phi}\sigma_{ac}, \tag{3.7b}$$

$$\sigma_{ac} = -\Gamma_{ac}\sigma_{ac} - i\Omega(\sigma_{aa} - \sigma_{cc}) + i\Omega\sigma_{bc} - i\Omega_\mu^* e^{i\Phi}\sigma_{ab}, \tag{3.7c}$$

$$\sigma_{bb} = \gamma_c\sigma_{aa} - i\Omega\sigma_{ba} + i\Omega^*\sigma_{ab} - i\Omega_\mu e^{-i\Phi}\sigma_{bc} + i\Omega_\mu^* e^{i\Phi}\sigma_{cb}, \tag{3.7d}$$

$$\sigma_{bc} = -\Gamma_{bc}\sigma_{bc} - i\Omega\sigma_{ba} + i\Omega^*\sigma_{ac} - i\Omega_\mu^* e^{i\Phi}(\sigma_{bb} - \sigma_{cc}), \tag{3.7e}$$

$$\sigma_{cc} = \gamma_b\sigma_{aa} - i\Omega\sigma_{ca} + i\Omega^*\sigma_{ac} + i\Omega_\mu e^{-i\Phi}\sigma_{bc} - \Omega_{\mu^*} e^{i\Phi}\sigma_{cb} \tag{3.7f}$$

where $\Phi = \nu t + \theta_\mu$. The space-time dependent Rabi frequency corresponding to the optical and microwave fields are defined by $\Omega(z,t) = \vec{\wp}\cdot\mathcal{E}/\hbar$ and $\Omega_\mu(z,t) = \vec{\wp}_{cb}\cdot\mathcal{E}_\mu/\hbar$.

3.2.2 Field propagation equations

We use Maxwell's wave equations to investigate the non-linear response of the medium on the propagating optical fields in presence of the microwave field. The wave equation

for the net generated field under slowly varying envelope approximation at the output for thin atomic number density can be written as

$$\frac{\partial E(z,t)}{\partial z} + \frac{1}{c}\frac{\partial E(z,t)}{\partial t} = 2\pi i\kappa \mathcal{P}(z,t), \tag{3.8}$$

The induced macroscopic polarizations $\mathcal{P}(z,t)$ is connected to the coherences in the system by the relation,

$$\mathcal{P} = \left(\wp_{ab}\rho_{ab} + \wp_{ac}\rho_{ac}\right) e^{-i\nu_c t}. \tag{3.9}$$

Thus the dynamical behaviour of the field as it propagates in the system is governed by the generated coherences due to the atom-field interactions. For later convenience with simulation we rewrite Eq. (3.8) in terms of the Rabi frequencies of the field.

$$\left(\frac{\partial}{\partial z} + \frac{1}{c}\frac{\partial}{\partial t}\right)\Omega(z,t) = i\frac{\eta}{2}(\sigma_{ac} + \sigma_{ab}) \tag{3.10}$$

where $\eta = 3\lambda^2\mathcal{N}\gamma/4\pi$. Note that the coherences $\sigma_{ij}, (i = a, j \in b, c)$ in the original frame are given by $\rho_{ij}e^{-i\nu_c t}$.

3.2.3 Thermal Averaging

In a realistic gas medium, the finite velocity of the moving atoms cause a Doppler shift in frequencies as seen by the atoms. This results in an inhomogeneous line broadening. The response of the net generated field in an inhomogeneously broadened medium can be obtained by averaging the coherences over the Maxwell-Boltzmann velocity distribution of the moving atoms. We incorporate the atomic motion by introducing velocity-dependent field detunings $\Delta(v) = \Delta - kv$, where kv is the Doppler shift experienced by an atom with a velocity component v in the direction of the propagation of the fields. A complete account of the Doppler broadening is given in the appendix. The averaged value coherence is represented by writing it within angular brackets $\langle\sigma_{ij}\rangle$. It is defined as

$$\langle\sigma_{ij}\rangle = \frac{1}{\sqrt{2\pi \mathrm{D}^2}}\int \sigma_{ij} e^{-(kv)^2/2\mathrm{D}^2} d(kv). \tag{3.11}$$

The Doppler width D at temperature T is defined by $\mathrm{D} = \sqrt{k_B T\nu_c^2/Mc^2}$ where M is the atomic mass and k_B is the Boltzmann constant. We estimate the Doppler width D at T=313K as 50γ. Thus the dynamics of the generated fields is expressed by the propagation equation,

$$\left(\frac{\partial}{\partial z} + \frac{1}{c}\frac{\partial}{\partial t}\right)\Omega(z,t) = i\frac{\eta}{2}\langle(\sigma_{ac} + \sigma_{ab})\rangle \tag{3.12}$$

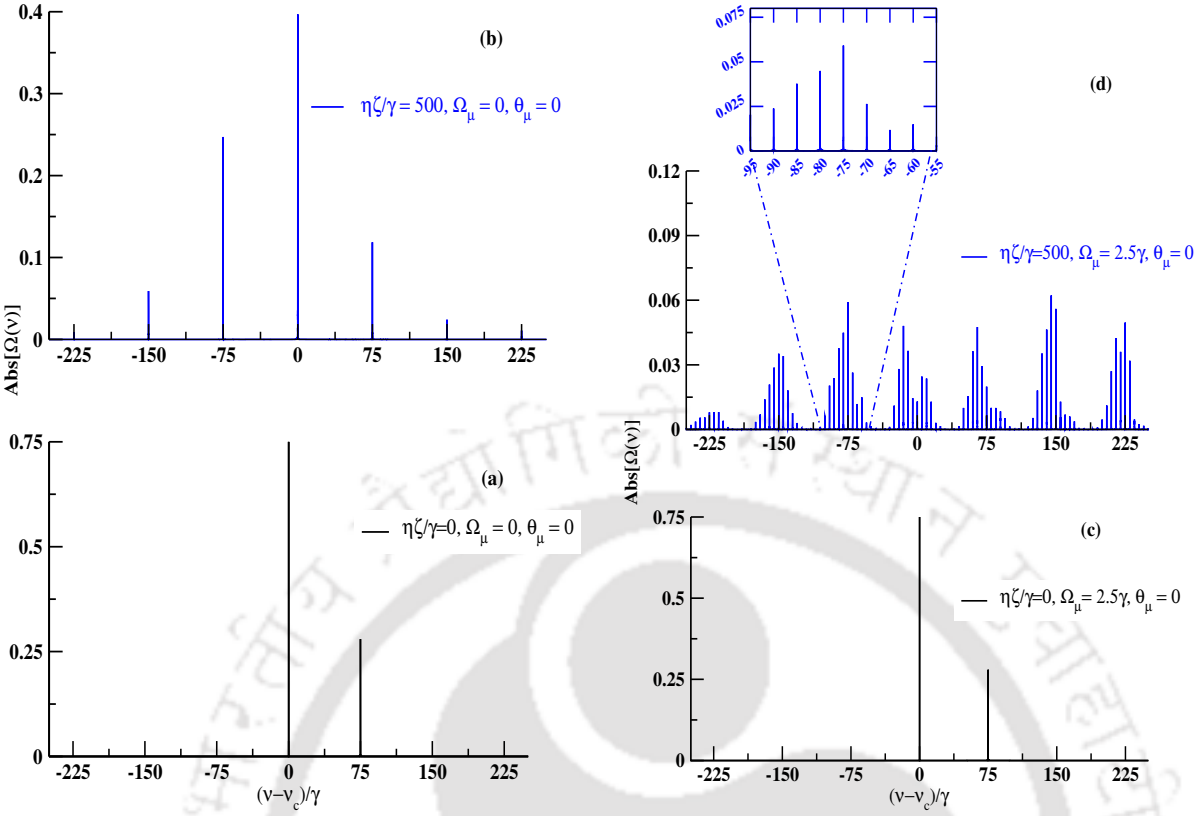

Fig. 3.2 The amplitudes of the different Fourier components of the input and output field is plotted against the normalised frequencies at different normalised propagation length $\eta\zeta/\gamma$. (a) & (b) shows the field amplitudes in the absence of microwave field, (c) &(d) depicts the generation of subraman fields with strong mocrowave coupling. The inset of (d) shows zoomed version of the generated Raman Stokes sub-harmonic fields in the presence of the microwave field. We choose the common parameters of above graphs as given by $\Omega = 0.75\gamma$, $\mathcal{E}_p/\mathcal{E}_c = 0.4$, $\Delta = \Delta' = 0$, $\gamma_p = 0$, $\omega_{bc} = 75\gamma$, $\gamma = 38 \times 10^6 s^{-1}$. The Doppler width parameter D is 50γ at T=313K and the wavelength $\lambda_c \approx 770$ nm.

3.3 Numerical Results and Discussions

Equation (3.5) for the atoms along with the propagation equation for the optical fields (3.12) are solved numerically in the moving co-ordinate system $\tau = t - z/c, \quad \zeta = z$ with the following initial conditions: atoms are initially in the state $|b\rangle$, microwave field is in resonance with the $|b\rangle \leftrightarrow |c\rangle$ transition and at the input face of the medium, control, probe and microwave fields are continuous waves. Furthermore, for numerical simplicity we have assumed that $\wp_{ab} = \wp_{ac} = \wp$ and $\gamma_b = \gamma_c = \gamma/2$. We calculate the output field $\mathcal{E}(l,\tau)$ in terms of the space-time dependent Rabi frequency $\Omega(l,\tau)$ and perform a fast Fourier transform to obtain the different Fourier components of the field at the output face of the medium.

3.3.1 Numerical results

We now present the key findings of our work - generation of the ground state coherence by the strong microwave field and its effect on the generated output field in an inhomogeneously broadened atomic medium. Our results are based on simulations carried out with experimental parameters corresponding to the level scheme $4S_{1/2}(F = 1) \equiv |b\rangle$, $4S_{1/2}(F = 2) \equiv |c\rangle$ and $4P_{1/2} \equiv |a\rangle$ of ^{39}K[110].

In Fig. 3.2 we show the amplitudes of frequency components in the field at the input and output face of the medium in the presence and absence of the microwave field. Without the microwave field, the output spectrum consists of control, probe, Raman Stokes and anti-Stokes field components and their higher harmonics. The higher order harmonics are weaker in intensity. It can be seen that in the presence of microwave field, new frequency components appeared in the output field spectrum. Each frequency harmonic of the Raman spectrum shows a comb of sub frequencies with frequency separation equal to two times the Rabi frequency of the microwave field as shown in Fig. 3.2(d). The numerical result leads to expressing the generated field expression at the output of the medium into the form

$$\mathcal{E}(t) = \sum_{m} \sum_{n} \mathcal{E}^{(\pm n, \pm m)} e^{\pm in\omega_{bc}t \pm 2im\Omega_{\mu}t} \tag{3.13}$$

Here $\mathcal{E}^{(\pm n, \pm m)}$ gives the strength of the mth order sub harmonic of nth order Raman fields for $n, m > 0$. The Rabi frequency of the microwave field is denoted by Ω_{μ}. It is also seen from Fig. 3.2(d)that the Raman sub-harmonic processes dominate over the Raman processes at length $\eta\zeta/\gamma = 500$. We also found that all Raman processes gradually diminishes whereas sub-Raman processes slowly enhance in amplitude during the length of propagation. The normalized propagation length $\eta\zeta/\gamma = 500$ corresponds to the actual length of the medium L$\sim$ 7 cm for the atomic density $\mathcal{N} = 5 \times 10^{10}$ atom/cm^3.

3.3.2 Discussion

To explain the generation of Raman sub-harmonic components in the Raman spectrum, we provide an intuitive picture of the process involved in terms of dressed states. The schematic explanation is shown in Fig.3.3. The bare state level configuration is shown in Fig.3.3a. The strong microwave driving of the lower two states $|c\rangle$ and $|b\rangle$ creates superposition dressed states $|+\rangle$ and $|-\rangle$ with an energy separation of $\omega_{bc} + 2\Omega_{\mu}$ as shown in Fig. 3.3b. Fig. 3.3c and 3.3d shows the sub-harmonic sideband generation in the Raman spectrum due to the formation of this dressed levels. The weak optical fields couple the levels $|a\rangle \leftrightarrow |+\rangle$ and $|a\rangle \leftrightarrow |-\rangle$ thereby generating all range of

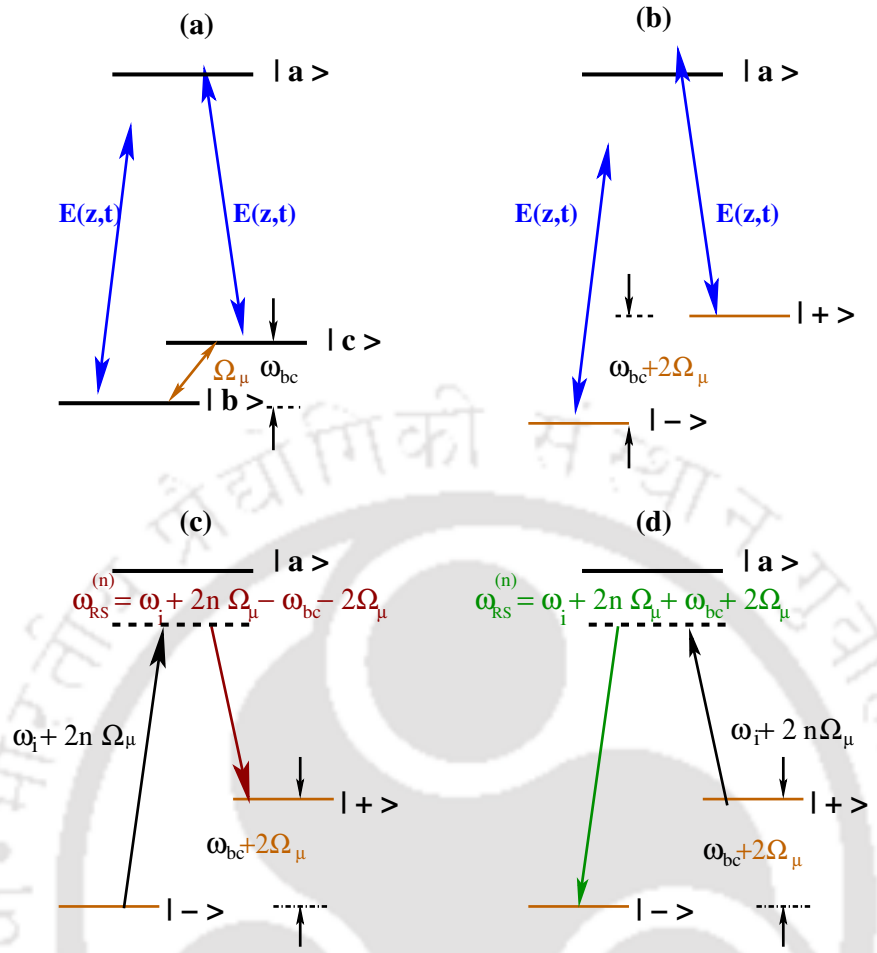

Fig. 3.3 Schematic explanation of generation of sub-harmonics in the Raman spectrum. (a) Bare state picture, (b) dressing of the lower levels due to presence of strong microwave coupling. (c) Generation of lower order Raman sub-harmonics ω_{RS} (d) generation of higher order Raman sub-harmonics ω_{RS} . $\omega_i = \omega_c \pm n\omega_{bc}$.

Raman harmonics and sub-harmonics as given in Eq. (3.13). Note that the Raman harmonic frequencies are $\omega_i = \omega_c \pm n\omega_{bc}$. The system emits the radiation at the Raman sub-harmonics that can be determined by the microwave Rabi frequency and energy separation between two lower levels of the Λ system.

Next we study the behaviour of Raman sub-harmonics with medium length at two different phases of the microwave field. The relative phase difference between the applied fields can drastically modify the coherences and populations of a closed loop three level atomic system [111]. Fig.3.4 depicts amplitude of the generated prominent sub-harmonic of stokes and anti-stokes fields as a function of propagation distance for two different values of θ_μ. The figure clearly shows that the spectral amplitudes of generated Raman sub-harmonics can be suppressed by the introduction of a phase θ_μ of $\pi/2$ of microwave field at low densities. In order to see the role of this microwave induced atomic coherence on the Raman sub-harmonic Stokes and anti-Stokes fields

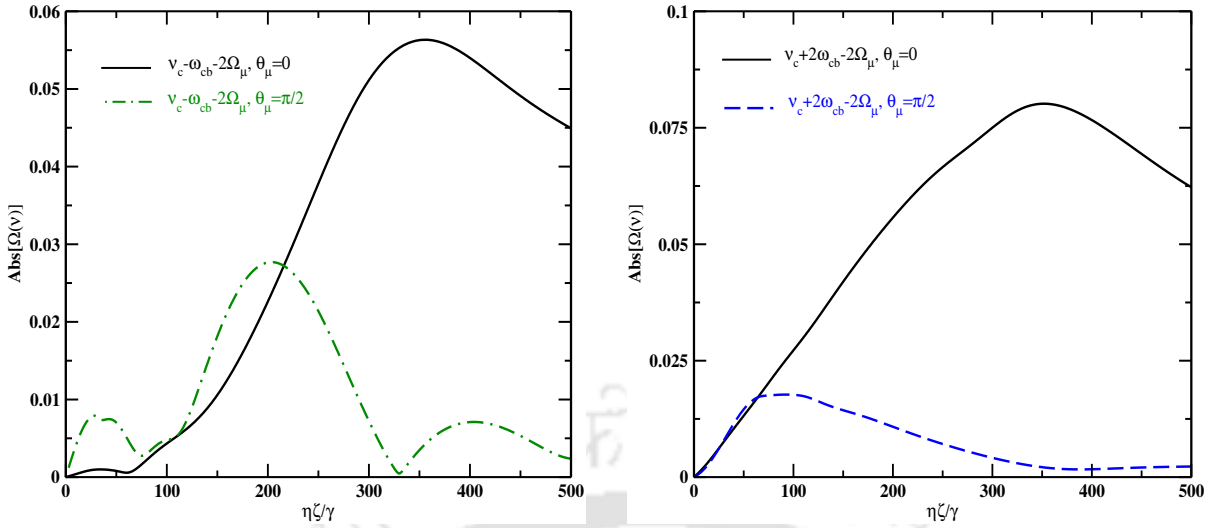

(a) (b)

Fig. 3.4 The spectral amplitudes of Raman sub-harmonic Stokes(a) and anti-Stokes(b) fields as a function of the medium length for a homogeneously broadened medium for two different phase parameter θ_μ The parameters are same as Fig.3.2.

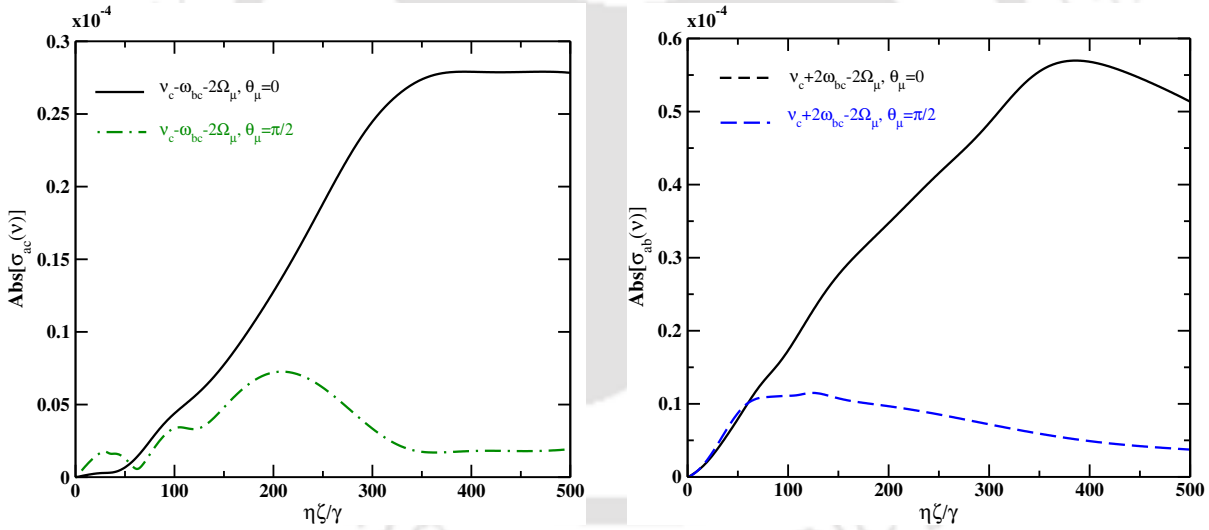

(a) (b)

Fig. 3.5 (a) The spectral amplitudes of coherences of corresponding Raman sub-harmonic Stokes and anti-Stokes fields in fig. 3.4 as a function of the medium length for a homogeneously broadened medium. The parameters are same as Fig.3.2.

generation, we investigate the Fourier components of the coherence between the levels $|a\rangle$ and $|c\rangle$ at frequency $\nu_c - \omega_{bc} - 2\Omega_\mu$ and that between the levels $|a\rangle$ and $|b\rangle$ at frequency $\nu_c + 2\omega_{bc} - 2\Omega_\mu$. These coherences are plotted in Fig. 3.5 for two values of microwave phase θ_μ, as in Fig. 3.4. It can be seen that the behaviour of the fields in Fig.3.4 and corresponding coherences in Fig.3.5 follow same pattern . This justify the

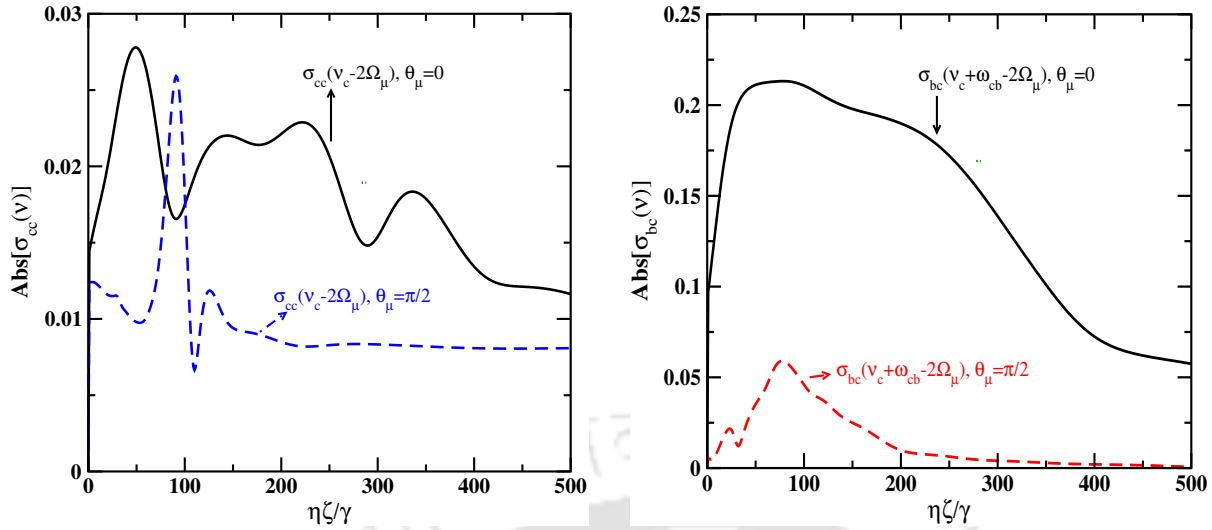

(a) (b)

Fig. 3.6 The spectral amplitudes of the (a) population $\sigma_{ii}, (i \in b, c)$ and (b) hyperfine coherence σ_{bc} are plotted as a function of medium length. Two lower level ground states populations have same amplitude and oscillation frequency $\nu_c - 2\Omega_\mu$. The parameters are same as in Fig.3.2.

intuitive explaination given before and shows that these are the sub-harmonic field components realated to the respective coherences.

Note that simulations have been carried out with $\gamma_p = 0$. However the results can be generalised to include buffer gas with $\gamma_p = 0.001\gamma$. We found that the nature of the Raman sub-harmonic spectrum is unaffected whereas the spectral amplitude is suppressed in the presence of buffer gas.

In Fig.3.6, we show the hyperfine coherence $\sigma_{bc}(\nu_c + \omega_{bc} - 2\Omega_\mu)$ and the populations in the ground states $\sigma_{ii}(\nu_c - 2\Omega_\mu)(i = b, c)$ as a function of optical density. We have noticed that the hyperfine coherence $\sigma_{bc}(\nu_c + \omega_{bc} - 2\Omega_\mu)$ and the population $\sigma_{ii}(\nu_c - 2\Omega_\mu)(i = b, c)$ are zero in absence of microwave field. The scattering between newly generated hyperfine coherence $\sigma_{bc}(\nu_c + \omega_{bc} - 2\Omega_\mu)$ with optical fields ν_i leads to nonlinear generation of Raman sub-harmonic field at sum and difference frequencies $\nu_i \pm (\nu_c + \omega_{bc} - 2\Omega_\mu)$ [52]. Hence the microwave induced hyperfine coherence modulates the refractive index of the medium and impress frequency sidebands into the laser field. Fig.3.6 also depicts that the hyperfine coherence can be greatly suppressed by changing the phase of the microwave field and generated Raman sub-harmonic fields are of small in amplitude as shown in Fig.3.4. Hence microwave induced hyperfine coherence is responsible for creation of the Raman sub-harmonic generation.

3.3.3 Comparison with cold atomic gas

When the medium consists of cold atoms, we can ignore the effects of atomic motion. The equations of motion can be solved without averaging the coherences over the velocity distribution due to Doppler effect. We have performed a comparative study of the results for the two cases. In Fig. 3.7, the amplitudes of subharmonic frequencies of fig. 3.2 is plotted with and without Doppler averaging. The graphs show that the Doppler averaging has the effect of reducing the generated field amplitudes to about half. Similar graphs corresponding to the coherences and populations in the previous section also shows the same behavior. The sub harmonic frequency spectrum remains unaffected.

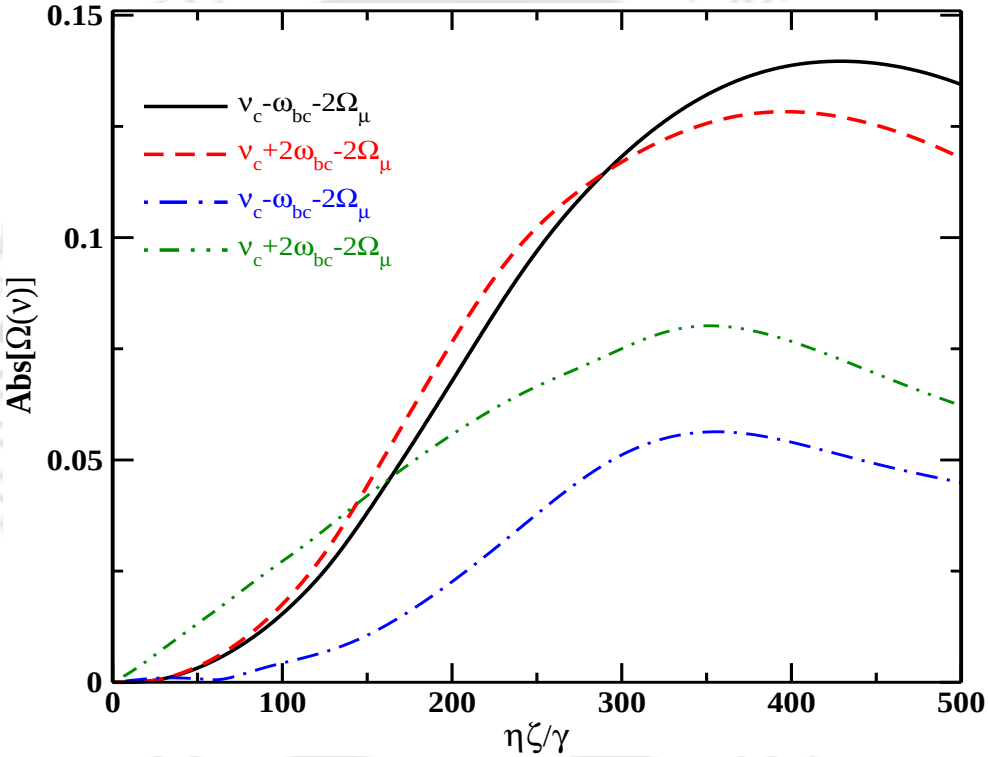

Fig. 3.7 The spectral amplitudes of the Raman sub-harmonic Stokes and anti-Stokes fields are plotted as a function of medium length. Black solid and red dashed graphs are plotted without Doppler averaging, blue dot-dashed and green double dot dashed plots are the same as in Fig. 3.4. The parameters are same as in Fig.3.2.

3.4 Chapter conclusion

To conclude, we have investigated efficient generation and manipulation of Raman sub-harmonic fields by microwave induced coherence between lower hyperfine levels in a typical Λ system. We compared the results with and without Doppler averaging the finite velocity of atoms. It is found that Doppler averaging suppresses the spectral

amplitudes of the generated fields. Our proposed scheme works at remarkable low optical densities and weak optical fields. Furthermore, we demonstrate that the phase of the microwave field can also be used as an additional control parameter in generation of the Raman sub-harmonic field. This microwave controlled Raman sub-harmonic generation can be used in sub femtosecond pulse train generation. Extension of this work beyond atomic vapors to photonic crystals or superstructures will help in making a significant step in the direction of bridging nano-photonics with microwave devices and promoting the practical use of quantum coherence in metamaterials [112] and photonic crystals to a wider domain.

Chapter 4

Microwave assisted arbitrary optical pulse generation in thermal vapour

4.1 Introduction

It is known that coherently prepared media enables optical frequency conversion through nonlinear wavemixing [113, 38, 114]. Conversion between low frequency microwave signals of giga-hertz range to high frequency optical signals of tera-hertz frequency is a highly desirable facility in information processing and communication networks. Electro optical modulators (EOM) are generally employed for bridging these two widely seperated frequency domains [115]. But the efficiency of these systems are not potent [116]. Finding new schemes for bidirectional as well as frequency up conversion methods are called for.

In the previous chapter we have shown how a frequency comb is generated in a closed Λ system with hyperfine coupling. In this work, we examine same closed loop Λ configuration but under different conditions of couplings. We exhibit how an optical pulse is generated at one transition frequency of a Λ system which has the shape of a microwave pulse coupling the lower levels, when a control field couples the other transition. This generation is shown to be most effective at three-photon resonance condition, which supresses the two-photon EIT effects.

4.2 Theoretical Model

In this work, we exploit microwave induced hyperfine coherence to enable efficient generation of the optical frequency pulse. In order to demonstrate efficient frequency conversion, we use an inhomogeneously broadened closed Λ atomic system consisting of an excited state $|1\rangle$ and two metastable states $|2\rangle$ and $|3\rangle$ as shown in Fig.4.1.

The electric dipole allowed transitions $|1\rangle \leftrightarrow |3\rangle$ and $|1\rangle \leftrightarrow |2\rangle$ are coupled by two optical fields, namely, probe and control fields, whereas the magnetic dipole allowed transition $|2\rangle \leftrightarrow |3\rangle$ is coupled by a microwave field to form a closed Λ-system. This level structure can be experimentally realized in ^{87}Rb which contain ground levels $|2\rangle = |5S_{1/2}, F = 2, m = 2\rangle$ and $|3\rangle = |5S_{1/2}, F = 1, m = 0\rangle$ and the excited level $|1\rangle = |5P_{3/2}, F' = 2, m = 1\rangle$. Numerical studies of the Maxwell-Bloch(MB) equation enable us to understand the coherent control of the optical frequency generation and subsequent propagation through inhomogeneously broadened system. The system is shown to exhibit interesting behavior under the condition when amplitudes and detunings of the microwave and other two optical fields are properly selected. The generated pulse is amplified and follows the temporal profile of microwave pulse. To interpret these results, we derive a simple expression for the atomic coherence at probe transmission in the Fourier domain. From this, we conclude that this generation of arbitrary shaped optical pulse is a direct manifestation of perturbed hyperfine coherence by microwave field.

4.2.1 Governing equations

The structure of the three coupling fields are given by

$$\vec{E}_i(z,t) = \hat{e}_i \mathcal{E}_i(z,t) e^{-i(\omega_i t - k_i z + \phi_i)} + \text{c.c. } (i \in p, c, \mu) \tag{4.1}$$

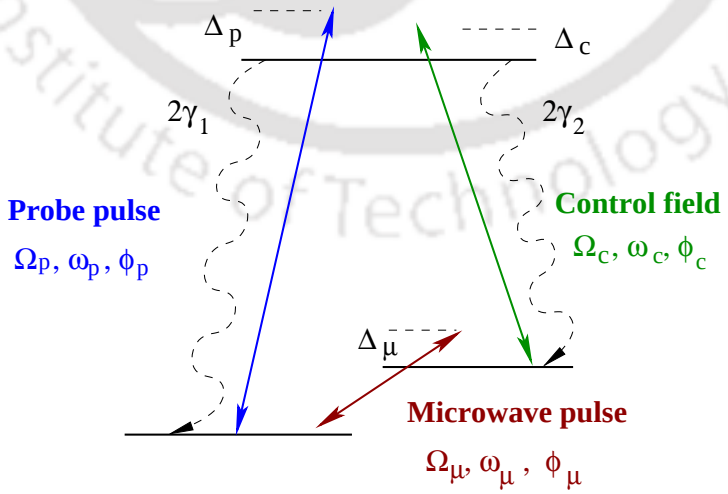

Fig. 4.1 Schematic representation of three level atoms in closed Λ configuration. The control field $\boldsymbol{E}_c$ couples to the transition $|1\rangle \leftrightarrow |2\rangle$, the probe field $\boldsymbol{E}_p$ interacts with the transition $|1\rangle \rightarrow |3\rangle$ and the microwave pulse $\boldsymbol{E}_\mu$ couples the hyperfine levels $|3\rangle \rightarrow |2\rangle$. For simplicity, we consider $\gamma_1 = \gamma_2 = \gamma/2$.

where $\mathcal{E}_i$ is the space time dependent amplitude, ω_i the frequency, ϕ_i phase of the corresponding fields. The Hamiltonian of the system under dipole and rotating wave approximations can be expressed as

$$\begin{aligned} H_{int} &= \hbar\omega_{13}|1\rangle\langle 1| + \hbar\omega_{12}|2\rangle\langle 2| - \hbar[\Omega_c e^{-i(\omega_c t - k_c z + \phi_c)}|1\rangle\langle 2| \\ &- \Omega_p e^{-i(\omega_p t - k_p z + \phi_p)}|1\rangle\langle 3| - \Omega_\mu e^{-i(\omega_\mu t - k_\mu z + \phi_\mu)}|2\rangle\langle 3|] + H.c., \end{aligned} \tag{4.2}$$

where the Rabi frequencies of the probe, control and microwave fields are defined by

$$\Omega_p = \vec{\boldsymbol{d}}_{13} \cdot \vec{\mathcal{E}}_p/\hbar, \quad \Omega_c = \vec{\boldsymbol{d}}_{12} \cdot \vec{\mathcal{E}}_c/\hbar, \quad \Omega_\mu = \vec{\boldsymbol{\mu}}_{23} \cdot \vec{\mathcal{E}}_\mu/\hbar \tag{4.3}$$

respectively. The electric and magnetic dipole matrix elements are represented by $\vec{\boldsymbol{d}}_{ij}$ and $\vec{\boldsymbol{\mu}}_{ij}$ respectively. Now we introduce a unitary transformation to the wave function of the system so that explicit time dependence is eliminated from the interaction terms of the Hamiltonian. The transformation operator U takes the form

$$U = e^{-i[(\omega_p t - k_c z + \phi_c)|1\rangle\langle 1| - ((\omega_p + \omega_c)t - (k_p + k_c)z + (\phi_p + \phi_c))|2\rangle\langle 2|]} \tag{4.4}$$

With the unitary transformation, the effective interaction Hamiltonian takes the form

$$\begin{aligned} H_{\text{int}} &= -\hbar\Delta_p|1\rangle\langle 1| - \hbar(\Delta_p - \Delta_c)|2\rangle\langle 2| - [|1\rangle\langle 3|\Omega_p \\ &+ |1\rangle\langle 2|\Omega_c + |2\rangle\langle 3|\Omega_\mu e^{-i(\Delta t + \Delta k z + \Phi)} + \text{H.c.}]. \end{aligned} \tag{4.5}$$

The relative phase and wave vector mismatch are defined as $\Phi = \phi_p - \phi_c - \phi_\mu$, and $\Delta k = k_p - k_c - k_\mu$ with k_i being the propagation constant of the respective field. The detunings of the three fields from the corresponding transition resonance are given by

$$\Delta_p = \omega_p - \omega_{13}, \quad \Delta_c = \omega_c - \omega_{12}, \quad \Delta_\mu = \omega_\mu - \omega_{23} \tag{4.6}$$

respectively. The three photon detuning Δ is defined as $\Delta = \Delta_p - \Delta_c - \Delta_\mu$. Now we impose the condition on the field frequencies $\omega_p = \omega_c + \omega_\mu$, which gives $\Delta = 0$, so that the time dependence is completely eliminated from the Hamiltonian. Note that the two photon resonance condition of electromagnetically induced transparency case, $\omega_p - \omega_c = \omega_{23}$ modifies into condition $\omega_p - \omega_c = \omega_{23} + \Delta_\mu$ satisfied by the three detunings, in the presence of additional coupling field between hyperfine levels. This condition not only simplifies the numerical integration but also turned out to be the important for effective frequency generation.

The spatiotemporal propagation of probe field is governed by the Maxwell's equations in the slowly varying envelope approximation as,

$$\left(\frac{\partial}{\partial z}+\frac{1}{c}\frac{\partial}{\partial t}\right)\Omega_p = i\eta_p\rho_{13}. \tag{4.7}$$

where the coupling constant is defined as $\eta_p = \gamma\mathcal{N}\lambda_p^2/8\pi$. Typical parameter values are $\mathcal{N} = 5\times10^{11}\text{atoms/cm}^3$, $\lambda_p = 780$ nm, and $\gamma = 2\pi\times10^6$ Hz. Note that the ratio $\eta_\mu/\eta_p = (\omega_m/\omega_p)\alpha^2$, where $\alpha\approx1/137$ is the fine structure constant. It follows that $\eta_\mu << \eta_p$. Also, $\Omega_c >> \Omega_p, \Omega_\mu$. So the spatiotemporal effects of the control and microwave fields are not taken into account in the numerical integration of Maxwell's equations. The quantum dynamics of the atoms is modeled by the master equation approach. The dynamics of atomic coherences that governs the propagation of probe field are given by Bloch equations

$$\begin{aligned}
\dot{\rho}_{11} &= -2\gamma\rho_{11} + i\Omega_c^*\rho_{21} - i\Omega_c^*\rho_{12} + i\Omega_p\rho_{31} - i\Omega_p^*\rho_{13},\\
\dot{\rho}_{12} &= -\left[\gamma - i\Delta_c\right]\rho_{12} - i\Omega_c(\rho_{11}-\rho_{22}) + i\Omega_p\rho_{32} - i\Omega_\mu^* e^{i\theta}\rho_{13},\\
\dot{\rho}_{13} &= -\left[\gamma - i\Delta_p\right]\rho_{13} + i\Omega_c\rho_{23} - i\Omega_p(\rho_{11}-\rho_{33}) - i\Omega_\mu e^{-i\theta}\rho_{12},\\
\dot{\rho}_{22} &= \gamma\rho_{11} - i\Omega_c\rho_{21} + i\Omega_c^*\rho_{12} + i\Omega_\mu e^{-i\theta}\rho_{32} - i\Omega_\mu^* e^{i\theta}\rho_{23},\\
\dot{\rho}_{23} &= -\left[\Gamma - i(\Delta_p-\Delta_c)\right]\rho_{23} + i\Omega_c^*\rho_{13} - i\Omega_p\rho_{21} + +i\Omega_\mu e^{-i\theta}(\rho_{33}-\rho_{22}),
\end{aligned} \tag{4.8}$$

where $\theta = \Phi + \Delta kz$. The spontaneous decay of excited state $|1\rangle$ to metastable states is denoted by γ whereas Γ is decay rate of the hyperfine coherence. In the weak probe and microwave fields limit, the ground state population $\rho_{33}\approx1$. So the Bloch equations can be approximated as

$$\begin{aligned}
\dot{\rho}_{13} &= -\left[\gamma - i\Delta_p\right]\rho_{13} + i\Omega_c\rho_{23} + i\Omega_p,\\
\dot{\rho}_{23} &= -\left[\Gamma - i(\Delta_p-\Delta_c)\right]\rho_{23} + i\Omega_c^*\rho_{13} + i\Omega_\mu e^{i\theta},
\end{aligned} \tag{4.9}$$

The atoms in the hot gas medium at room temperature is in random motion and has a velocity associated with each. The Doppler shift in frequency caused by the finite velocity of the atoms is taken into account in our simulation by averaging the coherences over the Maxwell-Boltzmann velocity distribution of the moving atoms.

$$\langle\rho_{ij}\rangle = \frac{1}{\sqrt{\pi w_D^2}}\int_{-\infty}^{\infty}\rho_{ij}(kv)e^{-\left(\frac{kv}{w_D}\right)^2}d(kv). \tag{4.10}$$

The Doppler width w_D at temperature T is defined by $\sqrt{2k_BT\nu_p^2/\mathcal{M}c^2}$ where $\mathcal{M}$ is the atomic mass and k_B Boltzmann constant. We have included velocity induced Doppler shift by replacing detunings Δ_i to $\Delta_i(v) = \Delta_i - k_iv(i\in p,c)$ in Eq. (4.8).

4.3 Numerical Results

We investigated the spatiotemporal evolution of the fields by numerically solving the coupled full as well as approximate Maxwell-Bloch(MB) equations. The results agree in both cases, so we present results for the solution of full MB equations. The control

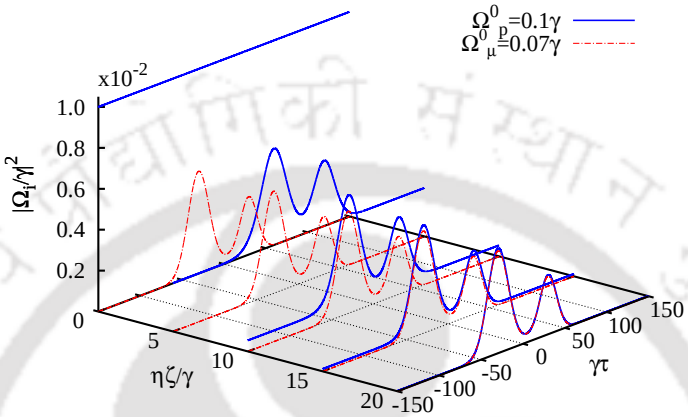

(a)

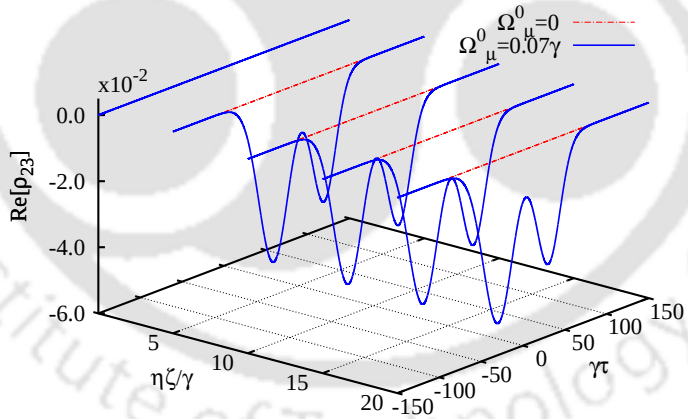

(b)

Fig. 4.2 (a) Temporal profiles of probe and microwave fields are plotted at different propagation distances $\eta\zeta/\gamma$ of the medium. Initial envelopes of probe and microwave fields are taken to be as cw and multi peak Gaussian structure respectively. (b) The spatiotemporal evolution of hyperfine coherence ρ_{23} is plotted in presence and absence of microwave field. The width, strength and location of individual peak for the microwave envelope are $\sigma_{\mu_1} = 25/\gamma$, $\sigma_{\mu_2} = 20/\gamma$, $f_{\mu_1} = 1$, $f_{\mu_2} = 0.75$, $\tau_{\mu_1} = -30/\gamma$, $\tau_{\mu_2} = 30/\gamma$ respectively. The following parameters have been used to generate these plots: $\Omega_c^0 = 1.41\gamma, \Delta_p = 2\gamma, \Delta_c = 0.6\gamma, \Delta_\mu = 1.4\gamma, w_D = 50\gamma, \Delta k/k = 1.8 \times 10^{-5}$, and $\Phi = 0$.

field can be on resonance or off-resonance with the transition $|1\rangle \leftrightarrow |2\rangle$. The probe and microwave fields are detuned accordingly from resonance to fulfill the resonance condition as stated earlier. The propagation equations Eq. (4.7) are solved in a rotating frame moving with the velocity of light in vacuum c; $\tau = t - z/c,\ \zeta = z$. With this choice of variables, the partial differential equation can be modified to ordinary differential equation as

$$\frac{d\Omega_p}{d\zeta} = i\eta_p\langle\rho_{13}\rangle \tag{4.11}$$

where the angular bracket denotes Doppler averaging. We start our discussion by investigation of the spatiotemporal evaluation of probe field with amplitude Ω_p^0 in presence of constant control field with amplitude Ω_c^0. We chose the temporal profile of the microwave field as multiple peaked Gaussian envelope. The time dependent field envelope for microwave as well as probe can be written as

$$\Omega_j(\zeta = 0, \tau) = \Omega_j^0 \sum_i f_{j_i} H\left[\frac{\tau - \tau_{j_i}}{\sigma_{j_i}}\right],\ (j \in p, \mu) \tag{4.12}$$

$$H[x] = e^{-x^{2\alpha_{j_i}}} \quad \text{Gaussian profile} \tag{4.13}$$

$$H[x] = Sech(x) \quad \text{sec-hyperbolic profile} \tag{4.14}$$

where Ω_j^0, σ_{j_i}, and f_{j_i} are the amplitude, temporal width and strength of the individual envelope respectively. The parameter α_{j_i} gives the flatness of individual envelope peak. The desired pulse shape can be obtained by using spatial light modulators [117]. The initial amplitudes of the three fields are taken as $\Omega_c^0 = 1.41\gamma, \Omega_p^0 = 0.1\gamma, \Omega_\mu^0 = 0.07\gamma$. Thus both probe and microwave field intensities are considerably smaller than the control field intensity. Fig.4.2a shows the temporal variation of probe and microwave pulse at different propagation distances. The shape of the probe field at medium boundary $\zeta = 0$ is chosen to be continuous wave(cw) whereas microwave field profile is double Gaussian. It can be seen that the shape of the microwave pulse has been generated in the probe profile. The initial cw probe field is fully suppressed and a pulse with shape of the double Gaussian pulse is generated towards exit of the medium. It is noticeable that the temporal profile of the pulse once formed propagates unaltered throughout the medium. In Fig.4.2b the hyperfine coherence is plotted in presence and absence of microwave field. We have noticed from Fig.4.2b that the hyperfine coherence is negligible in absence of microwave field whereas microwave field substantially modified the hyperfine coherences. The profile of induced coherence is identical to the shape of the microwave field. Hence the distinct characteristic of atomic coherence changes by microwave field lead to observed phenomena.

Next we examined the relative intensity dependence on the propagation dynamics of the probe field by taking higher microwave intensity. We take the initial shape

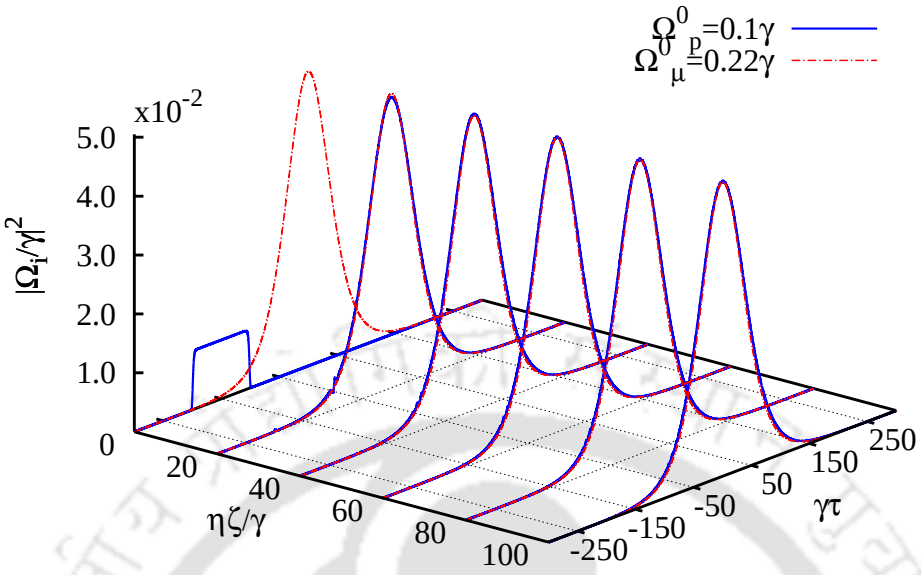

Fig. 4.3 Propagation dynamics of a weak probe pulse ($i = p$) and stronger *sec*-hyperbolic microwave pulse ($i = \mu$) is plotted along the length of the inhomogeneously broadened medium. The parameters are same as in Fig.4.2 except $\Delta_p = 1.75\gamma, \Delta_c = 0.45\gamma, \Delta_\mu = 1.30\gamma,\ \sigma_{p_1} = \sigma_{\mu_1} = 50/\gamma,\ \tau_{p_1} = -150/\gamma,\ \tau_{\mu_1} = 0,$ and $\alpha_{p_1} = 20$.

of probe pulse as super-Gaussian whereas microwave pulse is *sec*-hyperbolic shaped. As can be seen from Fig.4.3, the probe shape is replaced by the microwave profile and propagates as a soliton without distortion. The weak probe is amplified to the intensity of the microwave pulse and retains the amplitude through rest of the medium length. This shows that intensity of the generated temporal soliton can be efficiently controlled by suitably choosing the intensity and detuning of the microwave field.

The effect exhibited by the system is independent of the input shapes of probe and microwave fields. To verify this, we further studied the propagation dynamics of the probe field with different shapes of microwave fields. In all cases, it has been observed that the probe pulse is absorbed and got replaced by the microwave pulse shape and it follows the temporal location and dynamics of microwave pulse.

From these results it is evident that the initial probe field has no significant role in the subsequent dynamics of the generated pulse. The initial pulse is totally absorbed by the medium and a new pulse at the same frequency is generated with the shape of the microwave pulse. This fact is demonstrated by Fig. 4.4 where the probe pulse dynamics is shown without any input probe coupling. As the input probe is absent, we have taken $\Delta_p = 0$, and other two detunings take arbitrary values. As can be seen, a pulse is generated at the probe frequency which was initially absent. The generated

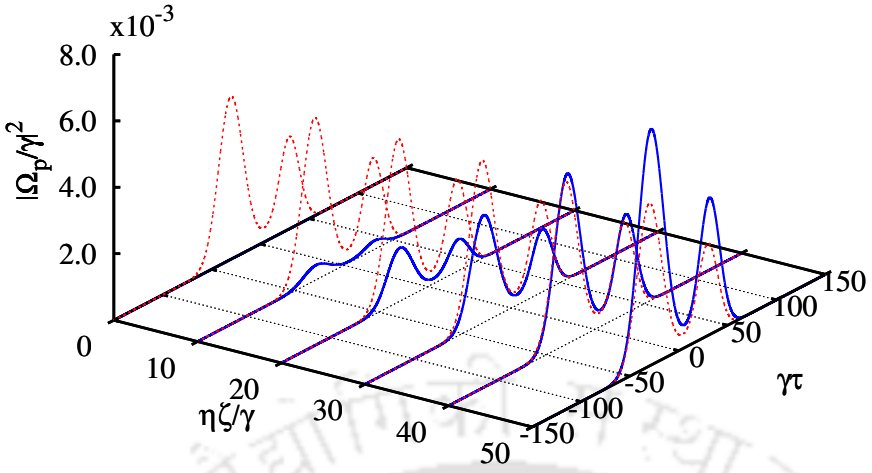

Fig. 4.4 Probe and microwave pulse intensities are plotted as function of time at different propagation distances $\eta\zeta/\gamma$ of the medium without input probe. The parameters are the same as in Fig.4.2 except that input probe intensity is zero. Initial profile of microwave is double Gaussian envelope with width $\sigma_{\mu_1} = 50/\gamma$. The parameters are fixed as follows: $\Delta_\mu = 2\gamma$ and $\Delta_c = 0$.

pulse is amplified. From the comparison with Fig.4.2, it is clear that the pulse is generated at a larger propagation distance in the absence of input probe coupling. So the input probe coupling field has no direct influence on the pulse dynamics, but it enhances the generation at smaller distances and subsequently gets absorbed by the medium. Finally we study how the arbitrary shaped optical pulse generation of a closed Λ-system is strongly dependent on two and three photon processes in presence of weak probe field. Fig.4.5 depicts the temporal behaviour of the generated optical pulse at a length of $\eta\zeta/\gamma = 40$. The normalized intensity profile of input microwave pulse is shown by the black solid line in Fig.4.5. It is observed from Fig.4.5 that the generated optical pulse develops oscillatory distorted behaviour by considering two particular conditions (i) all three fields are in resonance condition ($\Delta_c = \Delta_p = \Delta_\mu = 0$) and (ii) when control and probe fields fulfills two photon resonance condition ($\Delta_p - \Delta_c = 0$) whereas microwave field is on resonance $\Delta_\mu = 0$. It is clearly shown in Fig.4.5 that the efficient optical pulse generation is possible when three photon resonance condition is satisfied *i.e.*, $\Delta_p - \Delta_c - \Delta_\mu = 0$ and $\Delta_\mu \neq 0$. From this it is clear that the condition of three photon resonance where two photon resonance breaks down is crucial in observing efficient frequency generation and undistorted propagation. The detunings of the three fields can take any reasonable values as long as three photon resonance is satisfied. Hence the application of a microwave pulse connecting the two lower metastable states of a Λ system not only generates an optical pulse of arbitrary shape but also support propagation without distortion through medium.

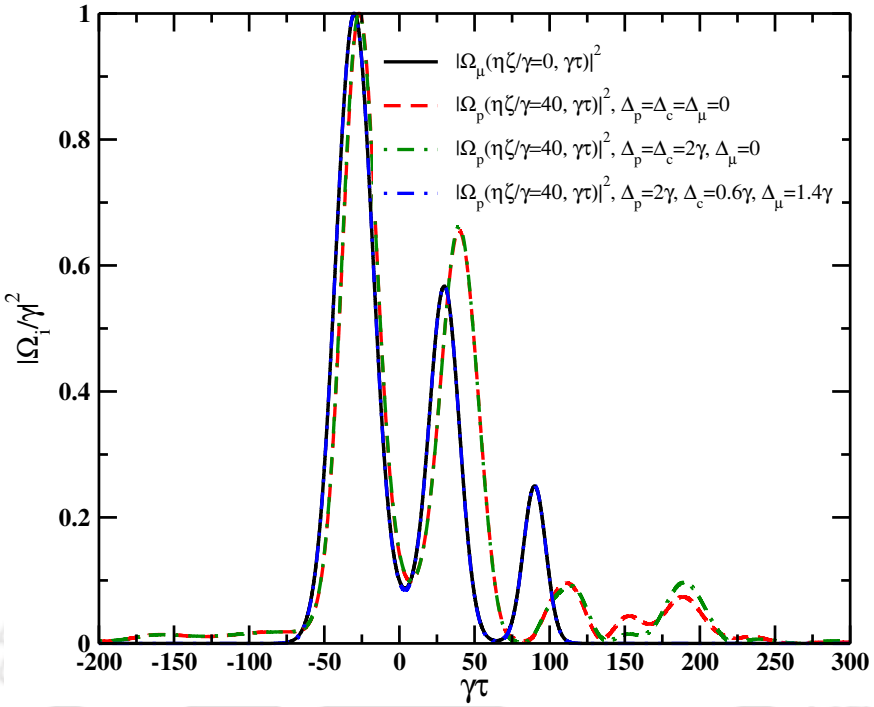

Fig. 4.5 The normalized intensities of generated optical pulses are plotted as function of time at a length $\eta\zeta/\gamma = 40$ of the medium in presence of weak probe field. The parameters are the same as in Fig.4.2 except that initial microwave profile. Initial profile of microwave is shown by solid black line. The width, strength and location of individual peak for the microwave envelope are $\sigma_{\mu_1} = 25/\gamma$, $\sigma_{\mu_2} = 20/\gamma$, $\sigma_{\mu_3} = 15/\gamma$, $f_{\mu_1} = 1$, $f_{\mu_2} = 0.75$, $f_{\mu_3} = 0.5$, $\tau_{\mu_1} = -30/\gamma$, $\tau_{\mu_2} = 30/\gamma$, $\tau_{\mu_3} = 90/\gamma$ respectively.

4.4 Analysis and Discussions

In order to analyze the results, we assume that the probe and microwave fields are sufficiently weak ($|\Omega_p|, |\Omega_\mu| \ll \gamma, |\Omega_c|$) so that we can pursue the perturbative approach. We considered terms of order first order in probe field and all orders in control and microwave fields. We decompose the Rabi frequency Ω_j, $(j \in p, \mu)$ into its Fourier components

$$\Omega_j(\zeta, \tau) = \int_{-\infty}^{\infty} e^{-i\omega\tau}\tilde{\Omega}_j(\zeta, \omega)d\omega \quad (j \in p, \mu). \tag{4.15}$$

$$\tilde{\rho}_{13}(\zeta, \omega) = \frac{i\Gamma_{23}\tilde{\Omega}_p - e^{i\phi}\Omega_c^0\tilde{\Omega}_\mu}{\Gamma_{13}\Gamma_{23} + |\Omega_c^0|^2} \tag{4.16}$$

where the relaxation rates are defined by $\Gamma_{13} = \gamma + i\Delta_p - i\omega, \Gamma_{23} = \Gamma + i(\Delta_c - \Delta_p) - i\omega$. The propagation of probe, Eq. (4.11) takes the form in the Fourier domain

$$\frac{\partial\tilde{\Omega}_p}{\partial\zeta} = i\eta_p\langle\tilde{\rho}_{13}\rangle \tag{4.17}$$

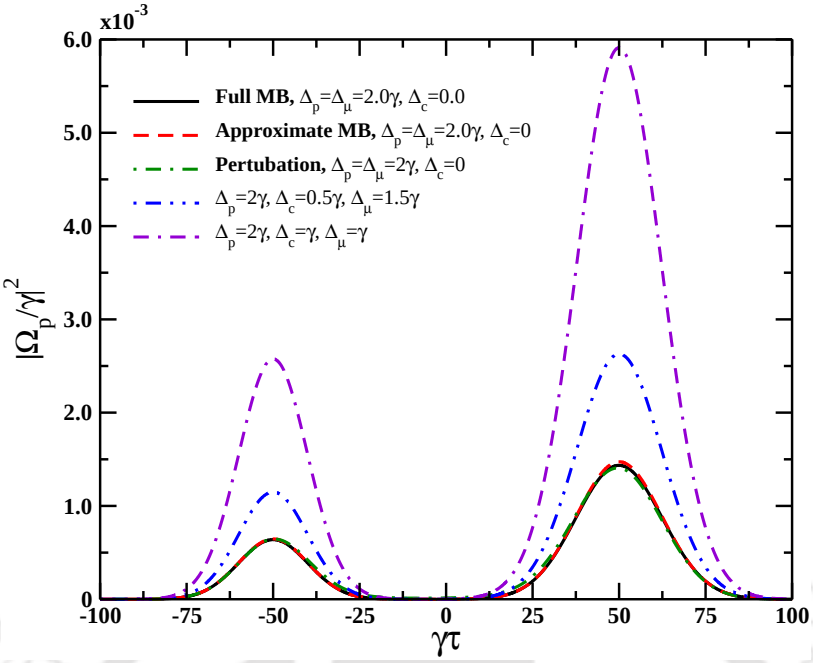

Fig. 4.6 Transmission of the cloned probe field at a distance $\eta\zeta/\gamma = 100$ in presence of double Gaussian shaped microwave field. The parameters are same as in Fig.4.2 except $\sigma_{\mu_1} = 20/\gamma, \sigma_{\mu_2} = 25/\gamma$.

Using equation (4.16),

$$\frac{\partial\tilde{\Omega}_p}{\partial\zeta} = i\eta_p \left\langle \frac{i\Gamma_{23}\tilde{\Omega}_p}{\Gamma_{13}\Gamma_{23} + |\Omega_c^0|^2} - \frac{e^{i\phi}\Omega_c^0\tilde{\Omega}_\mu}{\Gamma_{13}\Gamma_{23} + |\Omega_c^0|^2} \right\rangle. \tag{4.18}$$

The angular bracket denotes averaging over the inhomogeneous broadening for the detunings. The above equation (4.18) gives an insight into the pulse generation. The first term within the angular bracket refers to EIT phenomenon which renders opaque medium transparent for the probe field under two photon resonance condition. Second term corresponds to a gain process involving the microwave field at resonance condition. Therefore competition between these two terms governs the spatiotemporal evolution of the probe. The key to the optical frequency generation mechanism is three photon resonance in which two photon condition simultaneously breaks down. Hence the first term suppresses the initial probe envelope due to the presence of medium absorption at single photon probe detuning whereas second term generates a pulse with microwave envelope shape. Note that we considered a constant control field. The dynamics also depend on the total phase through the second term. This gives a better controllability on the probe dynamics.

Eq.(4.18) is to be integrated in order to compare the perturbative results with approximated as well as full MB equations. We assume initial profile of microwave field is a double peak structure while control and probe fields are cw and Gaussian

shape, respectively. The results shown in Fig.4.6 exhibit how the results obtained from approximate and perturbation theory are in full agreement with the results of full MB equations. In Fig.4.6, we have also shown that the transmission of the generated probe pulse can be varied by choosing different control and microwave field detunings. Hence the choice of detuning of the microwave field plays an important role to control transmission of generated pulse. The generated pulse travels with the velocity of light. These equations clearly shows that the result is a manifestation of competition between two and three photon processes. For the selected parameters, the three photon process dominates over the two photon process, which exhibit EIT, and the optical pulse is generated and amplified. It is evident from Eq. (4.18) that it is not necessary for an input probe pulse for the observed phenomena.

4.5 Chapter conclusion

In this chapter, we have shown a new scheme for generation of optical pulse of arbitrary shape in a three level Λ atomic medium exploiting the microwave induced atomic coherence between hyperfine levels. The optical pulse generated at the probe transition frequency follows the temporal profile of the input microwave pulse connecting the hyperfine levels of the atomic system. It is also demonstrated that the input probe pulse has only a transient effect in the generated pulse dynamics. The pulse generated propagates unaltered throughout the length of the medium. The phenomenon is shown to be a result of competition between two and three photon resonances where three photon resonance dominates over two photon resonance. This is made plausible with the selected parameters of the system. With this scheme optical pulse of desired shape can be efficiently generated and controlled. This may be exploited in precision measurements where stable optical frequency is preferred over microwave frequency.

Chapter 5

Phase controlled stable solitons in nonlinear fibers

5.1 Introduction

Self-induced transparency is a dramatic manifestation of nonlinear effects, leading to coherent localized pulse propagation in an atomic medium [10, 11, 54, 118]. The controlled, localized excitation and de-excitation of an ensemble of two level systems is effectively captured by the hyperbolic secant soliton pulse profile, which propagates as a stable soliton. Soliton is a shape preserving pulse which propagates undistorted through the medium over large distances, conserving energy and momentum. The optical soliton is formed by a balance between the group velocity dispersion and Kerr effect, nonlinear change of the index of refraction. The Maxwell-Bloch equations aptly describe the pulse and averaged atomic population dynamics, which have been extensively investigated for multi-level systems [54, 119–123]. Localized and nonlinear cnoidal wave solutions have been identified as exact solutions [119, 120], which has found experimental verification [124, 125].

The subject of pulse propagation in nonlinear fibers has also been well-studied, since its prediction by Hasegawa in 1974 [126]. The non-linear Schrödinger equation (NLSE), where the cubic nonlinearity arises due to Kerr effect, describes the pulse dynamics. This integrable system in one dimension possesses soliton solutions [127], which can be dark [128, 129], bright [130–133] or grey [134], depending on the nature of nonlinearity and dispersion. Bright solitons are the solution of the NLS equation in the anomalous GVD regime ($\beta_2 < 0$). These are stable light pulses of special shape formed where the chirping induced by SPM effect due to cubic nonlinearity balances the anomalous GVD. In the normal dispersion regime with $\beta_2 > 0$, the corresponding solution of NLSE supports the so called dark solitons, which appear as intensity dips or 'holes' set against

a continuous background that propagates like light pulse. Bright solitons have potential applications in areas like optical switch and pulse compression while dark solitons have better stability in presence of perturbation like noise, mutual interaction between two pulses etc, but not as useful as bright ones in high speed communication systems. Dark solitons are generally represented by the functional form of tan hyperbolic with phase function. Because of the antisymmetric nature of the "tanh" function, the soliton undergoes a π phase shift at he hole center, where the intensity also drops to zero, and the soliton is referred to as “black soliton”. In contrast, when the phase shift lies between zero to π, the minimum intensity does not drop to zero at the dip center; such solitons are called grey solitons. Grey solitons can be categorised as repetitive pulses with an intensity minimum in an optical background wave with a constant amplitude, where the minimum is not necessarily zero. Another interesting feature of dark solitons is that the phase of a dark soliton changes across its width, in contrast with bright solitons, which have a constant phase. Some of these solitons were experimentally observed, long after their prediction [135]. Soliton based optical communication systems have drawn wide attention in recent years because of their potential for increasing the capacity of the long distance light transmission systems. Optical solitons propagate in the form of light wave envelopes in optical fibers.

Gross-Pitaevskii equation in one-dimension, which captures the mean-field dynamics of Bose-Einstein condensate (BEC), being identical to NLSE, has also naturally evoked strong interest in solitons and their dynamics in cigar-shaped BEC [136–138]. Dark solitons in the repulsive regime and bright soliton and soliton trains in the attractive sector have been experimentally produced [128–131]. Several recent studies have been carried out on formation and dynamics of dark solitons in different physical systems including nonlinear fibers [139], carbon nanotubes [140], BEC [141], superfluid fermi gas [142, 143], P-T symmetric waveguide [144]. Also, the grey soliton, having complex profile has been produced through soliton collision in BEC [134]. Grey solitons have been the subject of some recent studies [145–147]. These are analogs of complex envelope Bloch solitons in condensed matter systems, which can connect differently ordered domains, without passing through the normal phase. This naturally makes it energetically favourable, as compared to the Neel’s soliton, wherein the soliton profile, being of the hyperbolic tangent type, passes through the normal phase, at the vanishing point of the above profile. It is interesting to note that the speed of the grey soliton can vary from zero to a maximum, depending on its depth. The co-existence of different types of solitons has been reported in several systems [148–150]. Recently, the experimental observation of bright-dark soliton pairs in fiber lattice has also been reported [151].

The doping of nonlinear fibers with suitable multilevel systems has opened up the

exciting possibility of naturally combining the atomic system with NLSE, which can possibly lead to effective soliton control and manipulation. Recently, the localized solitons of a nonlinear fiber with a three level dopant has been investigated, wherein exact solitons of tanh −sech type have been identified [152–154]. The constraints of this coupled nonlinear system has led to strong restrictions on the pulse dynamics. It was found that, the frequencies have to be perfectly matched for these solutions to exist [155].

In the present chapter, we present exact grey soliton profiles in a nonlinear fibre system doped with a three level atomic system. The system can be described by a two mode photonic crystal fiber, with the two mode frequencies equal to the transition frequencies of the lambda system. Nonlinear fibers doped with rare-earth elements can also be modelled by this system. Baldit *et. al* identified such a Λ-like three level system in an erbium doped solid state material wherein electromagnetically induced transparency has been experimentally observed [156]. We find that the complex profile's phase degree of freedom plays a crucial role in relaxing the constraint of frequency matching in this system. The grey solitons, apart from being energetically favourable, are found to undergo stable dynamical evolution over long distances. The fact that the phase degree of freedom can be controlled by atomic coherence opens up the possibility of controlled stable localized pulse propagation in this non-linear fiber system.

In the following, grey solitons with complex envelope are obtained as exact solutions of the coupled nonlinear system. It is explicitly shown how the phase degree of freedom removes the restrictive equal frequency conditions on the tanh −sech paired pulses [155]. Stability of the solitonic solutions is subsequently analyzed.

5.2 Coupled grey soliton solutions

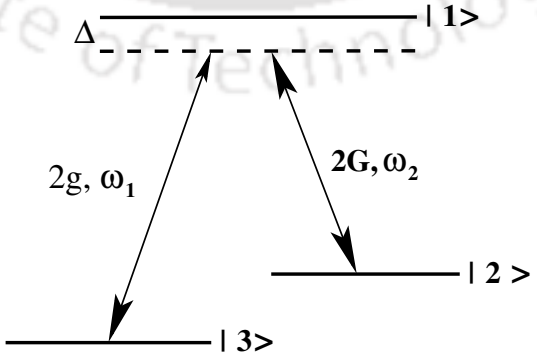

Fig. 5.1 A three level Λ atomic system whose transitions $1 \leftrightarrow 2$ and $1 \leftrightarrow 3$ are in near resonance with the two modes of the doped optical fiber. The Rabi frequencies of the two modes are $2G$ and $2g$. Δ denotes the single photon detuning.

We investigate the possibility of generalized solution for shape-preserving pulses in a Kerr nonlinear two-mode optical fiber doped with 3-level Λ atoms as shown in Fig.5.1. The system can be a birefringent fiber or bimodal fiber doped with rare-earth element which can be modelled by a three level Λ system. The modes of the fiber are near resonant with the transitions of the atomic system. The two modes of the optical fiber may be described by the profile,

$$\vec{E}_i(z,t) = \vec{A}_i e^{-i(\omega_i t - k_i z)} + c.c., (i = 1, 2), \tag{5.1}$$

$\vec{A}_i$ being the slowly varying envelope, ω_i and k_i, the carrier frequency and wave number respectively of the i^{th} mode. The time variation of the population of atomic levels are governed by optical Bloch equations. If $\zeta_i(z,t)$ denotes the probability amplitude of the i^{th} atomic level (Fig.5.1), then the following equations are obeyed within the rotating wave approximation

$$\dot{\zeta}_1 = -i\Delta\zeta_1 + iG\zeta_2 + ig\zeta_3 \tag{5.2}$$
$$\dot{\zeta}_2 = iG^*\zeta_1 \tag{5.3}$$
$$\dot{\zeta}_3 = ig^*\zeta_1 \tag{5.4}$$

The complex Rabi frequencies 2g and 2G for the two field modes are related to the slowly varying amplitudes $\vec{A}_i$ according to the relations

$$2g = \frac{2\vec{d}_{13}.\vec{A}_1}{\hbar}, 2G = \frac{2\vec{d}_{12}.\vec{A}_2}{\hbar},$$

where $\vec{d}_{ij}$ is the transition dipole moment matrix element. We take into account the effects of Kerr nonlinearity (proportional to the square of the electric field) and dispersion, in order to truly describe the spatio-temporal variation of the light pulses through the fiber. Using the approximation of slowly varying envelope, one can cast the NLSE in Rabi frequencies as,

$$\frac{\partial g}{\partial z} = -i\beta_1\frac{\partial^2 g}{\partial t^2} + i\gamma_1(|g|^2 + 2|G|^2)g + i\eta_1\zeta_3^*\zeta_1 \tag{5.5}$$
$$\frac{\partial G}{\partial z} = -i\beta_2\frac{\partial^2 G}{\partial t^2} + i\gamma_2(|G|^2 + 2|g|^2)G + i\eta_2\zeta_2^*\zeta_1 \tag{5.6}$$

where the terms with β_i are due to group velocity dispersion (GVD), those with γ_i and η_i represent the effect of Kerr nonlinearity and the coupling of the i^{th} mode with the atomic system respectively.

5.3 Ansatz

Motivated by the observed grey solitons in BEC [137, 145], we assume the following ansatz for the complex envelope solitons;

$$g = a\cos(\theta)\text{sech}\left[\frac{(t-uz)}{\sigma}\cos(\theta)\right]e^{i(p_1 z-\Omega_1 t)} \tag{5.7a}$$

$$G = b\left[\cos(\theta)\tanh\left[\frac{(t-uz)}{\sigma}\cos(\theta)\right]+i\sin(\theta)\right]e^{i(p_2 z-\Omega_2 t)} \tag{5.7b}$$

$$\zeta_1 = \frac{i\alpha\cos(\theta)}{a\sigma}\text{sech}\left[\frac{(t-uz)}{\sigma}\cos(\theta)\right]e^{i(p_1 z-\Omega_1 t)} \tag{5.7c}$$

$$\zeta_2 = -\frac{\alpha b\cos(\theta)}{a}\text{sech}\left[\frac{(t-uz)}{\sigma}\cos(\theta)\right]e^{i(p_1-p_2)z-i(\Omega_1-\Omega_2)t} \tag{5.7d}$$

$$\zeta_3 = \alpha\cos(\theta)\tanh\left[\frac{(t-uz)}{\sigma}\cos(\theta)\right]+(1-\alpha)\Gamma \tag{5.7e}$$

where u gives the envelope velocity in the moving frame, σ denotes the temporal width of the pulse. a and b are arbitrary parameters to be determined. θ gives the degree of blackness, α the absorption parameter. Note from the structure of the solutions g and G from RHS of the above equations that we have not imposed the condition $\Omega_1 = \Omega_2$ on the Rabi frequencies of pulse pair envelope. The Bloch equations (5.2-5.4) give

$$a^2 - b^2 = \frac{1}{\sigma^2}\,, \tag{5.8a}$$

$$\sin(\theta) = \sigma(\Omega_1 - \Omega_2)\,, \tag{5.8b}$$

$$\alpha = \frac{a^2\sigma^2}{a^2\sigma^2 + i(\Delta - \Omega_1 + b^2\sigma\sin(\theta))(\sigma/\Gamma)}\,. \tag{5.8c}$$

where the absorption parameter α is of Lorentzian shape and the width of the shape is decided by the pulse area. The second term in the denominator of Eq. (5.8c) gives the effective detuning of the laser frequencies from the resonance. The conservation of atomic probabilities leads to

$$|\Gamma|^2 = \frac{1-|\alpha|^2\cos^2(\theta)}{1-|\alpha|^2} \tag{5.9}$$

The nonlinear Schrodinger equations (5-6) then yield

$$p_1 = \frac{|\alpha|^2\eta_1(\Delta - \Omega_1 + b^2\sin(\theta)\sigma)}{a^4\sigma^2} + 2b^2\gamma_1 + \beta_1(\Omega_1^2 - \frac{\cos^2(\theta)}{\sigma^2}) \tag{5.10a}$$

$$p_2 = \gamma_2 b^2 + \beta_2\Omega_2^2 \tag{5.10b}$$

$$u = \frac{\eta_1|\alpha|^2}{a^2} + 2\beta_1\Omega_1 \tag{5.10c}$$

$$u = \frac{\eta_2|\alpha|^2}{a^2} + 2\beta_2\Omega_1 \tag{5.10d}$$

$$0 = \frac{2\beta_1}{\gamma_1\sigma^2} + (a^2 - 2b^2) \tag{5.10e}$$

$$0 = \frac{2\beta_2}{\gamma_2\sigma^2} + (2a^2 - b^2). \tag{5.10f}$$

Equation (5.10d) can alternately be cast as,

$$u = 2\beta_2\Omega_2 + (b^2 - 2a^2)\gamma_2\sigma\sin(\theta) + \eta_2\frac{|\alpha|^2}{a^2}. \tag{5.11}$$

For stable propagation of pulses, $\beta_1 \neq \beta_2$ [155]. From equations (5.10c) and (5.10d), we arrive at the following relations between the Rabi frequency and medium parameters,

$$\frac{|\alpha|^2}{a^2}(\eta_1 - \eta_2) + 2\Omega_1(\beta_1 - \beta_2) = 0 \text{ or } \Omega_1 = \frac{\frac{|\alpha|^2}{a^2}(\eta_2 - \eta_1)}{2(\beta_1 - \beta_2)} \tag{5.12}$$

Here, one important point to note is that, for $\theta = 0$, $\Omega_1 = \Omega_2$ is required. This is because of the consistency relation (5.8b) viz., $\sin\theta = \sigma\big(\Omega_1 - \Omega_2\big)$. If $\Omega_1 \neq \Omega_2$, then $\sigma = 0$ and the arguments of all the sech and tanh functions in the ansatz (5.7a-5.7e) diverge to give constant solutions. Hence for pure dark soliton solution for G, the condition $\Omega_1 = \Omega_2$ is enforced. In comparison, for the grey case, Ω_2 can take any value. Therefore the ansatz (5.7a-5.7e) represents valid solutions for all θ, given the consistency conditions are satisfied, showing that grey solitons of varying depths can be solutions of this dynamical system. It is observed that the conditions 5.11 and 5.12 do not restrict the values allowed for the dispersion and absorption coefficients for the observation of grey bright soliton solutions. We can choose the arbitrary parameters a and b , width of the pulse, Ω_i consistant with the above relations, for any physically possible values of medium parameters. In the next section, we numerically study the stability of the solutions and observed that these type of soliton solutions are observed for a good range of parameter values.

5.4 Stability of the coupled soliton pair

Stability analysis

We now investigate the propagation dynamics of the grey and bright solitons by integrating the full set of coupled nonlinear Schrodinger and Bloch equations. We have used Runge-Kutta method to solve the Bloch equations and split-step operator method

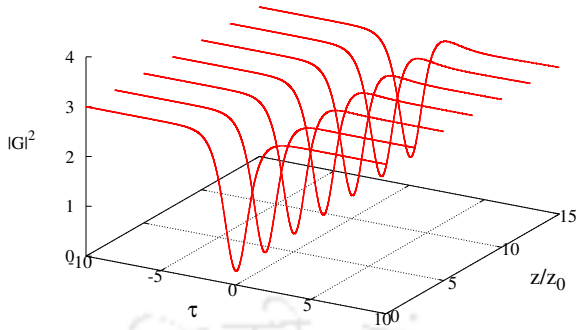

(a)

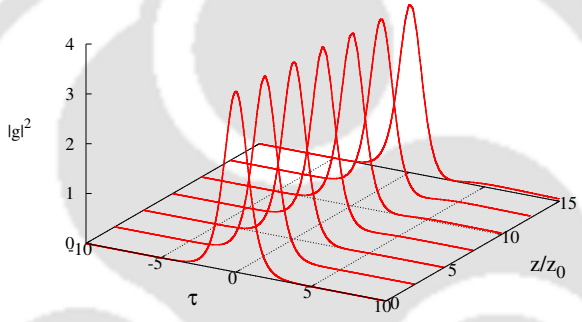

(b)

Fig. 5.2 Spatio-temporal evolution of the grey-bright solitons using parameters such that the group velocity dispersion have the opposite sign. We used $a = 0.17247$, $b = 0.14937$, $p_1 = 0.50083$, $p_2 = 0.02231$, $\Omega_1 = 0.026442$, $\Omega_2 = 0$, $\theta = 0.31164$, $\beta_1 = 1.0$, $\beta_2 = -2.5$,$\gamma_1 = 1$, $\gamma_2 = 1$, $\Delta = 2$, $u = 0.97835$, $\sigma = 11.596$, $\Gamma = 1.0013$, $\eta_1 = 1$, and $\eta_2 = 1.2$. All values are normalized in terms of z_0 and σ.

for solving the nonlinear Schrödinger equation and investigate the spatio-temporal evolution of the optical pulses through the medium. We have used the scalings, $\tau = t/\sigma, \zeta = z/z_0$
where σ is the width of input pulse and z_0 the dispersion length of the fibre.

The initial shapes of the input pulse and the initial atomic populations can be obtained in the limit of $z = 0$ and $t = 0$ from the analytical expressions (5.7a-5.7b) and (5.7c-5.7e) respectively. We use grey and bright solitons with same width 8.066 psec in the present investigation. Parameters used in the numerical simulation obey self consistency relations (5.12). The parameters can be experimentally attained in a birefringent two mode fiber with the two wavelengths selected to be of the order of 1.5μm and 1.65μm respectively [157]. It can also be realized in silica fibers doped

with Nd^{+3} ions [158]. By properly choosing the doping concentration and structural parameters, the consistency condition can be met with in this system. We explore the stable propagation of the grey and bright solitons in presence of GVD with opposite character. In Fig.5.2 the spatio-temporal propagation dynamics of the bright and grey soliton pair is plotted with GVD coefficients having opposite sign. It can be seen that the amplitudes of the output pulses are retaining their initial shape over considerable propagation distance. The length z is normalized with the dispersion length z_0 of the fiber, which can be of the order of a few metres for the pulse width considered [159]. Both solitons propagate undistorted over a long distance. A small oscillation though has been noticed at both the ends of the grey soliton after propagation through a distance $z \geq 10z_0$, due to the modulation instability. The numerical results obtained from the Runge-Kutta and split step operator methods match well with those obtained analytically.

Next we study how the choice of different parameters leads to stable propagation of soliton through the medium. For the selected values for detuning and fibre parameters, we have solved the algebraic expressions resulting from the various relations 5.8, 5.9 and 5.10 to find out all other parameter values consistently. The soliton velocity is found to be constant for a wide range of values of blackness parameter θ for a given consistent set of other parameters. However stable soliton propagation is possible for Δ equal to or higher than the value used.

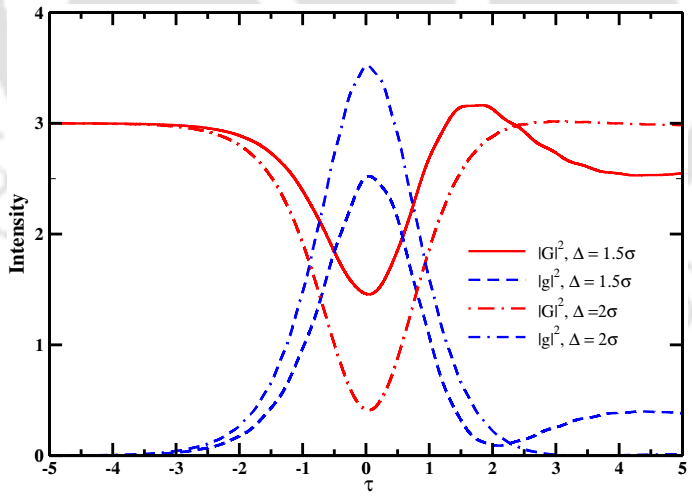

Fig. 5.3 Amplitude of the bright and grey solitons are plotted as a function of time at distance $z = 10z_0$ of the medium for two different values of Δ . All other parameters are as in Fig. 5.2.

As a comparative study, the amplitude of soliton pair at the output end of the medium with two different detuning is plotted in Fig. 5.3. It can be seen that for different detuning values Δ less than the one considered for stable soliton propagation, both grey

and bright solitons develop instability in anomalous GVD regime, with a reduction in amplitude of input signal. The high dispersive effects shown when $\Delta = 1.5\sigma$ shows that detuning is a crucial parameter for stable soliton propagation. By proper choice of signal detuning, the signal phase effects can be controlled and the instability can be compensated. Note that the selection of proper detuning is not a restrictive condition on the stable propagation, but a suitable parameter regime to observe the effect. A range of values can be assumed for the detuning, provided it is sufficiently detuned from resonance. We have verified the stable propagation for a range of detunings, greater than 2σ .

5.5 Chapter conclusion

In conclusion, grey solitons, analog of Bloch solitons in condensed matter systems, have been identified as exact solutions of the coupled nonlinear Schrodinger and Bloch equations in birefringent or bimode fiber systems doped with three level atoms. The complex nature of the profile played a crucial role in removing the restrictive frequency matching condition of tanh −sech paired solutions [155]. We numerically evolved our solution and found it to be stable over several orders of dispersion length. We note that, for the case of coupling with a two-level system ($g \to 0$, $\zeta_3 \to 0$) instead of the Λ system considered here, the pure tanh and grey solitonic profiles are prohibited for G while a pure sech profile is allowed. It is observed that the soliton phase is controlled by the atomic coherence and atomic population is governed by the area of the soliton. It is also observed that for near resonant frequencies, the solutions develops instability at larger diatances. But this can be compensted for fields sufficiently detuned from resosnance.

Chapter 6

Conclusions and Future outlook

This thesis discusses different coherent control schemes to effectively control the optical properties of atomic media and manipulate the light pulse propagation through it. The contents of the thesis is outlined below.

In chapter 1, we have introduced the theoretical background needed for the work. The semiclassical approach for light-matter interaction is described . Basic propagation equations of electromagnetic field through a polarized medium is derived. The density matrix formalism to treat the atomic medium is introduced and Bloch equations are derived. The atom-field coupled Hamiltonian and polarization expression in the dipole approximation is given. Basic features of light propagation through two-level and three level media are briefly discussed. The phenomenon of Electromagnetically Induced transparency and the modification of optical properties of the medium due to it is explained.

In chapter 2, the spatio-temporal evolution of a Gaussian probe pulse propagating through a four-level N-type atomic medium is investigated. Splitting of originally Gaussian pulse into sub-pulses is observed at reasonably high intensities of probe field, while distortionless propagation is observed at low intensities and at two photon resonance. The number of sub-pulses formed through the propagation is found to be controlled via a suitable choice of the probe and control field parameters. The splitting is also observed for non-Gaussian pulses like *sec*-hyperbolic.

In chapter 3, a novel scheme for efficient Raman sub-harmonic generation in a system of inhomogeneously broadened atomic vapor with atoms in a closed three level Λ-configuration is discussed. It is shown how a comb of Raman sub harmonic frequencies are generated in the system, making use of microwave induced hyperfine coherence between the two lower level metastable states. The phase dependence on the amplitude

of the generated field is also given.

In chapter 4, generation of optical frequency pulse is observed in a closed Λ atomic system by introducing a microwave pulse coupling the hyperfine levels. The generated pulse follows the temporal shape of the microwave pulse. This scheme can generate arbitrary shaped optical pulse from microwave pulse.

Considering the new possibilities in optical control by combining nonlinear fibre systems with atomic systems, in chapter 5, a system describing optical nonlinear birefringent fibers doped with three level atoms is investigated. The system is shown to exhibit bright and gray coupled solitons, with complex envelope, as solutions. The stability of generated solitons is studied and observed it to be stable over several dispersion lengths of the fibre.

Chapter 6 concludes the work and gives future outlooks.

Future perspectives

Coherent control studies are widely explored and actively carried out area of research for many years. The future scope of the content presented in this thesis is not limited to pulse propagation or atomic vapor systems. Because of its generalized nature, the work can be extended to any area of coherent control of optical systems. A full quantum mechanical treatment of light matter interaction can open up new insights and possibilities in this field. For example, N-level system studied in chapter 2 is already explored in few photon light levels and strong field polariton systems. Optical frequency harmonic generation and frequency mixing schemes have scope in areas of precision measurements, frequency standards etc.

We can extend our work to adaptive spectral pulse shaping, by tailoring the spectral phases of a pulse. One possible application for spectral shaped pulse is coherent control of backscattering experiments used in far-detection of scattering particles. For constructive interference between direct and reverse paths in the backscattering direction needed for the detection of backscattered beam, a controlled reflection and subsequent controlled multi-pulse interference is needed. Hence control over the spectral shape of the pulse enables applications in controlled lasing and multiphoton imaging in scattering materials.

Coherent control techniques extended to multiphoton regime allows access to dipole-forbidden transition states and has wider range of applicability. The requirement of high intensity laser pulses to achieve ultrafast Rabi oscillations, however, cause nonlinear effects and the Rabi oscillations are disrupted. The possibility to find new prospects for the ultrafast manipulation of multiphoton transition states thus need to be explored.

Coherent ultrafast radiation in the mid-infrared region is used in strong-field physics. This relaxes the requirement for high intensity optical radiation usually employed in light-matter interactions. The generation and control of mid-IR pulses is thus an interesting subject to look into. Parametric processes in atoms may be employed in achieving this task, and needs further investigation.

Possibility of employing atomic systems with other level structures such as double-lambda, double-A systems for multi-wave mixing and for higher nonlinear processes can also be investigated. Fields with different polarizations can be employed to produce multi-dark states and the nonlinear response can be measured. Chirped laser pulses can be employed in multi-level structures for selective population transfer and hence control of optical properties. In addition to detunings, chirp rate can also be used as an additional parameter for effective control of medium properties.

In the microwave to optical frequency conversion explained in chapter 4, the generated frequency is shown to follow the temporal dynamics of microwave pulse. We can look for ways to control the temporal delay between the pulses with high accuracy. By considering the realistic picture of all hyperfine levels in this system, we can explore the possibility of generation of multi-frequency pulses. By varying the relative phase of multi-photon components, processes like dissociation ionization in molecular systems can be analyzed.

References

[1] M. O. Scully and M. S. Zubairy, "Quantum Optics" (Cambridge University Press, Cambridge, 1997).

[2] I. Novikova, N. B. Phillips, and A. V. Gorshkov, Phys. Rev. A **78**, 021802(R) (2008).

[3] T. Guo, K. Deng, X. Chen, and Z. Wang, Applied Physics Letters **94**, 151108 (2009).

[4] A. Corney, Phil. Trans. R. Soc. Lond. A **307**, 573 (1982).

[5] M. M. Boyd, T. Zelevinsky, A. D. Ludlow, S. M. Foreman, S. Blatt, T. Ido, J. Ye, Science **314**, 1430 (2006).

[6] G. Katsoprinakis, D. Petrosyan, and I. K. Kominis, Phys. Rev. Lett. **97**, 230801 (2006).

[7] L. Guo-Bin, D. Run-Chang, L. Chao-Yang, and G. Si-Hong, Chinese Physics Letters **25**, 472 (2008).

[8] V. I. Yudin, A. V. Taichenachev, Y. O. Dudin, V. L. Velichansky, A. S. Zibrov, and S. A. Zibrov, Phys. Rev. A **82**, 033807 (2010).

[9] J. E. Thomas, P. R. Hemmer, S. Ezekiel, C. C. Leiby, Jr., R. H. Picard, and C. R. Willis, Phys. Rev. Lett. **48**, 867 (1982).

[10] S. L. McCall and E. L. Hahn, Phys. Rev. **183**, 457 (1969).

[11] S. L. McCall and E. L. Hahn, Phys. Rev. Lett. **18**, 908 (1967).

[12] E. Arimondo, Prog. Opt. **35**, 257 (1996).

[13] G. Alzetta, A. Gozzini, L. Moi, and G. Orriols, Nuovo Cimento B **36**, 5 (1976); G. Alzetta, L. Moi, and G. Orriols, Nuovo Cimento B **52**, 209 (1979).

[14] S. E. Harris, Phys. Today **50**, 36 (1997).

[15] L. V. Hau, S. E. Harris, Z. Dutton, and C. H. Behroozi, Nature **397**, 594 (1999).

[16] M. M. Kash, V. A. Sautenkov, A. S. Zibrov, L. Hollberg, G. R. Welch, M. D. Lukin, Y. Rostovtsev, E. S. Fry, and M. O. Scully, Phys. Rev. Lett. **82**, 5229 (1999).

[17] D. Budker, D. F. Kimball, S. M. Rochester, and V. V. Yashchuk, Phys. Rev. Lett. **83**, 1767 (1999).

[18] O. Kocharovskaya, and Y. I. Khanin, JETP Lett. **48**, 630 (1988); O. Kocharovskaya, and P. Mandel, Phys. Rev. A. **42**, 523 (1990); S. E. Harris, Phys. Rev. Lett. **62**, 1033 (1989).

[19] A. S. Zibrov, M. D. Lukin, D. E. Nikonov, L. Hollberg, M. O. Scully, V. L. Velichansky, and H. G. Robinson, Phys. Rev. Lett. **75**, 1499 (1995); G. G. Padmabandu, G. R. Welch, I. N. Shubin, E. S. Fry, D. E. Nikonov, M. D. Lukin, and M. O. Scully, Phys. Rev. Lett. **76**, 2053 (1996).

[20] D. S. Lee, and K. J. Malloy, IEEE Jl quant. Electron. **30**, 85 (1994).

[21] A. Imamoglu, and R. J. Ram, Optics Lett. **19**, 1744 (1994).

[22] M. Fleischhauer and M. D. Lukin, Phys. Rev. Lett. **84**, 5094 (2000); Phys. Rev. A **65**, 022314 (2002).

[23] D. F. Phillips, A. Fleischhauer, A. Mair, R. L. Walsworth, and M. D. Lukin, Phys. Rev. Lett. **86**, 783 (2001).

[24] A. V. Turukhin, V. S. Sudarhanam, M. S. Shahriar, J. A. Musser, B. S. Ham, and P. R. Hemmer, Phys. Rev. Lett. **88**, 023602 (2002).

[25] G. Heinze, C. Hubrich, and T. Halfmann, Phys. Rev. Lett. **11**, 033601 (2013).

[26] K. P. Heeg, J. Haber, D. Schumacher, L. Bocklage, H. C. Wille, K. S. Schulze, R. Loetzsch, I. Uschmann, G. G. Paulus, R. Rüffer, R. Röhlsberger, and J. Evers, Phys. Rev. Lett. **114**, 203601 (2015).

[27] T. N. Dey and G. S.Agarwal, Phys. Rev. A **67**, 033813 (2003).

[28] A. André and M. D. Lukin, Phys. Rev. Lett. **89**, 143602 (2002).

[29] M. Bajcsy, A. S. Zibrov, and M. D. Lukin, Nature **426**, 638 (2003).

[30] F. E. Zimmer, A. André, M. D. Lukin, and M. Fleischhauer, Opt. Commun. **264**, 441 (2006).

[31] F. E. Zimmer, J. Otterbach, R. G. Unanyan, B. W. Shore, and M. Fleischhauer, Phys. Rev. A **77**, 063823 (2008).

[32] S. A. Moiseev and B. S. Ham, Phys. Rev. A **71**, 053802 (2005).

[33] S. A. Moiseev and B. S. Ham, Phys. Rev. A **73**, 033812 (2006).

[34] M. Fleischhauer, J.Otterbach, and R. G. Unanyan, Phys. Rev. Lett. **101**, 163601 (2008).

[35] Y. W. Lin, W. T. Liao, T. Peters, H. C. Chou, J. S. Wang, H. W. Cho, P. C. Kuan, and I. A. Yu, Phys. Rev. Lett. **102**, 213601 (2009).

[36] G. Nikoghosyan and M. Fleischhauer, Phys. Rev. A **80**, 013818 (2009).

[37] M. Kiffner and M. J. Hartmann, Phys. Rev. A **82**, 033813 (2010).

[38] S. E. Harris, J. E. Field, A. Imamoglu, Phys. Rev. Lett. **64**, 1107 (1990).

[39] H. Wang, D. Goorskey and M. Xiao, Phys. Rev. Lett. **87**, 073601 (2001).

[40] M. Fleischhauer, A. Imamoglu, J. P. Marangos, Rev. Mod. Phys. **77**, 633 (2005).

[41] J. P. Marangos, J. Mod. Opt. **45**, 471 (1998).

[42] R. Fleischhaker and J. Evers, Phys. Rev. A **77**, 043805 (2008).

[43] G. S. Agarwal, T.N. Dey, and S. Menon, Phys. Rev. A **64**, 053809 (2001).

[44] Y. Niu, S. Gong, R. Li, Z. Xu, and X. Liang, Opt. Lett. **30**, 3371 (2005).

[45] S. F. Yelin, V. A. Sautenkov, M. M. Kash, G. R. Welch, and M.D. Lukin, Phys. Rev. A **68**, 063801 (2003).

[46] C. Y. Ye, A. S. Zibrov, Y. V. Rostovtsev, and M. O. Scully, Phys. Rev. A **65**, 043805 (2002).

[47] C. Y. Ye, and A. S. Zibrov, Phys. Rev. A **65**, 023806 (2002).

[48] H. Schmidt and A. Imamoglu, Opt. Lett. **21**, 1936 (1996).

[49] C. Goren, A. D. Wilson-Gordon, M. Rosenbluh, and H. Friedmann, Phys. Rev. A. **69**, 053818 (2004).

[50] L. B. Kong, X. H. Tu, J. Wang, Y. Zhu, and M. S. Zhan, Opt. Comm. **269**, 362 (2007).

[51] P. R. Hemmer, D. P. Katz, J. Donoghue, M. Cronin-Golomb, M. S. Shahriar, and P. Kumar, Opt. Lett. **20**, 982 (1995).

[52] M. Jain, H. Xia, G. Y. Yin, A. J. Merriam and S. E. Harris Phys. Rev. Lett. **77**, 4326 (1996).

[53] Y. Q. Li and M. Xiao, Opt. Lett. **21**, 1064 (1996).

[54] L. Allen and J. H. Eberly, "Optical resonance and two-level atoms" (Dover Publications, Mineola, NY, 1987).

[55] M.O. Scully, Phys. Rep. **219**, 191 (1992).

[56] T. W. Hansch, M. D. Levenson, and A. L. Schawlow, Phys. Rev. Lett. **26**, 946 (1971), M. Nilsson and S. Kroll, Opt. Commun. **247**, 393 (2005).

[57] G. L. Lamb, Jr., Rev. Mod. Phys. **43**, 99 (1971).

[58] H. A. Haus, Rev. Mod. Phys. **51**, 331 (1979).

[59] U. Fano, Phys. Rev. **124**, 1866 (1961).

[60] G. Vemuri, G. S. Agarwal, and B. D. Nageswara Rao, Phys. Rev. A **53**, 2842 (1996).

[61] A. Javan, O. Kocharovskaya, H. Lee, and M. O. Scully, Phys. Rev. A **66**, 013805 (2002).

[62] T. N. Dey, "Subluminal and Superluminal Propagation of Electromagnetic Fields" (Doctoral dissertation), (2004).

[63] K. I. Harada, T. Kanbashi, M. Mitsunaga, and K. Motomura, Phys. Rev. A **73**, 013807 (2006).

[64] T. N. Dey and G. S. Agarwal, Phys. Rev. A **67**, 033813 (2003).

[65] H. Kang and Y. Zhu, Phys. Rev. Lett. **91**, 093601 (2003).

[66] G. F. Sinclair and N. Korolkova, Phys. Rev. A **76**, 033803 (2007).

[67] J. H. Li, X. Y. Lu, J. M. Luo, and Q. J. Huang, Phys. Rev. A **74**, 035801 (2006).

[68] J. Sheng, X. Yang, U. Khadka and M. Xiao, Opt. Exp. **19**, 17059 (2011).

[69] M. Bajcsy, S. Hofferberth, V. Balic, T. Peyronel, M. Hafezi, A. S. Zibrov, V. Vuletic, and M. D. Lukin, Phys. Rev. Lett. **102**, 203902 (2009).

[70] A. Andre, M. Bajcsy, A. S. Zibrov, and M. D. Lukin, Phys. Rev. Lett. **94**, 063902 (2005).

[71] S. E. Harris and Y. Yamamoto, Phys. Rev. Lett. **81**, 2675 (1998).

[72] D. E. Chang, V. Gritsev, G. Morigi, V. Vuletic, M. D. Lukin, and E. A. Demler, Nat. Phys. **4**, 884 (2008).

[73] M. Kiffner and M. J. Hartmann, Phys. Rev. A **81**, 021806(R) (2010).

[74] M. Hafezi, D. E. Chang, V. Gritsev, E. A. Demler and M. D. Lukin, EPL **94**, 54006 (2011).

[75] L. E. Zohravi, M. Abedi and M. Mahmoudi, Commun. Theor. Phys. **61**, 506 (2014).

[76] D. Maxwell, D. J. Szwer, D. Paredes-Barato, H. Busche, J. D. Pritchard, A. Gauguet, K. J. Weatherill, M. P. A. Jones, and C. S. Adams, Phys. Rev. Lett. **110**, 103001 (2013).

[77] A. V. Gorshkov, J. Otterbach, M. Fleischhauer, T. Pohl, and M. D. Lukin, **107**, 133602 (2011).

[78] C. S. Hofmann, G. Günter, H. Schempp, M. Robert-de-Saint-Vincent, M. Gärttner, J. Evers, S. Whitlock, and M. Weidemüller **110**, 203601 (2013).

[79] S. Sevincli, N. Henkel, C. Ates, and T. Pohl **107**, 153001 (2011).

[80] G. P. Agrawal, "Nonlinear Fiber Optics" (Academic, Boston, 1989).

[81] M. Kiffner and K. P. Marzlin, Phys. Rev. A **71**, 033811 (2005).

[82] M. Kiffner, U. Dorner and D. Jaksch, Phys. Rev. A **85**, 023812 (2012).

[83] M. S. Shahriar and P. R. Hemmer, Phys. Rev. Lett. **65**, 1865 (1990).

[84] D. V. Kosachiov, B. G. Matisov, Y. V. Rozhdestvensky, Journal of Physics B-Atomic Molecular and Optical Physics **25**, 2473 (1992).

[85] A. S. Zibrov, A. B. Matsko, and M. O. Scully, Phys. Rev. Lett. **89**, 103601 (2002).

[86] A. S. Zibrov, A. A. Zhukov, V. P. Yakovlev, and V. L. Velichansky, JETP Lett. **83**, 136 (2006).

[87] K. Yamamoto, K. Ichimura, and N. Gemma, Phys. Rev. A **58**, 2460 (1998).

[88] G. S. Agarwal, T. N. Dey, and S. Menon, Phys. Rev A. **64**, 053809 (2001).

[89] H. Li, V. A. Sautenkov, Y. V. Rostovtsev, G. R. Welch, P. R. Hemmer and M. O. Scully, Phys. Rev. A **80**, 023820 (2009).

[90] D. V. Kosachiov and E. A. Korsunsky, Eur. Phys. J. D **11**, 457 (2000).

[91] Rajitha K. V., T. N. Dey S. Das and P. K. Jha, Opt. Lett. **40**, 2229 (2015).

[92] S. Davuluri and Y. Rostovtsev, Phys. Rev. A **88**, 053847 (2013).

[93] L. Li and G. X. Huang, Eur. Phys. J. D **58**, 339 (2010).

[94] A. Eilam, A. D. Wilson-Gordon, and H. Friedmann, Opt. Lett. **34**, 1834 (2009).

[95] F. Renzoni, S. Cartaleva, G. Alzetta, and E. A. Arimondo, Phys. Rev. A **63**, 065401 (2001).

[96] A. Mair, J. Hager, D. F. Phillips, R. L. Walsworth, and M. D. Lukin, Phys. Rev. A **65**, 031802 (2002).

[97] R. W. Boyd, "Nonlinear Optics" (Academic Press, New York, 1992).

[98] G. S. Agarwal, Phys. Rev. A **43**, 1523 (1991).

[99] J. Q. Liang, M. Katsuragawa, F. L. Kien, and K. Hakuta, Phys. Rev. Lett. **85**, 2474 (2000).

[100] M. Katsuragawa, J. Q. Liang, F. L. Kien, and K. Hakuta, Phys. Rev. A **65**, 025801 (2002).

[101] S. E. Harris and A. V. Sokolov, Phys. Rev. A **55**, R4019 (1997).

[102] A. V. Sokolov, D. R. Walker, D. D. Yavuz, G. Y. Yin, and S. E. Harris, Phys. Rev. Lett. **85**, 562 (2000).

[103] Y. Wu, L. L. Wen and Y. F. Zhu, Opt. Lett. **28**, 631 (2003).

[104] S. E. Harris and A. V. Sokolov, Phys. Rev. Lett. **81**, 2894 (1998).

[105] F. L. Kien, A. K. Patnaik, and K. Hakuta, Phys. Rev. A **68**, 063803 (2003).

[106] G. S. Agarwal, T. N. Dey, and D. J. Gauthier, Phys. Rev. A **74**, 043805 (2006).

[107] F. Levi, A. Godone, J. Vanier, S. Micalizio, and G. Modugno, Eur. Phys. J. D **12**, 53 (2000).

[108] G. S. Agarwal, T. N. Dey, S. Menon, Phys. Rev. A **64**, 053809 (2001).

[109] H. Li, V. A. Sautenkov, Y. V. Rostovtsev, G. R. Welch, P. R. Hemmer and M. O. Scully Phys. Rev. A **80**, 023820 (2009).

[110] H. M. Concannon, W. J. Brown, J. R. Gardner, and D. J. Gauthier, Phys. Rev. A **56**, 1519 (1997).

[111] D. V. Kosachiov, B. G. Matisov, and Y. V. Rozhdestvensky, J. Phys. B **25**, 2473 (1992).

[112] K. E. Dorfman, P. K. Jha, D. V. Voronine, P. Genevet, F. Capasso, and M.O. Scully, Phys. Rev. Lett. **111**, 043601 (2013).

[113] S. P. Tewari, G. S. Agarwal, Phys. Rev. Lett. **56**, 1811 (1986).

[114] K. Hakuta, L. Marmet, and B. P. Stoicheff, Phys. Rev. Lett. **66**, 596 (1991).

[115] M. Tsang, Phys. Rev. A **84**, 043845 (2011).

[116] D. V. Strekalov, A. A. Savchenkov, A. B. Matsko, and N. Yu, Opt. Lett. **34**, 713 (2009).

[117] A. M. Weiner, Rev. Sci. Instrum. **71**, 1929 (2000).

[118] A. I. Maimistov, A. M. Bhasrov, S. O. Elyutin and M. Y. Sklyarov, Phys. Rep. **191**, 1 (1990).

[119] T. W. Barnard, Phys. Rev. A **7**, 373 (1973).

[120] F. T. Arecchi, V. DeGiorgio and S. G. Someda, Phys. Lett. A **27**, 588 (1968).

[121] M. D. Crisp, Phys. Rev. Lett. **22**, 820 (1969).

[122] P. K. Panigrahi and G. S. Agarwal, Phys. Rev. A **67**, 033817 (2003).

[123] R. Grobe, F. T. Hioe and J. H. Eberly, Phys. Rev. Lett. **73**, 3183 (1994).

[124] M. A. Newbold and G. J. Salamo, Phys. Rev. Lett. **42**, 887 (1979).

[125] J. L. Shultz and G. J. Salamo, Phys. Rev. Lett. **78**, 855 (1997).

[126] T. S. Raju and P. K. Panigrahi, Phys. Rev. A **81**, 043820 (2010).

[127] V. E. Zakharov and A. B. Shabat, Sov. J. Exp. Theor. Phys. **34**, 62 (1972).

[128] S. Burger, K. Bongs, S. Dettmer, W. Ertmer, K. Sengstock, A. Sanpera, G. V. Shlyapnikov and M. Lewenstein, Phys. Rev. Lett. **83**, 5198 (1999).

[129] J. Denschlag, J. E. Simsarian, D. L. Feder, C. W. Clark, L. A. Collins, J. Cubizolles, L. Deng, E. W. Hagley, K. Helmerson, W. P. Reinhardt, S. L. Rolston, B. I. Schneider and W. D. Phillips, Science **287**, 97 (2000).

[130] L. Khaykovich, F. Schreck, G. Ferrari, T. Bourdel, J. Cubizolles, L. D. Carr, Y. Castin and C. Salomon, Science **296**, 1290 (2002).

[131] K. E. Strecker, G. B. Partridge, A. G. Truscott and R. G. Hulet, Nature (London) **417**, 150 (2002).

[132] U. Al Khawaja, H. T. C. Stoof, R. G. Hulet, K. E. Strecker and G. B. Partridge, Phys. Rev. Lett. **89**, 200404 (2002).

[133] S. L. Cornish, S. T. Thompson and C. E. Wieman, Phys. Rev. Lett. **96**, 170401 (2006).

[134] I. Shomroni, E. Lahoud, S. Levy and J. Steinhauer, Nature Phys. **5**, 193 (2009).

[135] L. F. Mollenauer, R. H. Stolen and J. P. Gordon, Phys. Rev. Lett. **45**, 1095 (1980).

[136] S. Komineas and N. Papanicolaou, Phys. Rev. Lett. **89**, 070402 (2002).

[137] A. D. Jackson and G. M. Kavoulakis, Phys. Rev. Lett. **89**, 070403 (2002).

[138] C. J. Pethick and H. Smith, "Bose-Einstein Condensation in Dilute Gases," (Cambridge University Press, Cambridge, UK, 2002).

[139] D. Y. tang, L. Li, Y. F. Song, L. M. Zhao, H. Zhang and D. Y. Shen, Phys. Rev. A **88**, 013849 (2013).

[140] H. Leblond and D. Mihalache, Phys. Rev. A **86**, 043832 (2012).

[141] O. Fialko, J. Brand and U. Z. licke, Phys. Rev. A **85**, 051605 (2012).

[142] R. G. Scott, F. Dalfovo, L. P. Pitaevskii and S. Stringari, Phys. Rev. Lett. **106**, 185301 (2011).

[143] R. Liao and J. Brand, Phys. Rev. A **83**, 041604 (2011).

[144] N. V. Alexeeva, I. V. Barashenkov, A. A. Sukhorukov and Y. S. Kivshar, Phys. Rev. A **85**, 063837 (2012).

[145] A. Khan, R. Atre and P. K. Panigrahi, arXiv:0903.4859v2.

[146] P. Das, S. Gangopadhyay and P. K. Panigrahi, arXiv:1003.5745v1.

[147] Andrea Spuntarelli, Lincoln D Carr, Pierbiagio Pieri, and Giancarlo C Strinati, New. J. Phys. **13**, 035010 (2011).

[148] X. Liu, Opt. Express **19**, 5874 (2011).

[149] D. Y. Tang, L. M. Zhao, G. Q. Xie and L. J. Qian, Phys. Rev. A **75**, 063810 (2007).

[150] D. Mao, X. Liu, L. Wang, Hua Lu, and L Duan, Opt. Express **19**, 16303 (2011).

[151] L. Wang, Opt. Communications **297**, 129 (2013).

[152] J. H. Eberly, Quantum Semiclass. Opt. **7**, 373 (1995).

[153] A. Rahman and J. H. Eberly, Phys. Rev. A **58**, R805 (1998).

[154] J. H. Eberly and V. V. Kozlov, Phys. Rev. Lett. **88**, 243604 (2002).

[155] T. N. Dey, S. Dutta Gupta and G. S. Agarwal, Opt. Express **16**, 17441 (2008).

[156] E. Baldit, K. Bencheikh, P. Monnier, S. Briaudeau, and J. A. Levenson, Phys. Rev. B **81**, 144303 (2010).

[157] F. Shi, Y. Wu, M. Li, Y. Zhao, and L. Zhao, Photonics Journal, IEEE **3**, 1181 (2011).

[158] "Rare-Earth-Doped Fibre Lasers and Amplifiers," edited by Michel J.F. Digonnet, 2nd Ed.(Marcel Dekker, Inc., 1993).

[159] G. P. Agrawal, "Nonlinear Fiber Optics" (2nd Ed. Academic Press, San Diego CA 1995).

List of publications

1. Rajitha K. V. , Tarak N. Dey, Jörg Evers, and Martin Kiffner, "*Pulse-splitting in light propagation through N-type atomic media due to an interplay of Kerr-nonlinearity and group velocity dispersion*", Phy. Rev. A **92**, 023840 (2015).

2. Rajitha K. V. , Tarak N. Dey, Sumanta Das, and Pankaj K. Jha, "*Microwave controlled efficient Raman sub-harmonic generation*", Opt. Lett. **40**, 2229 (2015).

3. Rajitha K. V. and Tarak N. Dey, "*Microwave assisted arbitrary optical pulse generation in thermal vapour*" (accepted in PRA).

4. "*Phase controlled stable solitons in nonlinear fibers,*" (under communication).

Schools and Conferences attended

1. XXVII IUPAP Conference on Computational Physics, 2-5 Dec 2015.

2. ICTS School & Discussion Meeting on Frontiers in Light-Matter Interactions, 8-18 Dec 2014.